

Searching for Additional Planets in *TESS* Multi-Planet Systems: Testing Empirical Models Based on *Kepler* Data

EMMA V. TURTELBOOM ¹, JAMIE DIETRICH ², COURTNEY D. DRESSING ¹ AND CALEB K. HARADA ^{1,*}

¹*Department of Astronomy, 501 Campbell Hall, University of California, Berkeley, CA 94720, USA*

²*School of Earth and Space Exploration, Arizona State University, Tempe, AZ 85287, USA*

(Received 5 August 2024)

Submitted to AJ

ABSTRACT

Multi-planet system architectures are frequently used to constrain possible formation and evolutionary pathways of observed exoplanets. Therefore, understanding the predictive and descriptive power of empirical models of these systems is critical to understanding their formation histories. Additionally, if empirical models can reproduce architectures over a range of scales, transit and radial velocity observations can be more easily and effectively used to inform future microlensing, astrometric, and direct imaging surveys. We analyze 52 *TESS* multi-planet systems previously studied using DYNAMITE (Dietrich & Apai 2020), who used *TESS* data alongside empirical models based on *Kepler* planets to predict additional planets in each system. We analyze additional *TESS* data to search for these predicted planets. We thereby evaluate the degree to which these models can be used to predict planets in *TESS* multi-planet systems. Specifically, we study whether a period ratio method or clustered period model is more predictive. We find that the period ratio model predictions are most consistent with the planets discovered since 2020, accounting for detection sensitivity. However, neither model is highly predictive, highlighting the need for additional data and nuanced models to describe the full population. Improved eccentricity and dynamical stability prescriptions incorporated into DYNAMITE provide a modest improvement in the prediction accuracy. We also find that the current sample of 183 *TESS* multi-planet systems are highly dynamically packed, and appear truncated relative to detection biases. These attributes are consistent with the *Kepler* sample, and suggest a highly efficient formation process.

1. INTRODUCTION

A large fraction of exoplanets with orbital periods $\lesssim 100$ d are members of multi-planet systems (e.g. Lissauer et al. 2011; Sandford et al. 2019). Of the 500 confirmed planets in the systems discovered by the Transiting Exoplanet Survey Satellite (*TESS*), 243 are in 97 multi-planet systems¹. This sample builds upon the extensive population of multi-planet systems found by the *Kepler* mission, which discovered 525 multi-planet systems containing over 1300 confirmed planets. Extensive

analyses of the *Kepler* multi-planet systems (e.g. Xie et al. 2016) have revealed demographic features such as the excess of planet pairs wide of resonance (Steffen & Hwang 2015; Fabrycky et al. 2014), and the tendency towards correlated radii and masses of small ($< 4R_{\oplus}$) planets in multi-planet systems (Millholland et al. 2017; Weiss et al. 2018).

Planetary system architectures and demographics encapsulate the outcomes of a diverse set of formation and evolutionary processes, wherein planets dynamically influence each other throughout their lifetimes. Theoretical models of multi-planet systems aim to connect relevant physical processes with the observed population of planets (see Mordasini 2018; Drążkowska et al. 2023 and references therein). Empirical models, on the other hand, seek to characterize the detection biases and

Corresponding author: Emma V. Turtelboom
eturtelboom@berkeley.edu

* NSF Graduate Research Fellow

¹ NASA Exoplanet Archive, <https://exoplanetarchive.ipac.caltech.edu/>, accessed 12 June 2024.

observational strategies involved in generating the observed planet population.

Large-scale transit and radial velocity surveys are currently the largest contributors (74% and 19%, respectively) to the confirmed exoplanet sample. However, these methods are most sensitive to Jovian planets with short orbital periods. Complementary methods, such as direct imaging, astrometry, and microlensing are primarily sensitive to planets at wide separations. Future missions will use these methods to probe currently under-sampled regions of parameter space. Direct imaging is particularly sensitive to long-period planets (at 10s of AU), with a bias towards young (and thus, luminous), giant planets (Chauvin 2024). The microlensing method is most sensitive to giant planets at moderately wide separations ($\sim 1\text{-}10$ AU) from their host stars, with the added capability of detecting free-floating planets (e.g. Bennett & Rhie 2002; Sumi et al. 2011; Barclay et al. 2017). The Nancy Grace Roman Space Telescope (Spergel et al. 2015) is predicted to discover ~ 1000 bound and ~ 250 free-floating planets via microlensing (Penny et al. 2019), as well as $\sim 100,000$ transiting planets (Montet et al. 2017; Wilson et al. 2023; Tamburo et al. 2023). By detecting both transiting (and thus, likely close-in) and microlensed (at preferentially intermediate separations) planets, Roman will provide a large-scale view of exoplanet systems (Montet et al. 2017) relative to our current understanding. Robust models of the inner regions of planetary systems will be critical to contextualize these observations. However, we must be cautious when using models of exoplanetary systems based on prior surveys which are not generalizable. Relying too heavily on models fit to past results from other survey may introduce unknown biases in our analyses of future surveys such as the the Roman Galactic Bulge Time Domain Survey (GBTDS) and cloud our picture of planet demographics.

Several models have been put forth to describe the *Kepler* multi-planet systems (e.g., Mulders et al. 2018; Batalha 2014; Zhu et al. 2018; Yang et al. 2020). These models characterize the detection sensitivity function associated with the *Kepler* mission, and aim to describe the observed exoplanet population and distribution of planetary system architectures. A “*Kepler* multi” has come to mean a largely co-planar compact multi-planet system hosting relatively small, roughly uniformly sized planets with similar masses evenly spaced in log-period space. However, this architecture does not describe the full *Kepler* sample of planets, and may not be generalizable to other observed populations. We seek to investigate whether two of the empirical models developed using the *Kepler* sample accurately describe the

multi-planet systems discovered by *Kepler*’s successor, the *TESS* mission.

The empirical models that we study were initially introduced by Mulders et al. (2018) and He et al. (2019). In 2020, these models were used to predict an additional planet in the *TESS* multi-planet systems using DYNAMITE (the DYNAMical Multi-planet Injection TEster², Dietrich & Apai 2020, henceforth D20). We measure the descriptive power of a model by evaluating how accurately it is able to predict additional planets in a given system.

This work is structured as follows: in Section 3, we discuss the sample of *TESS* multi-planet systems with additional DYNAMITE predicted planets, as well as the current sample of *TESS* multi-planet systems. In Section 4, we test the model predictions by comparing the planets predicted by these models to the new planets detected with additional *TESS* observations and radial velocity (RV) data since 2020. We then quantify the detection sensitivity for each predicted additional planet using injection-recovery tests and analytical signal-to-noise calculations. In Section 5, we evaluate which model most accurately predicted the new planets found since 2020, and apply an updated version of DYNAMITE to predict additional planets in the current *TESS* sample of multi-planet systems. We discuss our results in Section 6, and conclude in Section 7.

2. DATA

The *TESS* mission is an all-sky survey searching for transiting exoplanets, and has completed over 4 years of observations since its launch in 2019. Observations are taken in sectors, each covering $24'' \times 96''$ and lasting two spacecraft orbits (~ 27 days). *TESS* has completed its Prime (Cycles 1 and 2) and First Extended (Cycles 3 and 4) missions, and has re-observed stars across multiple sectors. All of the stars discussed in this paper were observed by *TESS* for at least one sector. We devote the majority of this paper to discussing a subset of 52 stars that were first observed prior to February 2020 and then re-observed (albeit not continuously) between February 2020 and March 2024. For readability, we refer to *TESS* observations of our sample up to and including sector 21 as “initial” observations, data collected between sectors 22 and 76 inclusive as “recent” observations, and all available *TESS* observations of a target up to and including sector 76 as “full” observations.

2.1. Initial *TESS* Observations

² <https://github.com/jamiedietrich/dynamite>

In 2020, *TESS* had completed 21 sectors of observations, and had detected 1800 *TESS* Objects of Interest (TOIs). D20 investigated the architectures of the 52 *TESS* multiplanet systems that had been discovered at the time. In the Prime mission, targets selected for high cadence monitoring were initially observed at 2-minute cadence, and full-frame images (FFIs) were collected every 30 minutes. D20 used *TESS* data up to and including Sector 21 to calculate posterior period and radius probability distributions for an additional planet in each of the 52 multi-planet systems. The *TESS* data available varied substantially between targets; 16 stars were only observed for 1 sector, while 8 stars had 10 or more sectors of data. Most of the observations (for 33/52 targets) included small data gaps of 1 or 2 sectors, but 5 targets were observed at times 3 or more sectors apart.

2.2. Recent *TESS* Observations

We define the recent *TESS* observations as spanning sectors 22 to 76, which include the end of the Prime mission, the First Extended mission, and the start of the Second Extended mission. *TESS*'s First Extended mission covered sectors 27-55 (Cycles 3 and 4), and lasted approximately two years. For these sectors, an even shorter exposure time of 20 seconds was introduced alongside the 2-minute cadence, and the FFI exposure time was reduced to 10 minutes. In the Second Extended mission (Cycles 5-7, sectors 56-96), the FFI exposure time was further reduced to 200 seconds. As of August 1 2024, *TESS* is conducting observations of sector 81. When considering recent *TESS* observations of our sample, we include data collected between sectors 22 and 76. As in the initial *TESS* observations, the data coverage was heterogeneous; 5 targets were only observed for 1 sector out of 54, while 15 of the 52 targets were observed for more than 15 sectors between sectors 22 and 76 (inclusive). We use the full data set available (up to and including sector 76) for our analyses in Section 4.

3. SAMPLE

The goals of this paper are to assess the extent to which empirical models can be used to predict the presence of additional planets in multiplanet systems, and to analyze the architectures of these systems. Accordingly, our primary target sample is a set of systems that were first observed prior to 2020 and then re-observed by *TESS* in subsequent sectors. D20 analyzed the initial *TESS* photometry to make predictions about additional planets. Specifically, they considered the set of 52 *TESS* targets with multiple detected planets or planet candidates and made predictions about the periods and radii of possible additional planets in those systems. D20 in-

troduced and made use of the software package DYNAMITE, which returns posterior probability distributions for planet radius and orbital period under two empirical models: a clustered period model, and a period ratio model. The period ratio model (henceforth PRM) suggests that planet pairs in a multi-planet system have similar spacing in log-period space, as in [Mulders et al. \(2018\)](#). The clustered period model (henceforth PCM) suggests that planets in multi-planet systems are found in clusters centered on periods that are determined by a system's period distribution ([He et al. 2019](#)).

In this paper, we first use more recently obtained *TESS* photometry to assess the performance of the model predictions applied by D20. We discuss the sample of targets used in D20 in Section 3.1. Next, we broaden our analysis to the current sample of systems with multiple transiting planets or planet candidates observed by *TESS*. We discuss this larger sample in Section 3.2.

3.1. *TESS* Multi-Planet Systems Observed Prior to 2020 & Subsequently Re-Observed

D20 created their sample by selecting stars in the ExoFOP-*TESS* archive which hosted more than one TOI. They excluded four systems which hosted planets $> 5R_{\oplus}$, as the period distributions implemented in DYNAMITE are not representative of giant planets (e.g. [Dong & Zhu 2013](#)). Their sample included 39 systems hosting 2 TOIs, 11 systems hosting 3 TOIs, and 2 systems hosting 4 TOIs. They only included transiting planets and planet candidates as inputs to their models as DYNAMITE returns posterior distributions for planet radius. The posterior distributions returned by DYNAMITE under the clustered period model strictly peaked at shorter periods than those under the period ratio model ($P_{median,PCM} = 2.7$ days, $P_{median,PRM} = 20.3$ days).

3.1.1. Insights From Additional Observations

All of the 52 systems in the sample were re-observed for between 1 and 25 additional sectors and a median of 5 additional sectors of data in recent *TESS* observations. Figure 1 shows that both the number of sectors and the number of transits (assuming linear ephemerides) observed for each target has increased by at least a factor of 2 for the majority of the sample. The candidates with the largest increase in *TESS* data now have six times more sectors of data and 4.5 times more transits than in the initial *TESS* observations. With this extended baseline, we can not only search for longer-period transiting planets, but also improve our detection sensitivity for short-period transiting planets. Of the original sample, 24 systems have had additional planets found and re-

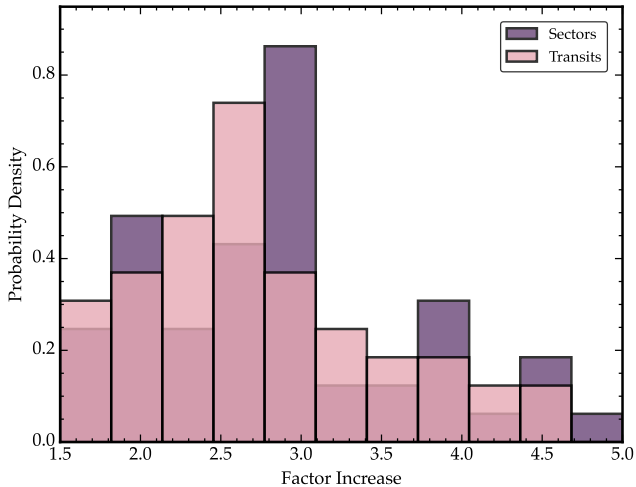


Figure 1. Histogram of the ratio of the total number of *TESS* sectors (up to and including Sector 76) to the number of sectors available in 2020 (prior to Sector 21, in purple) for each system in our sample. We also plot the histogram of the ratio of the number of transits in the currently available data to the number of transits in the pre-sector 21 *TESS* light curves (pink). We calculate this ratio as the mean of transit ratio for each planet candidate in a system. All 52 systems have substantially increased photometric baselines.

ported on ExoFOP³, for a total of 31 new confirmed or candidate planets. These newly discovered planets allow us to evaluate the accuracy of the predictions made in 2020.

The newly discovered (candidate) planets are both transiting and non-transiting, and are strikingly diverse; these planets range from the size of Venus to that of Neptune, and have orbital periods ranging from 1.91 d to over 4000 d. Furthermore, the newly discovered planets and planet candidates are interior, in-between, and exterior to previously known planets.

Since the publication of D20, follow-up observations have been conducted for many of the 52 systems considered in the paper. By analyzing these follow-up observations and the recent *TESS* data, three of the planet candidates in the D20 sample have been revealed to be False Alarms.

1. TOI-282, also known as HD 28109, was thought to host four transiting planet candidates in 2020. The planet candidate TOI-282.02 had an orbital period of 31 d, was included in the D20 analysis of this system. However, it has since been found to be a False Alarm. The two outermost planets in this system are near the 3:2 MMR and all three

confirmed planets exhibit transit timing variations (TTVs) of up to 60 minutes. These TTVs induced the signal initially labelled as TOI-282.02. We include the three confirmed transiting planets ((HD 28109 b: $22.9d$, $2.199^{+0.098}_{-0.10} R_{\oplus}$, $18.5^{+9.1}_{-7.6} M_{\oplus}$, HD 28109 c: $56.0d$, $4.23 \pm 0.11 R_{\oplus}$, $7.94^{+4.23}_{-3.05} M_{\oplus}$, and HD 28109 d: $84.3d$, $3.25 \pm 0.11 R_{\oplus}$, $5.69^{+2.74}_{-2.11} M_{\oplus}$, Dransfield et al. 2022) in all analyses in this work (Section 4.2 onwards).

2. TOI-1277 is a K dwarf that had two planet candidates at the time of publication of D20. TOI-1277.02, with a period of 14.9 days, is still classified as an active planet candidate. TOI-1277.01, on the other hand, only had 1 associated transit-like event, and has been retired as a False Alarm. Therefore, this system currently hosts only one planet or planet candidate, and we exclude it from further analysis (see Section 3.2).
3. TOI-1449 is a M dwarf which was previously thought to host two planet candidates. Similarly to TOI-1277, one of the planet candidates (TOI-1449.01) only had one transit-like event, and has been retired as a False Alarm. There is currently with one active planet candidate at 2.3 d, TOI-1449.02. We therefore exclude this system from the updated sample list (see Section 3.2).
4. TOI-1339, also known as HD 191939, is a high multiplicity system, and there is some discussion in the literature about the number of planets in the system (Lubin et al. 2022; Badenas-Agusti et al. 2020; Orell-Miquel et al. 2023). At the time of D20, the system was believed to host 3 planet candidates, with periods of ~ 8 , ~ 25 and ~ 28 d. As of 12 June 2024, the system hosts three confirmed planets with updated periods of 8.9 d, 28.6 d, and 38 d (HD 191939 b: 8.9 d, $3.41 \pm 0.08 R_{\oplus}$, $10.0 \pm 0.7 M_{\oplus}$, HD 191939 c: 28.6 d, $3.20 \pm 0.08 R_{\oplus}$, $8.0 \pm 1.0 M_{\oplus}$, HD 191939 d: 38.4 d, $3.00 \pm 0.07 R_{\oplus}$, $2.8 \pm 0.6 M_{\oplus}$, Badenas-Agusti et al. 2020). The inaccuracies of the earlier period measurements were likely due to the fact that the host star fell outside of the CCD’s science image area in sector 14 (Badenas-Agusti et al. 2020), which was not flagged in the initial *TESS* Quick-Look Pipeline planet search (Huang et al. 2020). The HD 191939 system also includes non-transiting planets. Lubin et al. (2022) reported 2 additional non-transiting planets in the system (HD 191939 e: 397 ± 16 d, $M \sin(i) = 112.2 \pm 1.0 M_{\oplus}$, HD 191939 f: 12.2 ± 3.9 yr, $M \sin(i) = 6.5 \pm 4.5 M_{Jup}$). Orell-Miquel et al. (2023) found a

³ ExoFOP, <https://exofop.ipac.caltech.edu/tess/>, accessed 11 July 2024

third non-transiting planet in the Habitable Zone of this system (HD 191939 g: $284_{-8}^{+10}d$, $M\sin(i) = 13.5 \pm 2.0M_{\oplus}$), for a total of six confirmed planets. We incorporate the six confirmed planets HD 191939 b-g in our analysis.

3.2. *TESS Multi-Planet Systems in 2024*

As well as increasing the baseline of the 52 systems in the original D20 sample, *TESS*'s continued observations have revealed additional multi-planet systems. As of 26 Feb 2024, there are 183 TOIs with at least 2 planet candidates (PCs), confirmed planets (CPs), ambiguous planet candidates (APCs), or known planets (KPs)³. We note that only 50 of the 52 TOIs analysed in D20 are included in the current sample, as two systems in the original sample currently have only one PC, APC, CP, or KP (TOI-1277 and TOI-1449).

4. METHODS

In this section, we describe the methods used to search the full *TESS* observations for the predicted additional planets in each system in our sample. We used both an empirical (see Section 4.2) and analytical (see Section 4.3) approach to quantify the detection sensitivity.

4.1. *Planet Search*

We developed a planet search pipeline in order to search for transits (injected or real) in the light curves of targets in our sample. Our pipeline considers a combination of light curves produced by the *TESS* Science Processing Operations Center (SPOC, Jenkins et al. 2016) and the *TESS-Gaia* Light Curve (TGLC, Han & Brandt 2023) pipelines. For each sector of observations, we selected the 120-second SPOC cadence light curve if available. If this data product was not available for a given sector, we used the light curve with the highest cadence (shortest exposure time), in order to maximise the signal-to-noise ratio of transit signals in the data. For some sectors, targets were only observed in the *TESS* Full-Frame Images (FFIs). If only FFI-derived light curves are available, we selected the TGLC data products, which make use of the *Gaia* DR3 data as position priors for individual targets (Han & Brandt 2023).

We first flattened the light curves using the *wotan* Python package (Hippke et al. 2019). This procedure uses a B-spline Huber regression to fit variability, with the number of knots set by the window function. We set the window function to 0.5 days, in order to capture the typical time scales of photometric variability in the light curves in our sample. However, this approach limited our sensitivity to detecting transits with durations on the order of 0.4 days or longer, as these features

were often flattened out during this step. However, for the bulk of stars in our sample, transit durations of 0.4 days correspond to orbital periods $\gtrsim 10x$ larger than those of the predicted additional planets. We removed outliers that lie more than 5 standard deviations above the median flux. We did not remove outliers below the median flux in order to avoid removing data points in transits. We then used a Box-Least Squares (BLS) periodogram (Kovács et al. 2002) to search for periodic transit-like features in the light curves. We used a period grid between 0.5 and 730 days (as in D20) and a duration grid with 50 values between 0.02 and 0.4 days (0.5 - 9.6 hours) when calculating the BLS periodogram. We optimized the period grid spacing in order to limit the periodogram's size to 10,000 points for computational tractability. We searched each light curve 7 times, masking transits (or transit-like events) associated with the strongest peak in the BLS periodogram after each iteration.

For each candidate period found by these searches, we phase-folded the light curve using the period and epoch associated with the strongest peak in the BLS periodogram in each iteration of the search. We then calculated the mean number of data points between phases of -0.05 and 0.05 of the phase-folded light curve. We discarded search results where this number was more than twice that outside the phase range surrounding the transit. This indicated that the periodic signal identified by this iteration of BLS was a periodic data gap or ramp feature sometimes seen near the start of *TESS* sectors, and was not a transit.

We observed substantial quasi-periodic, heteroskedastic structure at long periods in the BLS periodograms of several light curves, which we attribute to several-month data gaps between *TESS* observations of a target. For example, TOI-125 (TIC 522368076) has three sectors of *TESS* data, but the system was observed for 1 sector at a time with 2 year gaps between sectors (see Figure 2). Nine of the 183 systems had predicted additional planets beyond 100 d. In these cases, the peak in BLS periodograms at the predicted period was frequently lost in the long-period structure, which reduced the recovery fraction for these signals. For the 95% of systems with predicted additional planets within 100 d, the BLS peaks associated with the predicted period were often swamped by this long-period structure. As a result, signals corresponding to the additional predicted planet were not recovered even if the associated BLS peaks were locally maximal.

The long-period structure observed in the BLS periodograms is likely due to the pattern of *TESS* pointings across cycles. The spacecraft has mostly alternated an-

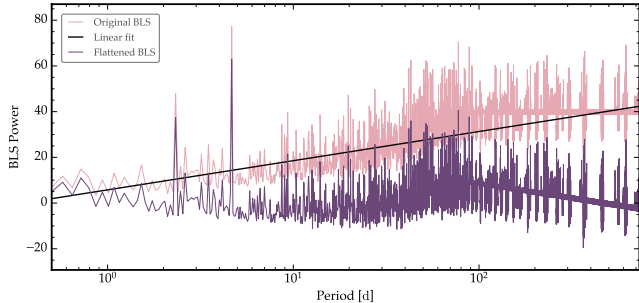


Figure 2. Box-Least Squares periodogram (BLS, pink) of the light curve of TOI-125 (observed in cycles 1, 3 and 5, with gaps of ~ 2 years between each data segment). Quasi-periodic, heteroskedastic structure is present at periods beyond ~ 50 days. We fit a weighted linear function (black) to the original periodogram (pink) and return a flattened BLS periodogram (purple). Thereby, we remove the general upwards trend with increasing orbital period and thus minimize the impact of the long-period structure on the recovery of injected planets.

nually between observing the Northern and Southern hemispheres, with some sectors observing the ecliptic. Previous works have used a variety of models to remove long-term trends from BLS periodograms. These include subtracting the median-filtered periodogram (Ofr 2014), and quadratic smoothing using 20 equally-spaced spline knots (Gondhalekar et al. 2023). In order to mitigate the impact of these features, we fit and subtracted a weighted linear function to the BLS periodogram. The function weighted periodogram values at periods > 100 d 100 times more strongly than those at shorter periods. This method suppressed the strong, unphysical structure at longer periods in the periodogram, and thus increased the detection sensitivity for planets at all orbital periods.

We also discarded signals which were found multiple times by our algorithm. In each iteration of the planet search, we mask potential ‘transit events’ using the period and epoch associated with the highest power peak in the periodogram. As such, if a candidate period is returned several times, it is likely attributable to the periodic data gaps created by transit masks in previous iterations. Therefore, if a candidate period is returned more than two times by the BLS search, we restrict the period space being searched to be shorter than this period for the remainder of the BLS searches.

4.2. Transit Injection & Recovery

In order to quantify our detection sensitivity to the predicted additional planets, we performed transit injection and recovery tests. For each target, we injected a `batman` (Kreidberg 2015) transit model into the light curve, after masking the transit events associated with

known TOIs in each system. We set the injected planet period and radius using the peak of the D20 posterior probability distributions. We drew a transit epoch for the injected planet from a uniform distribution spanning the target’s observational baseline, and an impact parameter from a uniform distribution between 0 and 1. We then flattened the light curve and performed an uninformed search for periodic transit-like features as described in Section 4.1. Additionally, we considered the 10 strongest peaks in the BLS periodogram in each of the 7 iterations of the planet search, in order to further mitigate the impact of strong non-physical peaks at long periods due to the window function of observations. For each of the 10 strongest peaks in the periodogram, we checked whether the associated period was consistent with the injected period, and whether there was data at phase of 0 when the light curve was folded at this orbital period and associated transit midpoint.

We consider an injected signal recovered if it has a reported period within 10% of the injected period (or an integer multiple up to 4 of the injected period). We consider the transit epoch recovered if it falls within 0.1 phase of the injected transit midpoint. We also consider the radius of the planet recovered if it is consistent with the predicted radius to 1σ using the errors associated with the predicted radius distribution. We only consider a planet recovered if both the period and transit midpoint are recovered, and if the Signal Detection Efficiency is greater than 7.3 (as is required for detection by the *TESS* SPOC pipeline). We perform 100 injection/recovery tests on each target in the sample, and show the fraction of injected planets recovered Figure 5.3.

4.3. Analytical Detection Sensitivity

We also used analytical calculations to evaluate the detectability of each predicted planet. For each target, we generated a grid of planet radius (R_p) vs. orbital period (P) in the following ranges: $0.5-5 R_\oplus$, $0.5-730$ d. These ranges are consistent with the parameter space explored by D20. For each (P , R_p) combination, we calculated the signal-to-noise ratio associated with such a transit,

$$SNR = \frac{(R_p/R_*)^2}{CDPP_{\text{eff}}} \sqrt{\frac{t_{\text{obs}} f_0}{P}} \quad (1)$$

where R_* is stellar radius, $CDPP_{\text{eff}}$ is the effective Combined Differential Photometric Precision, t_{obs} is the time span of the *TESS* observations of a target, and f_0 is the duty cycle of the light curve (i.e. the fraction of the baseline during which the target was observed). In order to calculate $CDPP_{\text{eff}}$, we used the `lightkurve.estimate_cdpp` function, which calculates

a quasi-CDPP for a given transit duration and light curve (Aigrain et al. 2015). We note that $CDPP_{\text{eff}}$ depends on the cadence of the light curve, with longer exposure times (i.e., lower cadence) associated with higher $CDPP_{\text{eff}}$ and thus lower SNR for a given set of planet parameters. For light curves made up of sectors with different cadences, we calculate $CDPP_{\text{eff}}$ for a putative planet signal for each cadence, using only the sectors with that cadence. We then compute the median $CDPP_{\text{eff}}$ across all cadences, and use this value to calculate the SNR.

We calculated transit durations using the planet parameters associated with the peak of the posterior probability distributions returned by DYNAMITE. We drew eccentricity samples from a truncated Rayleigh distribution with a mode of 0.0355 (as per Mills et al. 2019), and drew inclinations from a uniform distribution of $\cos(i)$ ranging from 0 to $\cos(i_{\text{min,transit}})$, where $i_{\text{min,transit}}$ is the minimum inclination possible for a putative planet to still transit the host star. We find that all of the putative additional planets in both models would have calculated $\text{SNR} > 7.3$, and thus would pass the detection threshold of the TESS mission. This is contrary to the recovery fractions found in Section 4.2; the 86th percentile of the recovery fraction across our sample is 56% for the PRM and 44% for the PCM. This discrepancy highlights the impact of drawing transit midpoints and impact parameters for the injected planets, which can lead to fewer and shallower transits, respectively. Furthermore, in some cases, the injected flux will not contain any transits due to the placement of injected transits in data gaps. The injection-recovery method also includes a more nuanced treatment of noise. The quasi-CDPP used in the analytical SNR calculations is an approximation of the scatter in a light curve after removing long-term trends; performing injection-recovery tests allowed us to sample the true noise distribution in each light curve.

5. RESULTS

5.1. DYNAMITE predictions for 2020 sample

We set out to determine which model used in D20 to predict additional planets was most accurate, using extended *TESS* observations, injection-recovery tests, and the results of radial velocity studies of these systems. Additional observations of a given system can verify model predictions in several ways: 1) reveal an additional planet with an orbital period corresponding to the peak of the posterior probability distribution, and 2) reveal an additional planet with an orbital period with some other, non-zero posterior probability. We evaluated model performance for case 1 by computing the

overlap between the normalized posteriors and probability distributions of new TOIs. The ideal scenario for case 1 involves a new planet with a tightly constrained period lying at the peak of the DYNAMITE posterior period distribution. However, a caveat of the overlap method is that it also favours newly discovered planets with poorly constrained (and thus, wide) orbital periods. For case 2, we measured the difference in period between new TOIs and the peaks in the posterior distributions to evaluate model performance. A representative example is shown in Figure 6.2.

Of the 52 systems analyzed, 24 of them have been found to have additional planets, for a total of 31 new planets and planet candidates in these systems. We find that 8 of the additional planets in the systems have orbital periods that are consistent to 1σ with the peak period posterior returned by the PRM, and 4 are consistent with the predictions from the PCM to 1σ . Accordingly, the overlap between the PRM posteriors and the period distributions of the new planets is ~ 1.5 times that for the PCM posteriors. We note that these results are not mutually exclusive, as the PRM and PCM can predict a similar period range where an additional planet is then found. This is the case for two of the systems (TOI-174 and TOI-178). Of the additional transiting planets found, 15 of them are consistent with the radius predictions to 1σ (which are agnostic to the period model), and 9 of these 15 planets also match at least one of the peaks of the period posteriors.

5.2. Updated DYNAMITE predictions for 2020 sample

Since D20, DYNAMITE has been expanded with more planet parameter models and a more robust dynamical stability criterion (Dietrich et al. 2022). In particular, multiplicity-dependent log-normal distributions for the eccentricity and the mutual inclination were taken from He et al. (2020). These distributions empirically matched the observed Kepler population, and were added to DYNAMITE to compare with the previous Rayleigh distribution for mutual inclination from Mulders et al. (2018). We ran the newest version of DYNAMITE on the dataset from 2020; the new results more accurately predicted the newly discovered planets in the 52 systems in our sample. One exception was in the TOI-797 system, where both the PRM and PCM models in the original version of DYNAMITE accurately predicted an additional planet found at 2.7 d. However, the updated version of DYNAMITE returned a reduced likelihood of an additional planet at 2.7 d, likely due to the additional dynamical stability constraints implemented in Dietrich et al. (2022).

We found that 13 of the newly discovered planets in the systems matched the PRM period predictions, compared with 8 planets matching the previous version of DYNAMITE. Three of these 13 matching planets were found iteratively after adding one planet with period and radius set to the peaks of the posteriors and running DYNAMITE again. 11 of the new planets matched the predictions from the PCM (relative to 4 matches found previously), the same 3 of which were found iteratively. The PRM and PCM predictions were more consistent for these systems using this version of DYNAMITE than the previous version, with 8 of the planets found by both orbital period models and 16 of them found by at least one model. Of the 25 additional planets that were found to transit, 17 of them matched the radius predictions. Including the eccentricity distribution and an updated orbital inclination distribution improved the efficacy of the new dynamical stability criterion used to determine the likelihood of additional planets in close pairs with known planets, as dynamical stability and dynamical packing is significantly affected by planet orbital eccentricity (e.g., [Obertas et al. 2023](#)). These changes particularly improved the performance of PCM, as the period clustering model tends to pack planets as close together as is dynamically possible. This was reflected in the calculated overlap between the updated PCM and PRM posteriors and the newly discovered planets. We found that the overlap between the updated PCM posteriors and the newly discovered planets was 1.1 times that for the updated PRM posteriors and newly discovered planets; the two models performed similar when including a nuanced eccentricity and inclination treatment.

5.3. Updated DYNAMITE predictions for 2024 sample

We also considered the current sample of 183 multi-planet systems observed by *TESS*, as defined in Section 3.2. We run the most recent version of DYNAMITE² on this sample, and present our results in Figure 5.3 and Tables 1 and 2. Of this sample, 136 targets (66%) have been re-observed since sector 76 or will be re-observed during the planned *TESS* Cycle 7 observations. These stars will receive between 1 and 11 (with a median of 4) additional sectors of data. We find that $\sim 80\%$ of predicted additional planets have recovery fractions $< 50\%$ with the full *TESS* data, suggesting that these additional planets may be challenging to detect in the current *TESS* data set. *TESS* observations beyond sector 76 will increase the number of sectors by a median factor of 1.25, and provide a similar boost in the number of observable transits of predicted planets. These additional *TESS* observations will improve our sensitivity to detecting the predicted additional planets in each sys-

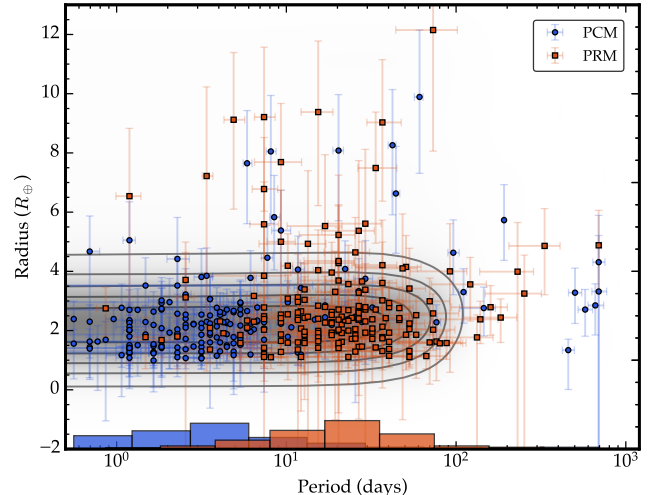


Figure 3. Predicted planet orbital period and radius peaks of the 2023 DYNAMITE posterior distributions (PCM: blue circles, PRM: orange squares) for the current sample of 183 *TESS* multi-planet systems. A Gaussian kernel density estimate of the period and radius distributions of the known planets and planet candidates in these systems is shown in grey, with contour lines added in black. The distribution of the orbital periods of the predicted additional planet in each system under the two models are shown as histograms at the bottom of the plot. The period ratio model predicts additional planets at longer orbital periods than the clustered period model.

tem. Figures 3 and 5.3 show the peaks of the most up-to-date DYNAMITE posteriors for the 183 *TESS* multi-planet systems, as well as the recovery fractions for these predicted planets.

6. DISCUSSION

6.1. How accurately did the PRM and PCM predict additional planets?

We found that of the 25 transiting planets discovered since 2020 in our sample, 8 have non-negligible period overlaps with either of the original PCM and PRM posteriors reported in D20. Furthermore, 13 of the newly discovered planets match the PCM and/or PRM predictions using the latest version of DYNAMITE ([Dietrich et al. 2022](#)). Using the original version of DYNAMITE, which assumed circular orbits, the posteriors under the period ratio model are more consistent with the newly discovered planets and planet candidates. Using the updated DYNAMITE PRM and PCM posteriors, which include eccentricity and inclination, we find that the models performed comparably well. In cases where multiple additional planets have been discovered in a system, we calculated each overlap separately, as each newly detected planet is an independent check of the models' performances. This result is modulated by

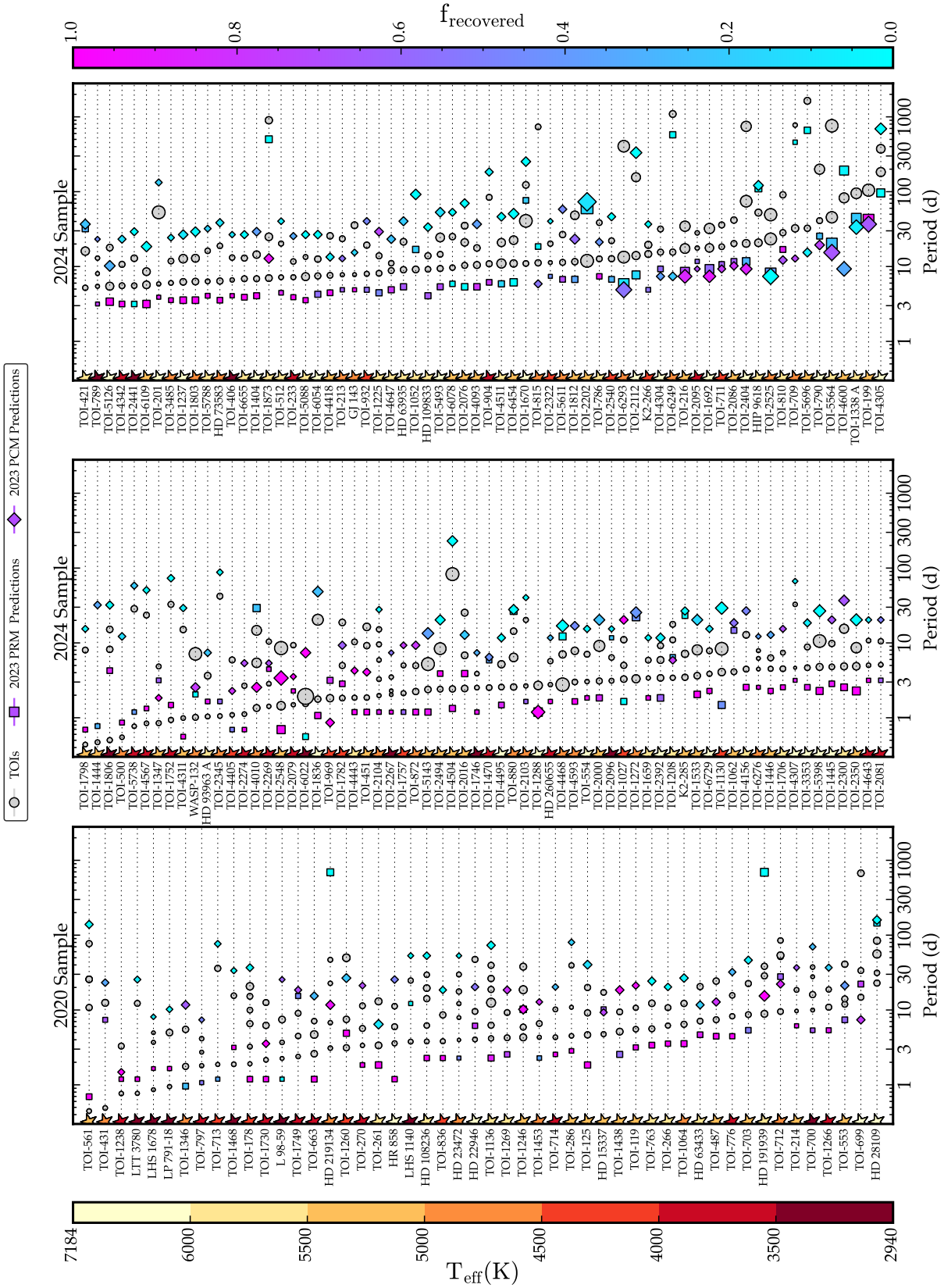


Figure 4. *TESS* systems with multiple planets and/or confirmed planets (grey circles), with the peak of the DYNAMITE orbital period posterior distributions based on the current sample of *TESS* multi-planet systems under the period ratio model (PRM, diamonds) and clustered period model (PCM, squares) shaded according to their recovery fraction. The PCM predictions lie at systematically shorter periods, and have higher recovery fractions than the PRM predictions.

the fact that the planets predicted under the period ratio model were typically at longer orbital periods ($P_{median,PCM} = 3.55$ days, $P_{median,PRM} = 20.3$ days, see Figure 5.3) and thus both less detectable in a given light curve and less likely to transit. We also found that the periods of the newly discovered planets are closer to the primary peak in the PRM period posteriors than the primary peak in the PCM posteriors (see Figure 6.2).

However, the improvement in model performance between PRM and PCM is not statistically significant; both models have limited predictive power. The predictions from both models are more accurate when the newer version of DYNAMITE is used, but only a minority of systems are accurately described by PRM or PCM using either version of DYNAMITE. This results showcases the limitations in these empirical models; they are not representative of all observed multi-planet systems.

6.2. How does the *TESS* observing strategy impact detectability?

Our sensitivity to detected additional transiting planets in multi-planet systems was greatly impacted by the observing pattern of the *TESS* mission. During its prime mission, *TESS* observed first the southern and then the northern ecliptic hemispheres, repeating this pattern in the First Extended mission (which also included some pointings along the ecliptic plane). In its Second Extended mission, which began in September 2022, *TESS* has generally observed the southern ecliptic hemisphere. This observing strategy has led to many targets being observed for a few sectors every other year; the median duty cycle of our targets is only 13%, and each light curve has two gaps (corresponding to cycles observing the other hemisphere) which are at least 14 (and up to 40) sectors long. These large gaps substantially inhibit our sensitivity to detecting additional planets. Even TOIs with orbital periods as short as half a sector length (roughly 13 days) may be observed in transit only once per sector due to the timing of transits relative to data gaps. These transit events lead to poorly constrained orbital periods, and require intensive photometric follow-up to characterize (e.g. [Tuson et al. 2023](#); [Ulmer-Moll et al. 2022](#)). Additionally, transiting planets with periods longer than a sector length (~ 30 days) will not transit multiple times each time *TESS* is observing the system, resulting in mono- and duo-transits across the full light curve. The planet detection pipeline used in this work searches for periodic transit-like signals; it is not sensitive to mono-transits.

6.3. How do *TESS* multi-planet systems compare to the confirmed planet population?

The models used to predict additional planets in these *TESS* multi-planet systems are based on the observed *Kepler* sample of multi-planet systems. As such, it is important to compare the two stellar samples. We used the one-sided Kolmogorov-Smirnov test ([Smirnov 1939](#)) to evaluate the likelihood of our sample stellar properties being drawn from the Gaia-*Kepler* Stellar Properties Catalog (GKSPC, [Berger et al. 2020](#)), the sample of confirmed planet and planet candidate *Kepler* Objects of Interest (KOIs⁴), and the sample of *Kepler* multi-planet systems⁴. The GKSPC homogeneously derived stellar properties for 186,301 *Kepler* stars, using isochrones, broadband photometry, *Gaia* DR2 parallaxes, and spectroscopic metallicities. When considering stellar mass, radius, effective temperature, surface gravity, and metallicity ([Fe/H]), we found that we can reject the null hypothesis (that our stars were drawn from the GKSPC distribution) in all cases with p-value $< 10^{-10}$. We can also reject the null hypotheses when comparing the *TESS* multi-planet system stellar sample with the KOI and multi-planet KOI samples with p-values $< 10^{-13}$. However, when comparing the the KOI samples with the full GKSPC, the null hypothesis is also rejected with p-value $< 10^{-19}$. This highlights the impact of detection biases; planets orbiting bright, hot stars are most easily detected and followed up. Nevertheless, we find that the stellar properties in our sample are not representative of the wider *Kepler* sample used to develop the predictive models. This result highlights the importance of acknowledging the influence of stellar properties on trends in exoplanetary systems (e.g. [Berger et al. 2020](#); [Fulton & Petigura 2018](#); [Fischer & Valenti 2005](#)).

We also compared the period distribution of our sample of planets (including additional predicted planets) to the period distribution of the confirmed planet population⁵ in Figure 6. All of the distributions included the known excess of planet pairs wide of resonance ([Lithwick et al. 2012](#)). However, compared to the distribution for confirmed planets, the period ratio distribution under the period ratio model over-predicted the frequency of pairs wide of resonance, and under-predicted pairs interior to first-order mean-motion resonances. These discrepancies imply that the evolution of observed planets under this model would either involve enhanced near-resonant pair formation (e.g. [Choksi & Chiang 2020](#)), or

⁴ ExoFOP-KOIs, https://exofop.ipac.caltech.edu/tess/view_koi.php, accessed 30/04/2024

⁵ NASA Exoplanet Archive, accessed 30/04/2024

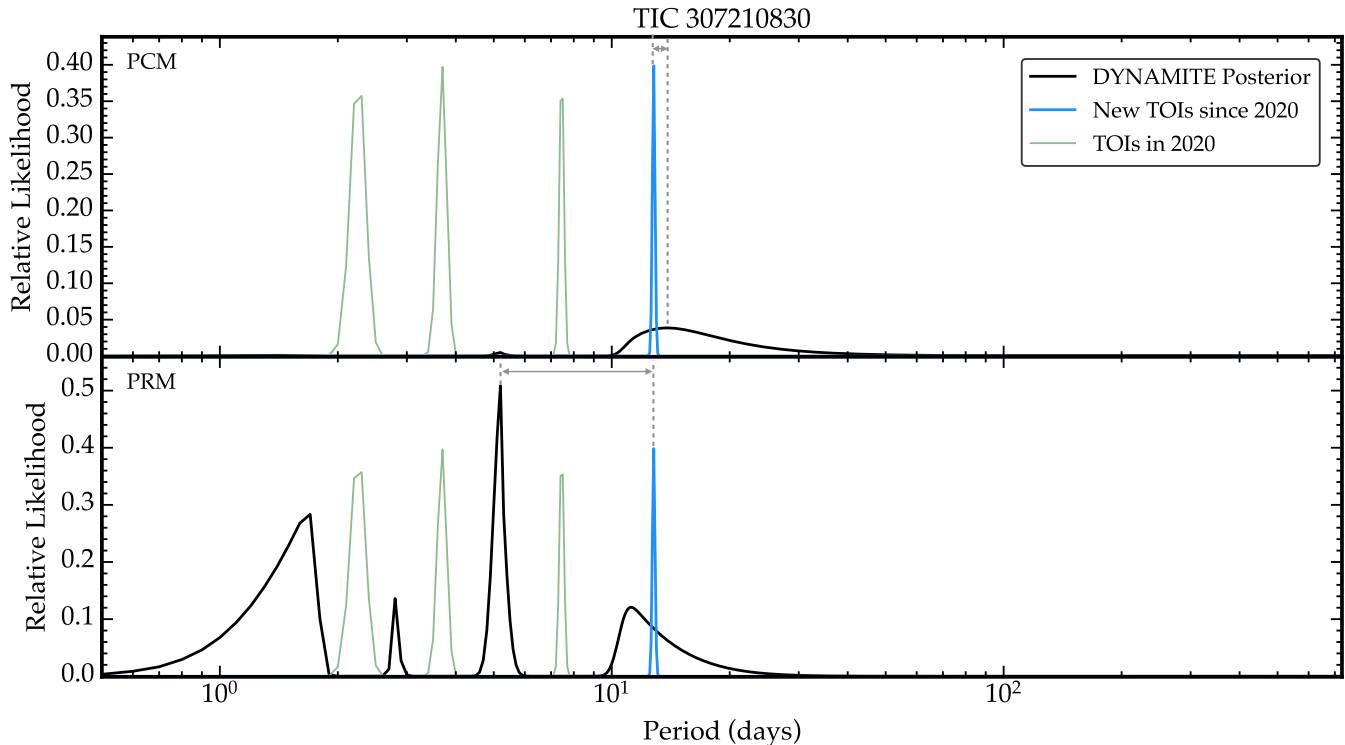


Figure 5. DYNAMITE posterior period probability distributions (black, Dietrich et al. 2022) for the clustered (PCM, top) and period ratio (PRM, bottom) models for TOI-175 (TIC 307210830, L 98-59). The relative likelihoods are multiplied by a factor of 10 for improved visual clarity. The orbital period distributions (assuming Gaussian errors) of TOIs known in 2020 are shown in light green, and those that have since been discovered are shown in blue. In 2020, three confirmed planets were known in this system (Kostov et al. 2019). An additional, non-transiting planet (L 98-59 e) with an orbital period of 12.796 ± 0.020 d was found by Demangeon et al. (2021). The overlap between the newly discovered planet’s period and the PRM posterior is 1.5 times larger than that with the PCM posterior. However, in this case, the period of L 98-59 e is closer to that of the highest peak in the PCM posterior; the highest probability period for a new planet under the PRM was at ~ 5 d. This nearness is illustrated using grey arrows and dashed lines.

reduced disruption of resonant pairs (e.g. Izidoro et al. 2021).

6.4. What is the discovery space for additional planets?

All of the *TESS* multi-planet systems will be re-observed by *TESS*, as well as other ground-based facilities collecting both photometry and spectroscopy. We can make use of the posterior probability distributions returned by DYNAMITE and the sensitivity distributions calculated in this work to evaluate regions of parameter space where additional planets are both most likely to exist and be detected by *TESS*. In order to do so, we generated grids of detectability in period-radius space, parameterized by the SNR of the transits of a putative planet with a given (R_p, P) in the light curve of a given star using Equation 1. We also computed a mesh of the radius and period posteriors returned by DYNAMITE using the dot product. We then down-sampled the posterior grid in order to match the sampling of the SNR grid, and convolved the posterior and detectability grids

together. We include a representative example in Figure 7, and make the rest of the plots publicly available on Zenodo⁶. The detectability grid modulates the DYNAMITE posteriors, demonstrating that additional planets at shorter periods and with larger radii will be most detectable in additional *TESS* observations. These results may be of use in planning follow-up observations of these systems to maximise the return of limited telescope resources. For example, TOI-1339 (HD 191939) is a bright star (*V* magnitude ~ 9) that hosts at least 3 transiting and 3 non-transiting planets. The updated DYNAMITE posterior distributions peak at > 50 ; this region of parameter space not yet been searched well.

6.5. Are these systems dynamically packed?

The current sample of 183 *TESS* multi-planet systems host a total of 453 planets and candidate planets. We

⁶ <https://zenodo.org/>

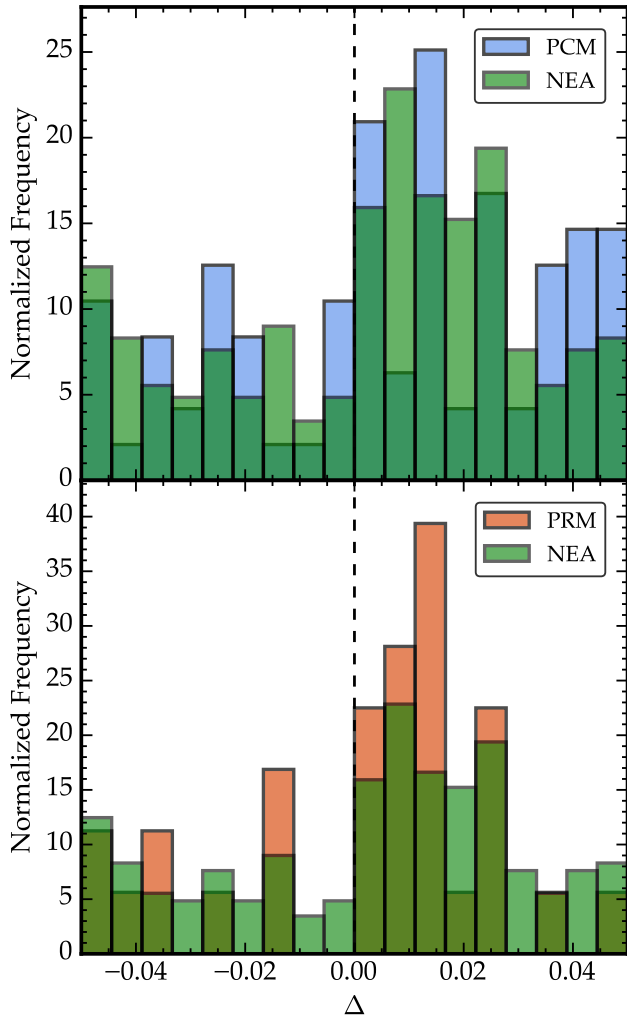


Figure 6. Histograms showing the normalized frequency of adjacent planet pairs’ nearness to resonance, as parameterized by Δ (Lithwick et al. 2012). The predictions for additional planets in the 52 TESS multi-planet systems are included for the period ratio model (blue, upper panel) and the clustered period model (orange, lower panel). The sample of confirmed multi-planet systems in the NASA Exoplanet Archive¹ are shown for reference (green, both panels). The clustered period model more accurately matches the confirmed planet sample, while the period ratio model predicts an excess of planet pairs wide of resonance.

evaluated the degree to which the systems in this sample are dynamically packed. The Packed Planetary System hypothesis suggests that planet formation is highly efficient, and that as a result, each system will have as many planets as dynamically feasible (Barnes & Raymond 2004). Previous works have shown that the multi-planet systems discovered by *Kepler* are mostly dynamically packed (Fang & Margot 2013; Pu & Wu 2015; He et al. 2019; Tió Humphrey & Quintana 2020).

For each system, we estimated the mass of the predicted additional planets using *spright* (Parviainen et al. 2024). We also used *spright* to predict the masses for the 70 planets/planet candidates with radii less than $5R_{\oplus}$ and without measured masses. This package uses the planet radius to infer a mass distribution using mass-radius relationship inferred from either the sample of small transiting confirmed planets orbiting M dwarfs (STPM, Luque & Pallé 2022) or orbiting FGK stars (TEPCat⁷, Southworth 2011). For the 38 planets or planet candidates without measured masses and with radii greater than $5R_{\oplus}$, we used *Forecaster*. This package implements the probabilistic mass-radius relationship presented in Chen & Kipping (2017), which was conditioned using a sample that included both dwarf planets and late-type stars. We then used these predicted masses to determine whether the planet pairs including the additional predicted planet were allowable after imposing a minimum dynamical spacing of Δ_{crit} between two adjacent planets, following the heuristic methodology of Tió Humphrey & Quintana (2020). In D20, this was done assuming $\Delta_{crit} = 8$, and all added planets were required to not destabilise the system. We used Δ_{crit} values of 10 (circular orbits, Pu & Wu 2015), 12.3 (eccentric orbits, Pu & Wu 2015), and 21.7 (Fang & Margot 2013). As expected, with more conservative values of Δ_{crit} , some of the predicted additional planets would destabilise the system. Under these stricter stability criteria, the additional predicted planets would need to be less massive than predicted using *spright* in order to remain dynamically stable over the systems’ lifetimes. This less massive sub-population of planets would be more challenging to detect and characterize using radial velocity observations they do not transit.

When considering the sub-sample of *TESS* multi-planet systems hosting confirmed planets with $P < 200$ d and $1.5 - 30 R_{\oplus}$ and assuming $\Delta_{crit} = 21.7$ (as in Fang & Margot 2013), we find that the observed packing fraction of the observed planets is high. Namely, 96%, 67%, and 100% of 2-, 3-, and >3-planet systems ($N_{2pl} = 27$, $N_{3pl} = 12$, $N_{>3pl} = 5$) are packed. Furthermore, 89% of all systems in this sample are packed. These results are consistent with those reported in Fang & Margot (2013), who found that > 31%, > 35% and > 45% of 2-, 3-, 4-planet *Kepler* systems are dynamically packed on \sim Gyr timescales. Additional work by Tió Humphrey & Quintana (2020) found that > 19% of planet pairs in 691 *Kepler* multi-planet-candidate systems were packed assuming $\Delta_{crit} = 12.3$. More recent

⁷ TEPCat, <https://www.astro.keele.ac.uk/jkt/tepcat/>

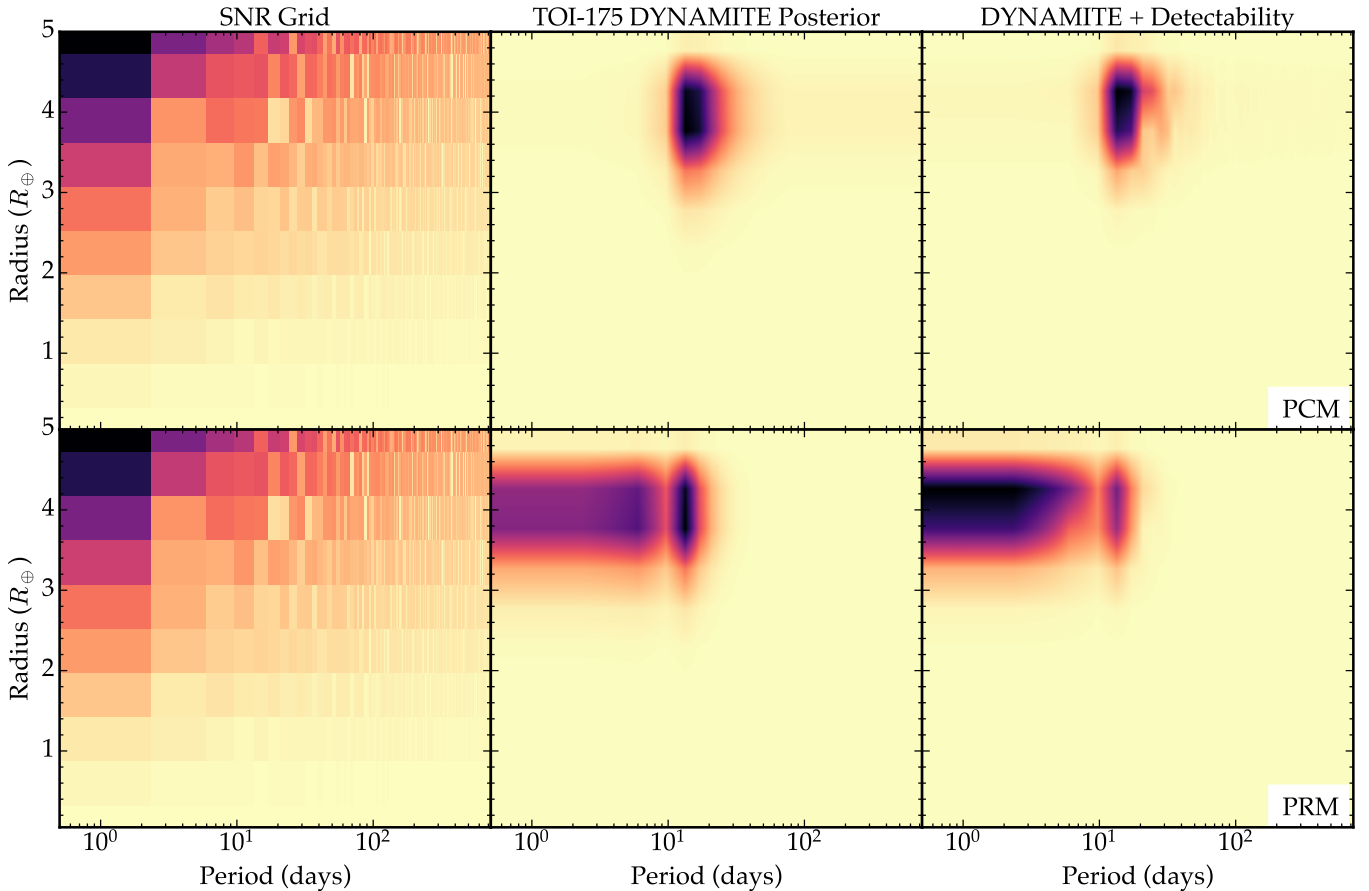


Figure 7. *Left:* Signal-to-Noise Ratio (SNR) of simulated transits in the *TESS* light curve of TOI-175. *Middle:* Mesh of radius and period posteriors generated by DYNAMITE for TOI-1751. *Right:* Detectability modulated by the DYNAMITE posterior for TOI-1751, showing the location in (P, R_p) space where an additional planet in this system is most likely to be detected under the period ratio model

work by Obertas et al. (2023) found that by not requiring circular orbits and strictly central placing of additional planets between known planets, an even larger fraction (60 – 90%) of *Kepler* multi-planet systems are strongly packed. The packing fraction that we found for this sub-sample of confirmed *TESS* planets is also very high, possibly implying a highly efficient formation history.

6.6. Are these systems truncated?

We also studied the observed outer edges of these multi-planet systems. Millholland et al. (2022) found that $\sim 35\%$ of *Kepler* multi-planet systems are truncated. This truncation refers to the lack of detected transiting planets with orbital periods $\sim 100 - 300$ days, even when accounting for the reduced transit probability at longer orbital periods. This result implies that the outer regions of these multi-planet systems either have a dearth of planets, or contain only small, and specifically un-detectable, planets. A decrease in the typical planet radius with increasing orbital period may reveal a break-

down of the peas-in-a-pod architecture that is observed in the inner regions of some multi-planet systems (Weiss et al. 2018; Millholland et al. 2017).

There are several possible mechanisms that could drive this breakdown. Firstly, small planets may be more susceptible to migration traps, preventing them from migrating inwards, unlike larger planets formed in the system. Secondly, Adams et al. (2020) find that for systems with $\gtrsim 40M_{\oplus}$ in total planetary mass, mass uniformity is no longer the most energetically favourable architecture at semi-major axes of $\sim 0.5 - 1AU$. Indeed, including planets’ self-gravity alongside the conservation of angular momentum and total mass suggest that planets preferentially exhibit runaway growth when the total mass in the system exceeds some critical mass ($\sim 40M_{\oplus}$). Runaway growth would cause to high mass partitioning between planets, which could lead to small, un-detectable planets between ~ 100 and 300 days. Thirdly, giant outer planets with orbital periods > 300 days may destabilize planets in this period range (e.g. Denham et al. 2019), leading to a dearth

of planets in these intermediate regions of multi-planet systems. We sought to investigate whether the *TESS* multi-planet systems also exhibit signs of truncation.

We performed a heuristic investigation into the outer edges of the 35 TOIs with 3 or more planets or planet candidates, following the methodology of Millholland et al. (2022). Firstly, we defined a putative external transiting planet in each system, based on the period spacing and radius uniformity seen in peas-in-a-pod architectures. A caveat of this approach is that, as demonstrated in Section 5, we find that this model of multi-planet systems is not fully descriptive of the observed population. We assigned a radius to the putative planet equal to the radius of the outermost transiting planet, and a period set by the linear spacing of the two outermost transiting planets in the system. We then calculated the minimum radius of a putative transiting planet with this orbital period that would be detectable to $> 7.3\sigma$ in each system using the full *TESS* data set, using Equation 1.

We then compare the calculated minimum detectable radius with the radius of the putative outer planet. We find that for all but two of the 35 systems in the sample, the ratio of the hypothetical radius and the minimum detectable radius is greater than one. This result implies that the putative transiting outer planets should be detectable in the current *TESS* light curve of the system (see Figure 8).

However, there are no detected transiting planets or planet candidates at the periods of the putative outer planets. This indicates that planets at these orbital periods, if they do exist, are either too small to detect using current *TESS* data, or inclined such that they do not transit. We used a combination of literature inclinations for confirmed planets and measured inclinations (using TATER, Mayo et al., in prep) for planet candidates to calculate the mutual inclination of each system. We found that the mutual inclinations of all but one (TOI-2104) of these systems are $\lesssim 3^\circ$. This result is consistent with the distribution of mutual inclinations in the *Kepler* multi-planet systems (Lissauer et al. 2011; Fabrycky et al. 2014), which is well-described by a Rayleigh distribution with scale parameter $\sigma_i \sim 1 - 2^\circ$. Additionally, with the exception of Mercury, the orbits of the Solar System planets lie within a few degrees of the ecliptic plane⁸. Mutual inclination is a probe of the dynamical temperature of a system; nearly co-planar systems are “cooler” than those where planet eccentricities and

inclinations have been excited by e.g. the Kozai-Lidov mechanism (e.g. Kozai 1962; Lidov 1962; Fabrycky & Tremaine 2007) or tidally-driven migration (e.g. Jackson et al. 2008; Wu et al. 2024). For 11 of the 36 high-multiplicity *TESS* systems, the minimum transiting inclination of the putative outer planet implies that if an additional, evenly-spaced outer planet were to exist and not transit, these systems would be dynamically hotter than currently understood.

The *TESS* multi-planet systems appear to be truncated relative to detection sensitivity limits when considering transiting planets, similarly to the *Kepler* systems. However, we cannot test the hypothesis of the dearth of planets in the 100-300 d orbital period range described in Millholland et al. (2022) due to the heterogeneous and shorter photometric baselines of *TESS* systems compared to the *Kepler* sample.

7. CONCLUSIONS

We used an additional 4 years (54 sectors) of *TESS* observations to search for predicted additional planets in each of 52 multi-planet systems, under two predictive models based on results from the *Kepler* mission. We found that a period ratio model more accurately predicted additional planets in these multi-planet systems. However, neither the period ratio model (Mulders et al. 2018) nor a clustered period model (He et al. 2019) accurately predicted all of the additional planets found in these multi-planet systems. This result highlights the need for additional data to continue to improve models of multi-planet systems, as well as the need for prescriptions for eccentricity and inclination, as in Dietrich et al. (2022).

We use an updated set of predictive models from DYNAMITE, (Dietrich et al. 2022) to iteratively predict additional planets in the 183 current *TESS* systems with multiple planets or planet candidates. We modulate these posterior probabilities with these putative planets’ detectability and provide the most detectable planet location in orbital period and radius space. The majority of these systems will be re-observed by *TESS* in Cycle 7, and the remainder will likely be re-observed in the third extended mission. These additional observations will enable further testing and refinement of the models discussed here, and continue to expand our understanding of these multi-planet systems.

We also found that the high-multiplicity ($N_{pl} \geq 3$) transiting systems observed by *TESS* appear to be truncated and highly dynamically packed. While the nature of the *TESS* mission makes homogeneous analyses analogous to those done with *Kepler* data challenging, continued and sustained follow-up efforts of these rich

⁸ NASA Solar System Fact Sheet, <https://nssdc.gsfc.nasa.gov/planetary/factsheet/>

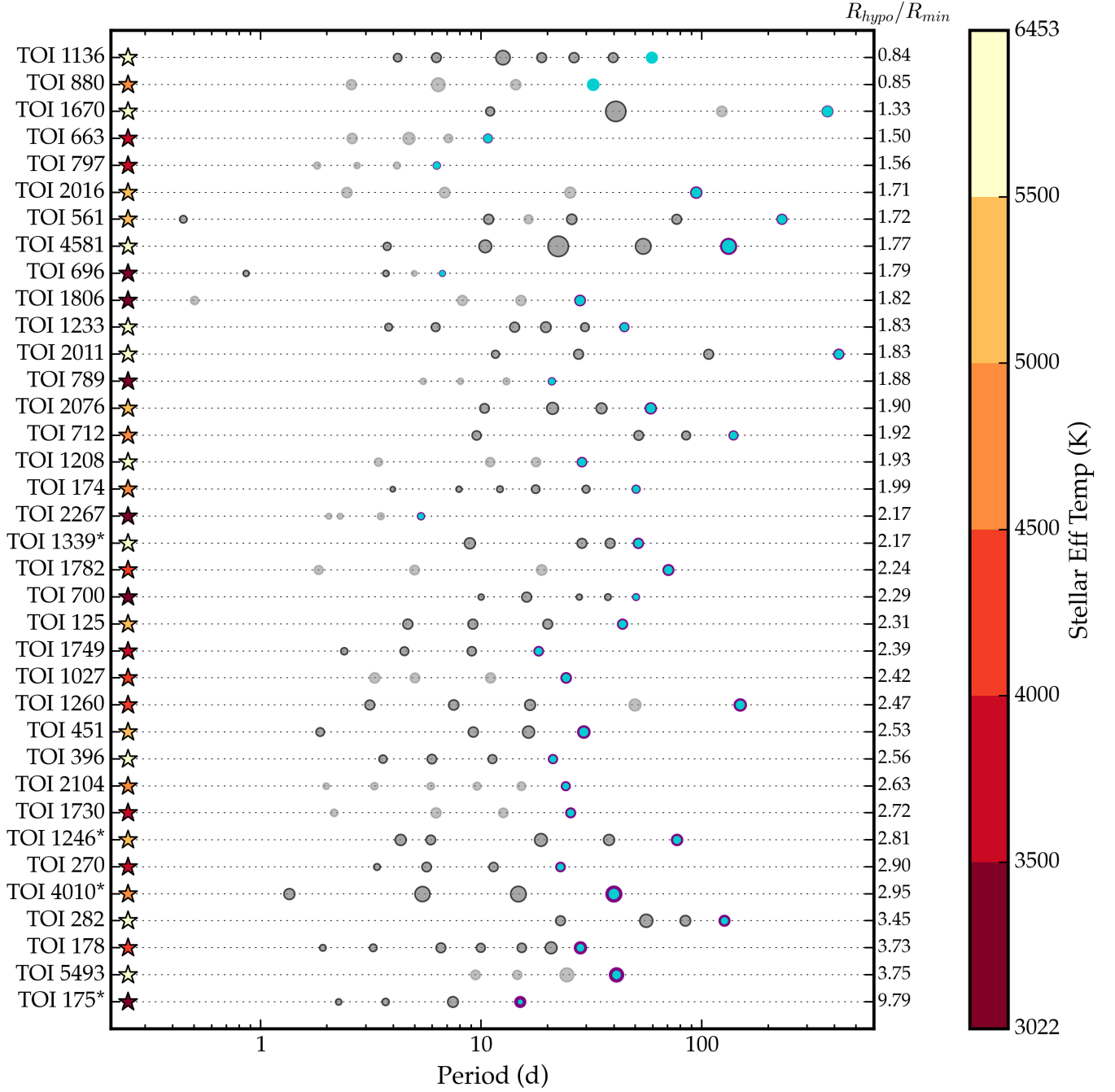


Figure 8. Transiting planets (grey, outlined in black) and planet candidates (grey, no outlines) in the 36 *TESS* systems with 3 or more planets or planet candidates. Systems with additional non-transiting confirmed planets are indicated with a single asterisk. All points are scaled according to planet radius. A putative outer planet (purple) is included for each system, with a hypothetical radius equal to that of the outermost transiting planet in the system. The minimum detectable radius at the hypothetical planet's orbital period is shown in blue. On the right of the plot, the ratio between the hypothetical and minimum detectable radii for the putative planets is shown. On the left of the plot, the effective temperature of the stellar host is shown in the colour of a star-shaped marker. If the purple putative planet is not visible (as is the case for TOIs 1136 and 880), the putative planet is smaller than the minimum detectable radius, and thus would not be detectable in the current *TESS* light curve.

systems is warranted to understand how these planets formed and came to be as they are observed today.

We thank Guy Nir and Massimo Pascale for useful conversations in the preparation of this work. E. Turtelboom acknowledges support from a David & Lucile Packard Foundation grant. C. Harada acknowledges support from the National Science Foundation Graduate Research Fellowship Program under Grant No. DGE 2146752. C.D.Dressing gratefully acknowledges support from the NASA Exoplanets Research Program (XRP) via grant 80NSSC20K0250, the Hellman Faculty Fellows Fund, the Sloan Foundation, and the David & Lucile Packard Foundation.

This research has made use of the Exoplanet Follow-up Observation Program (ExoFOP; DOI: [10.26134/ExoFOP5](https://doi.org/10.26134/ExoFOP5)) website, which is operated by the California Institute of Technology, under contract with the National Aeronautics and Space Administration under the Exoplanet Exploration Program. This paper made use of data collected by the TESS mission and are publicly available from the Mikulski Archive for Space Telescopes (MAST) operated by the Space Telescope Science Institute ([10.17909/fwdt-2x66](https://doi.org/10.17909/fwdt-2x66)). Funding for the TESS mission is provided by NASA’s Science Mission Directorate. We acknowledge the use of public TESS data from pipelines at the TESS Science Office and at the TESS Science Processing Operations Center. Resources supporting this work were provided by the NASA High-End Computing (HEC) Program through the NASA Advanced Supercomputing (NAS) Division at Ames Research Center for the production of the SPOC data products. This research has made use of NASA’s Astrophysics Data System, and of the NASA Exoplanet Archive ([10.26133/NEA1](https://doi.org/10.26133/NEA1)).

Facilities: TESS

Software: `astropy` (Astropy Collaboration et al. 2013, 2018, 2022), `batman` (Kreidberg 2015), `lightkurve` (Lightkurve Collaboration et al. 2018), `wotan` (Hipke et al. 2019)

REFERENCES

- Adams, F. C., Batygin, K., Bloch, A. M., & Laughlin, G. 2020, MNRAS, 493, 5520, doi: [10.1093/mnras/staa624](https://doi.org/10.1093/mnras/staa624)
- Aigrain, S., Hodgkin, S. T., Irwin, M. J., Lewis, J. R., & Roberts, S. J. 2015, MNRAS, 447, 2880, doi: [10.1093/mnras/stu2638](https://doi.org/10.1093/mnras/stu2638)
- Astropy Collaboration, Robitaille, T. P., Tollerud, E. J., et al. 2013, A&A, 558, A33, doi: [10.1051/0004-6361/201322068](https://doi.org/10.1051/0004-6361/201322068)
- Astropy Collaboration, Price-Whelan, A. M., Sipőcz, B. M., et al. 2018, AJ, 156, 123, doi: [10.3847/1538-3881/aabc4f](https://doi.org/10.3847/1538-3881/aabc4f)
- Astropy Collaboration, Price-Whelan, A. M., Lim, P. L., et al. 2022, ApJ, 935, 167, doi: [10.3847/1538-4357/ac7c74](https://doi.org/10.3847/1538-4357/ac7c74)
- Badenas-Agusti, M., Günther, M. N., Daylan, T., et al. 2020, AJ, 160, 113, doi: [10.3847/1538-3881/aba0b5](https://doi.org/10.3847/1538-3881/aba0b5)
- Barclay, T., Quintana, E. V., Raymond, S. N., & Penny, M. T. 2017, ApJ, 841, 86, doi: [10.3847/1538-4357/aa705b](https://doi.org/10.3847/1538-4357/aa705b)
- Barnes, R., & Raymond, S. N. 2004, ApJ, 617, 569, doi: [10.1086/423419](https://doi.org/10.1086/423419)
- Batalha, N. M. 2014, Proceedings of the National Academy of Science, 111, 12647, doi: [10.1073/pnas.1304196111](https://doi.org/10.1073/pnas.1304196111)

- Bennett, D. P., & Rhie, S. H. 2002, *ApJ*, 574, 985, doi: [10.1086/340977](https://doi.org/10.1086/340977)
- Berger, T. A., Huber, D., van Saders, J. L., et al. 2020, *AJ*, 159, 280, doi: [10.3847/1538-3881/159/6/280](https://doi.org/10.3847/1538-3881/159/6/280)
- Chauvin, G. 2024, *Comptes Rendus Physique*, 24, 139, doi: [10.5802/crphys.139](https://doi.org/10.5802/crphys.139)
- Chen, J., & Kipping, D. 2017, *ApJ*, 834, 17, doi: [10.3847/1538-4357/834/1/17](https://doi.org/10.3847/1538-4357/834/1/17)
- Choksi, N., & Chiang, E. 2020, *MNRAS*, 495, 4192, doi: [10.1093/mnras/staa1421](https://doi.org/10.1093/mnras/staa1421)
- Demangeon, O. D. S., Zapatero Osorio, M. R., Alibert, Y., et al. 2021, *A&A*, 653, A41, doi: [10.1051/0004-6361/202140728](https://doi.org/10.1051/0004-6361/202140728)
- Denham, P., Naoz, S., Hoang, B.-M., Stephan, A. P., & Farr, W. M. 2019, *MNRAS*, 482, 4146, doi: [10.1093/mnras/sty2830](https://doi.org/10.1093/mnras/sty2830)
- Dietrich, J., & Apai, D. 2020, *AJ*, 160, 107, doi: [10.3847/1538-3881/aba61d](https://doi.org/10.3847/1538-3881/aba61d)
- Dietrich, J., Apai, D., & Malhotra, R. 2022, *AJ*, 163, 88, doi: [10.3847/1538-3881/ac4166](https://doi.org/10.3847/1538-3881/ac4166)
- Dong, S., & Zhu, Z. 2013, *ApJ*, 778, 53, doi: [10.1088/0004-637X/778/1/53](https://doi.org/10.1088/0004-637X/778/1/53)
- Dransfield, G., Triaud, A. H. M. J., Guillot, T., et al. 2022, *MNRAS*, 515, 1328, doi: [10.1093/mnras/stac1383](https://doi.org/10.1093/mnras/stac1383)
- Drażkowska, J., Bitsch, B., Lambrechts, M., et al. 2023, in *Astronomical Society of the Pacific Conference Series*, Vol. 534, *Protostars and Planets VII*, ed. S. Inutsuka, Y. Aikawa, T. Muto, K. Tomida, & M. Tamura, 717, doi: [10.48550/arXiv.2203.09759](https://doi.org/10.48550/arXiv.2203.09759)
- Fabrycky, D., & Tremaine, S. 2007, *ApJ*, 669, 1298, doi: [10.1086/521702](https://doi.org/10.1086/521702)
- Fabrycky, D. C., Lissauer, J. J., Ragozzine, D., et al. 2014, *ApJ*, 790, 146, doi: [10.1088/0004-637X/790/2/146](https://doi.org/10.1088/0004-637X/790/2/146)
- Fang, J., & Margot, J.-L. 2013, *ApJ*, 767, 115, doi: [10.1088/0004-637X/767/2/115](https://doi.org/10.1088/0004-637X/767/2/115)
- Fischer, D. A., & Valenti, J. 2005, *ApJ*, 622, 1102, doi: [10.1086/428383](https://doi.org/10.1086/428383)
- Fulton, B. J., & Petigura, E. A. 2018, *AJ*, 156, 264, doi: [10.3847/1538-3881/aae828](https://doi.org/10.3847/1538-3881/aae828)
- Gondhalekar, Y., Feigelson, E. D., Caceres, G. A., Montalto, M., & Saha, S. 2023, *ApJL*, 959, L16, doi: [10.3847/2041-8213/ad0844](https://doi.org/10.3847/2041-8213/ad0844)
- Han, T., & Brandt, T. D. 2023, *AJ*, 165, 71, doi: [10.3847/1538-3881/acaaa7](https://doi.org/10.3847/1538-3881/acaaa7)
- He, M. Y., Ford, E. B., & Ragozzine, D. 2019, *MNRAS*, 490, 4575, doi: [10.1093/mnras/stz2869](https://doi.org/10.1093/mnras/stz2869)
- He, M. Y., Ford, E. B., Ragozzine, D., & Carrera, D. 2020, *AJ*, 160, 276, doi: [10.3847/1538-3881/abba18](https://doi.org/10.3847/1538-3881/abba18)
- Hippke, M., David, T. J., Mulders, G. D., & Heller, R. 2019, *AJ*, 158, 143, doi: [10.3847/1538-3881/ab3984](https://doi.org/10.3847/1538-3881/ab3984)
- Huang, C. X., Vanderburg, A., Pál, A., et al. 2020, *Research Notes of the American Astronomical Society*, 4, 204, doi: [10.3847/2515-5172/abca2e](https://doi.org/10.3847/2515-5172/abca2e)
- Izidoro, A., Bitsch, B., Raymond, S. N., et al. 2021, *A&A*, 650, A152, doi: [10.1051/0004-6361/201935336](https://doi.org/10.1051/0004-6361/201935336)
- Jackson, B., Greenberg, R., & Barnes, R. 2008, *ApJ*, 678, 1396, doi: [10.1086/529187](https://doi.org/10.1086/529187)
- Jenkins, J. M., Twicken, J. D., McCauliff, S., et al. 2016, in *Proc. SPIE*, Vol. 9913, *Software and Cyberinfrastructure for Astronomy IV*, 99133E, doi: [10.1117/12.2233418](https://doi.org/10.1117/12.2233418)
- Kostov, V. B., Schlieder, J. E., Barclay, T., et al. 2019, *AJ*, 158, 32, doi: [10.3847/1538-3881/ab2459](https://doi.org/10.3847/1538-3881/ab2459)
- Kovács, G., Zucker, S., & Mazeh, T. 2002, *A&A*, 391, 369, doi: [10.1051/0004-6361:20020802](https://doi.org/10.1051/0004-6361:20020802)
- Kozai, Y. 1962, *AJ*, 67, 591, doi: [10.1086/108790](https://doi.org/10.1086/108790)
- Kreidberg, L. 2015, *PASP*, 127, 1161, doi: [10.1086/683602](https://doi.org/10.1086/683602)
- Lidov, M. L. 1962, *Planet. Space Sci.*, 9, 719, doi: [10.1016/0032-0633\(62\)90129-0](https://doi.org/10.1016/0032-0633(62)90129-0)
- Lightkurve Collaboration, Cardoso, J. V. d. M., Hedges, C., et al. 2018, *Lightkurve: Kepler and TESS time series analysis in Python*, *Astrophysics Source Code Library*. <http://ascl.net/1812.013>
- Lissauer, J. J., Ragozzine, D., Fabrycky, D. C., et al. 2011, *ApJS*, 197, 8, doi: [10.1088/0067-0049/197/1/8](https://doi.org/10.1088/0067-0049/197/1/8)
- Lithwick, Y., Xie, J., & Wu, Y. 2012, *ApJ*, 761, 122, doi: [10.1088/0004-637X/761/2/122](https://doi.org/10.1088/0004-637X/761/2/122)
- Lubin, J., Van Zandt, J., Holcomb, R., et al. 2022, *AJ*, 163, 101, doi: [10.3847/1538-3881/ac3d38](https://doi.org/10.3847/1538-3881/ac3d38)
- Luque, R., & Pallé, E. 2022, *Science*, 377, 1211, doi: [10.1126/science.abl7164](https://doi.org/10.1126/science.abl7164)
- Millholland, S., Wang, S., & Laughlin, G. 2017, *ApJL*, 849, L33, doi: [10.3847/2041-8213/aa9714](https://doi.org/10.3847/2041-8213/aa9714)
- Millholland, S. C., He, M. Y., & Zink, J. K. 2022, *AJ*, 164, 72, doi: [10.3847/1538-3881/ac7c67](https://doi.org/10.3847/1538-3881/ac7c67)
- Mills, S. M., Howard, A. W., Petigura, E. A., et al. 2019, *AJ*, 157, 198, doi: [10.3847/1538-3881/ab1009](https://doi.org/10.3847/1538-3881/ab1009)
- Montet, B. T., Yee, J. C., & Penny, M. T. 2017, *PASP*, 129, 044401, doi: [10.1088/1538-3873/aa57fb](https://doi.org/10.1088/1538-3873/aa57fb)
- Mordasini, C. 2018, in *Handbook of Exoplanets*, ed. H. J. Deeg & J. A. Belmonte, 143, doi: [10.1007/978-3-319-55333-7_143](https://doi.org/10.1007/978-3-319-55333-7_143)
- Mulders, G. D., Pascucci, I., Apai, D., & Ciesla, F. J. 2018, *AJ*, 156, 24, doi: [10.3847/1538-3881/aac5ea](https://doi.org/10.3847/1538-3881/aac5ea)
- Obertas, A., Tamayo, D., & Murray, N. 2023, *MNRAS*, 526, 2118, doi: [10.1093/mnras/stad1921](https://doi.org/10.1093/mnras/stad1921)
- Ofir, A. 2014, *A&A*, 561, A138, doi: [10.1051/0004-6361/201220860](https://doi.org/10.1051/0004-6361/201220860)
- Orell-Miquel, J., Nowak, G., Murgas, F., et al. 2023, *A&A*, 669, A40, doi: [10.1051/0004-6361/202244120](https://doi.org/10.1051/0004-6361/202244120)

- Parviainen, H., Luque, R., & Palle, E. 2024, MNRAS, 527, 5693, doi: [10.1093/mnras/stad3504](https://doi.org/10.1093/mnras/stad3504)
- Penny, M. T., Gaudi, B. S., Kerins, E., et al. 2019, ApJS, 241, 3, doi: [10.3847/1538-4365/aafb69](https://doi.org/10.3847/1538-4365/aafb69)
- Pu, B., & Wu, Y. 2015, ApJ, 807, 44, doi: [10.1088/0004-637X/807/1/44](https://doi.org/10.1088/0004-637X/807/1/44)
- Sandford, E., Kipping, D., & Collins, M. 2019, MNRAS, 489, 3162, doi: [10.1093/mnras/stz2350](https://doi.org/10.1093/mnras/stz2350)
- Smirnov, N. V. 1939, Bull. Math. Univ. Moscou, 2, 3
- Southworth, J. 2011, MNRAS, 417, 2166, doi: [10.1111/j.1365-2966.2011.19399.x](https://doi.org/10.1111/j.1365-2966.2011.19399.x)
- Spergel, D., Gehrels, N., Baltay, C., et al. 2015, arXiv e-prints, arXiv:1503.03757, doi: [10.48550/arXiv.1503.03757](https://doi.org/10.48550/arXiv.1503.03757)
- Steffen, J. H., & Hwang, J. A. 2015, MNRAS, 448, 1956, doi: [10.1093/mnras/stv104](https://doi.org/10.1093/mnras/stv104)
- Sumi, T., Kamiya, K., Bennett, D. P., et al. 2011, Nature, 473, 349, doi: [10.1038/nature10092](https://doi.org/10.1038/nature10092)
- Tamburo, P., Muirhead, P. S., & Dressing, C. D. 2023, AJ, 165, 251, doi: [10.3847/1538-3881/acd1de](https://doi.org/10.3847/1538-3881/acd1de)
- Ti o Humphrey, A. L., & Quintana, E. V. 2020, arXiv e-prints, arXiv:2011.03053, doi: [10.48550/arXiv.2011.03053](https://doi.org/10.48550/arXiv.2011.03053)
- Tuson, A., Queloz, D., Osborn, H. P., et al. 2023, MNRAS, 523, 3090, doi: [10.1093/mnras/stad1369](https://doi.org/10.1093/mnras/stad1369)
- Ulmer-Moll, S., Lendl, M., Gill, S., et al. 2022, A&A, 666, A46, doi: [10.1051/0004-6361/202243583](https://doi.org/10.1051/0004-6361/202243583)
- Weiss, L. M., Marcy, G. W., Petigura, E. A., et al. 2018, AJ, 155, 48, doi: [10.3847/1538-3881/aa9ff6](https://doi.org/10.3847/1538-3881/aa9ff6)
- Wilson, R. F., Barclay, T., Powell, B. P., et al. 2023, ApJS, 269, 5, doi: [10.3847/1538-4365/acf3df](https://doi.org/10.3847/1538-4365/acf3df)
- Wu, S. C., Dewberry, J. W., & Fuller, J. 2024, ApJ, 963, 34, doi: [10.3847/1538-4357/ad1e54](https://doi.org/10.3847/1538-4357/ad1e54)
- Xie, J.-W., Dong, S., Zhu, Z., et al. 2016, Proceedings of the National Academy of Science, 113, 11431, doi: [10.1073/pnas.1604692113](https://doi.org/10.1073/pnas.1604692113)
- Yang, J.-Y., Xie, J.-W., & Zhou, J.-L. 2020, AJ, 159, 164, doi: [10.3847/1538-3881/ab7373](https://doi.org/10.3847/1538-3881/ab7373)
- Zhu, W., Petrovich, C., Wu, Y., Dong, S., & Xie, J. 2018, ApJ, 860, 101, doi: [10.3847/1538-4357/aac6d5](https://doi.org/10.3847/1538-4357/aac6d5)

APPENDIX

In this Appendix, we include Tables 1 and 2, which detail the DYNAMITE predictions for the current sample of 183 *TESS* multi-planet systems.

Table 1. DYNAMITE v3 predictions for the 2023 dataset with the PCM model

Name	Period (d)	Radius (R_{\oplus})	Mass (M_{\oplus})	Inclination (deg)	Eccentricity	Transit Depth (ppm)	Transit Probability	RV Semi-amplitude (m/s)
HD22946	15.4 ^{+1.8} _{-0.5}	1.96 ^{+0.65} _{-1.1}	5.04 ^{+2.88} _{-1.87}	90.5 ^{+42.6} _{-43.4}	0.036 ^{+0.029} _{-0.016}	257 ⁺¹⁷¹ ₋₁₃₁	0.523 ^{+0.093} _{-0.001}	1.22 ^{+0.26} _{-0.69}
TOI - 1873	502.1 ^{+42.7} _{-47.9}	3.28 ^{+1.04} _{-0.83}	11.37 ^{+6.2} _{-4.2}	90.0 ^{+43.1} _{-43.2}	0.037 ^{+0.03} _{-0.017}	961 ⁺⁶¹⁷ ₋₄₉₆	0.502 ^{+0.007} _{-0.001}	0.91 ^{+0.25} _{-0.53}
HD191939	692.2 ^{+52.6} _{-61.7}	4.31 ^{+9.09} _{-1.58}	17.5 ^{+87.55} _{-8.99}	88.6 ^{+1.2} _{-0.8}	0.017 ^{+0.016} _{-0.008}	1770 ⁺⁷⁴⁵⁰ ₋₁₃₀₀	0.15 ^{+0.346} _{-0.001}	1.46 ^{+7.86} _{-0.79}
TOI - 797	7.39 ^{+2.1} _{-1.3}	1.17 ^{+0.41} _{-0.29}	1.55 ^{+2.81} _{-0.968}	90.0 ^{+43.1} _{-42.5}	0.042 ^{+0.038} _{-0.02}	513 ⁺⁵⁶¹ ₋₂₅₆	0.52 ^{+0.047} _{-0.001}	0.84 ^{+1.07} _{-0.63}
TOI - 2404	399.3 ^{+24.2} _{-30.5}	4.06 ^{+2.64} _{-1.13}	15.92 ^{+19.21} _{-6.03}	90.0 ^{+42.7} _{-42.3}	0.033 ^{+0.026} _{-0.013}	995 ⁺¹³⁰⁰ ₋₉₃₃	0.502 ^{+0.013} _{-0.001}	1.25 ^{+1.03} _{-0.66}
TOI - 4418	12.2 ^{+2.6} _{-1.6}	2.3 ^{+0.71} _{-0.57}	6.49 ^{+3.75} _{-2.35}	90.1 ^{+42.3} _{-42.3}	0.046 ^{+0.02} _{-0.013}	661 ⁺³³⁸ ₋₃₃₈	0.522 ^{+0.001} _{-0.001}	1.91 ^{+1.61} _{-1.12}
TOI - 561	0.694 ^{+0.0} _{-0.0}	2.3 ^{+0.77} _{-0.57}	6.49 ^{+3.75} _{-2.35}	90.0 ^{+1.5} _{-0.1}	0.021 ^{+0.019} _{-0.01}	630 ⁺³¹³ ₋₃₁₃	1.0 ^{+0.001} _{-0.001}	5.4 ^{+3.41} _{-2.06}
TOI - 554	4.46 ^{+0.8} _{-0.7}	1.41 ^{+1.33} _{-0.43}	2.94 ^{+26.19} _{-2.11}	90.0 ^{+42.9} _{-43.0}	0.045 ^{+0.029} _{-0.019}	82 ⁺¹⁵⁵ ₋₅₀	0.561 ^{+0.162} _{-0.001}	0.99 ^{+7.4} _{-0.81}
TOI - 663	12.2 ^{+3.8} _{-2.2}	2.35 ^{+0.81} _{-0.59}	6.71 ^{+4.0} _{-2.46}	89.8 ^{+43.1} _{-42.8}	0.041 ^{+0.038} _{-0.019}	1770 ⁺¹²²⁰ ₋₈₉₄	0.513 ^{+0.035} _{-0.001}	2.92 ^{+0.82} _{-1.71}
TOI - 1130	1.48 ^{+11.0} _{-9.0}	3.52 ^{+1.38} _{-0.94}	12.71 ^{+8.73} _{-4.93}	89.6 ^{+3.7} _{-4.6}	0.045 ^{+0.028} _{-0.019}	2190 ⁺¹⁷²⁰ ₋₁₁₇₀	0.947 ^{+0.001} _{-0.363}	8.97 ^{+13.07} _{-6.32}
TOI - 1225	25.5 ^{+4.0} _{-2.9}	2.71 ^{+0.91} _{-0.69}	8.41 ^{+4.88} _{-3.12}	89.8 ^{+42.8} _{-42.7}	0.057 ^{+0.043} _{-0.026}	783 ⁺⁵³³ ₋₄₀₈	0.512 ^{+0.046} _{-0.001}	1.87 ^{+0.61} _{-1.1}
TOI - 2269	4.46 ^{+1.3} _{-0.6}	1.45 ^{+0.5} _{-0.36}	3.24 ^{+5.77} _{-2.03}	89.8 ^{+42.7} _{-42.1}	0.047 ^{+0.031} _{-0.02}	584 ⁺⁴⁰⁵ ₋₂₉₃	0.53 ^{+0.094} _{-0.001}	1.89 ^{+2.29} _{-1.42}
TOI - 1468	3.16 ^{+0.6} _{-0.4}	1.3 ^{+0.46} _{-0.31}	2.23 ^{+4.1} _{-1.36}	90.0 ^{+4.4} _{-3.8}	0.047 ^{+0.03} _{-0.021}	1230 ⁺⁸⁷³ ₋₅₉₀	0.751 ^{+0.233} _{-0.119}	2.0 ^{+4.03} _{-1.45}
LP791 - 18	1.65 ^{+0.1} _{-0.1}	1.23 ^{+1.15} _{-0.37}	1.84 ^{+16.09} _{-1.3}	89.3 ^{+2.7} _{-2.3}	0.038 ^{+0.03} _{-0.018}	3920 ⁺⁷³⁵⁰ ₋₂₄₀₀	0.878 ^{+0.122} _{-0.001}	3.7 ^{+34.86} _{-2.68}
TOI - 1052	16.9 ^{+0.4} _{-0.4}	2.85 ^{+1.82} _{-0.76}	9.1 ^{+10.76} _{-3.55}	88.3 ^{+4.6} _{-4.5}	0.043 ^{+0.024} _{-0.018}	430 ⁺⁵⁵⁰ ₋₂₃₀	0.586 ^{+0.412} _{-0.001}	2.01 ^{+2.47} _{-0.81}
TOI - 2016	11.2 ^{+2.6} _{-1.6}	2.77 ^{+0.88} _{-0.68}	8.7 ^{+3.7} _{-2.4}	89.2 ^{+4.9} _{-4.9}	0.032 ^{+0.023} _{-0.014}	914 ⁺⁵⁶³ ₋₄₆₄	0.514 ^{+0.044} _{-0.001}	2.72 ^{+0.94} _{-0.84}
TOI - 2525	126.9 ^{+88.7} _{-6.6}	8.05 ^{+1.89} _{-1.89}	46.96 ^{+24.28} _{-16.19}	89.3 ^{+3.4} _{-3.4}	0.045 ^{+0.017} _{-0.019}	8730 ⁺⁵³¹⁰ ₋₄₁₅₀	0.488 ^{+0.263} _{-0.001}	6.67 ^{+2.52} _{-3.91}
TOI - 4443	3.10 ^{+0.3} _{-0.2}	1.8 ^{+0.46} _{-0.46}	4.4 ^{+14.04} _{-1.93}	90.2 ^{+42.8} _{-42.8}	0.047 ^{+0.033} _{-0.02}	263 ⁺¹⁷⁷ ₋₁₃₇	0.558 ^{+0.333} _{-0.001}	1.86 ^{+4.57} _{-1.18}
HR858	23.2 ^{+4.5} _{-3.0}	2.02 ^{+0.69} _{-0.52}	5.28 ^{+3.12} _{-1.98}	86.5 ^{+2.8} _{-2.2}	0.04 ^{+0.036} _{-0.019}	200 ⁺¹³⁷ ₋₁₀₃	0.364 ^{+0.595} _{-0.001}	1.08 ^{+0.8} _{-0.46}
TOI - 872	8.1 ^{+0.7} _{-0.4}	2.32 ^{+0.78} _{-0.564}	6.58 ^{+3.82} _{-2.34}	90.8 ^{+42.3} _{-42.9}	0.046 ^{+0.03} _{-0.02}	783 ⁺⁵³⁷ ₋₃₉₄	0.534 ^{+0.179} _{-0.001}	2.45 ^{+0.73} _{-1.41}
TOI - 1782	8.1 ^{+2.0} _{-1.6}	2.23 ^{+0.7} _{-0.55}	6.18 ^{+3.33} _{-2.23}	89.6 ^{+43.4} _{-42.5}	0.032 ^{+0.023} _{-0.014}	935 ⁺⁶⁰⁷ ₋₄₈₇	0.519 ^{+0.053} _{-0.001}	2.55 ^{+0.8} _{-1.52}
L98 - 59	1.19 ^{+0.2} _{-0.2}	1.27 ^{+0.45} _{-0.32}	2.05 ^{+3.79} _{-1.3}	87.4 ^{+1.5} _{-1.9}	0.029 ^{+0.028} _{-0.014}	1510 ⁺¹¹¹⁰ ₋₈₁₇	0.937 ^{+0.063} _{-0.001}	2.7 ^{+6.03} _{-1.82}
TOI - 836	14.7 ^{+0.7} _{-0.5}	1.8 ^{+0.6} _{-0.46}	4.4 ^{+14.04} _{-1.93}	89.1 ^{+4.4} _{-3.8}	0.047 ^{+0.03} _{-0.02}	607 ⁺⁴⁰⁵ ₋₃₁₁	0.569 ^{+0.424} _{-0.001}	1.49 ^{+5.05} _{-0.7}
TOI - 776	26.7 ^{+3.9} _{-2.7}	1.88 ^{+0.63} _{-0.49}	4.72 ^{+16.82} _{-1.91}	87.8 ^{+4.6} _{-3.6}	0.058 ^{+0.044} _{-0.026}	1020 ⁺⁶⁸⁷ ₋₅₃₆	0.48 ^{+0.321} _{-0.001}	1.52 ^{+5.92} _{-0.69}
TOI - 421	32.1 ^{+1.8} _{-1.5}	2.78 ^{+1.79} _{-0.79}	8.75 ^{+10.44} _{-3.59}	86.7 ^{+4.4} _{-3.8}	0.042 ^{+0.026} _{-0.017}	858 ⁺¹¹¹⁰ ₋₄₈₈	0.359 ^{+0.581} _{-0.001}	1.96 ^{+2.45} _{-0.85}
TOI - 2441	22.2 ^{+1.6} _{-1.2}	2.09 ^{+0.694} _{-0.51}	5.58 ^{+5.2} _{-1.99}	90.3 ^{+41.9} _{-43.0}	0.045 ^{+0.028} _{-0.019}	1680 ⁺¹¹²⁰ ₋₆₂₅	0.511 ^{+0.07} _{-0.001}	2.12 ^{+0.45} _{-0.46}
HIP9618	110.6 ^{+7.7} _{-7.7}	3.3 ^{+0.79} _{-0.79}	11.48 ^{+6.8} _{-4.2}	89.5 ^{+42.7} _{-42.1}	0.045 ^{+0.018} _{-0.018}	973 ⁺⁴⁶⁶ ₋₃₆₆	0.5 ^{+0.001} _{-0.001}	1.51 ^{+0.83} _{-0.83}
TOI - 4600	191.7 ^{+2.7} _{-2.7}	5.73 ^{+1.36} _{-1.2}	27.44 ^{+10.98} _{-8.51}	88.4 ^{+3.7} _{-3.7}	0.031 ^{+0.015} _{-0.012}	4210 ⁺²⁰²⁰ ₋₁₇₉₀	0.471 ^{+0.429} _{-0.001}	3.29 ^{+1.1} _{-1.1}
TOI - 1136	60.9 ^{+43.6} _{-43.6}	2.57 ^{+0.9} _{-0.66}	7.73 ^{+2.89} _{-2.89}	88.9 ^{+1.2} _{-0.8}	0.018 ^{+0.016} _{-0.012}	590 ⁺⁴¹⁶ ₋₃₀₇	0.499 ^{+0.023} _{-0.001}	1.24 ^{+1.85} _{-0.62}
TOI - 2300	8.1 ^{+1.5} _{-1.2}	3.22 ^{+1.82} _{-1.37}	11.04 ^{+11.37} _{-4.33}	90.5 ^{+42.7} _{-42.7}	0.042 ^{+0.026} _{-0.017}	1370 ⁺¹⁵⁶⁰ ₋₇₅₅	0.529 ^{+0.001} _{-0.001}	3.54 ^{+11.14} _{-2.19}
TOI - 431	7.39 ^{+0.5} _{-0.6}	1.69 ^{+0.77} _{-0.61}	3.99 ^{+6.18} _{-2.81}	85.1 ^{+2.8} _{-2.2}	0.039 ^{+0.031} _{-0.018}	450 ⁺⁹⁴⁴ ₋₃₁₀	0.257 ^{+0.738} _{-0.001}	1.54 ^{+25.9} _{-1.12}
TOI - 1470	5.87 ^{+0.2} _{-0.1}	2.08 ^{+0.64} _{-0.5}	5.53 ^{+2.92} _{-1.95}	88.6 ^{+4.4} _{-3.6}	0.042 ^{+0.023} _{-0.017}	1650 ⁺¹⁰¹⁶ ₋₇₉₁	0.632 ^{+0.368} _{-0.001}	3.24 ^{+1.79} _{-1.2}
HD93963A	1.65 ^{+0.1} _{-0.1}	1.54 ^{+1.61} _{-0.49}	3.90 ^{+43.15} _{-2.93}	84.6 ^{+4.5} _{-3.7}	0.049 ^{+0.033} _{-0.021}	184 ⁺³⁸⁵ ₋₁₁₇	0.88 ^{+0.12} _{-0.001}	2.01 ^{+22.59} _{-1.49}
TOI - 286	6.74 ^{+0.8} _{-0.5}	1.46 ^{+0.53} _{-0.36}	3.32 ^{+6.35} _{-2.07}	90.1 ^{+42.6} _{-42.5}	0.048 ^{+0.033} _{-0.02}	287 ⁺²¹² ₋₁₄₆	0.529 ^{+0.155} _{-0.001}	1.24 ^{+1.75} _{-0.94}
TOI - 4156	7.39 ^{+0.7} _{-0.5}	2.4 ^{+0.8} _{-0.58}	6.94 ^{+3.99} _{-2.46}	90.2 ^{+42.2} _{-42.2}	0.045 ^{+0.03} _{-0.019}	448 ⁺³⁰¹ ₋₂₂₁	0.535 ^{+0.177} _{-0.001}	2.14 ^{+0.6} _{-1.23}
TOI - 6276	9.29 ^{+2.0} _{-1.3}	1.07 ^{+0.36} _{-0.27}	1.14 ^{+1.95} _{-0.72}	90.2 ^{+42.5} _{-42.5}	0.061 ^{+0.049} _{-0.028}	242 ⁺¹⁶⁸ ₋₁₂₉	0.521 ^{+0.061} _{-0.001}	0.42 ^{+0.55} _{-0.32}

Table 1 continued

Table 1 (continued)

Name	Period (d)	Radius (R_{\oplus})	Mass (M_{\oplus})	Inclination (deg)	Eccentricity	Transit Depth (ppm)	Transit Probability	RV Semi-amplitude (m/s)
TOI-4342	18.5 ^{+2.7} _{-2.0}	2.24 ^{+0.76} _{-0.56}	6.22 ^{+3.65} _{-2.27}	88.4 ^{+3.6} _{-4.5}	0.056 ^{+0.043} _{-0.025}	1170 ⁺⁷⁹⁶ ₋₅₈₇	0.494 ^{+0.364} _{-0.001}	2.05 ^{+1.34} _{-0.81}
TOI-969	3.16 ^{+0.3} _{-0.1}	2.54 ^{+0.81} _{-0.63}	7.59 ^{+4.16} _{-2.75}	86.0 ^{+3.6} _{-4.6}	0.046 ^{+0.03} _{-0.02}	1210 ⁺⁷⁷¹ ₋₆₀₀	0.507 ^{+0.493} _{-0.001}	4.07 ^{+2.3} _{-1.57}
TOI-6729	12.2 ^{+1.1} _{-0.7}	1.86 ^{+0.64} _{-0.47}	4.64 ^{+16.6} _{-1.84}	90.6 ^{+42.5} _{-42.6}	0.047 ^{+0.032} _{-0.02}	84 ⁺⁵⁸ ₋₄₃	0.546 ^{+0.251} _{-0.001}	1.12 ^{+3.23} _{-0.69}
TOI-1260	26.7 ^{+1.5} _{-1.6}	2.67 ^{+0.85} _{-0.65}	8.21 ^{+4.5} _{-3.98}	88.7 ^{+1.6} _{-1.7}	0.025 ^{+0.021} _{-0.01}	1330 ⁺⁸⁵¹ ₋₆₉₁	0.499 ^{+0.494} _{-0.001}	2.27 ^{+1.34} _{-0.96}
TOI-2392	10.2 ^{+1.2} _{-1.2}	3.02 ^{+0.77} _{-0.77}	9.98 ^{+3.71} _{-3.71}	89.7 ^{+43.1} _{-43.1}	0.058 ^{+0.026} _{-0.026}	247 ⁺¹²² ₋₁₂₂	0.542 ^{+0.494} _{-0.001}	2.6 ^{+0.55} _{-0.55}
WASP-132	2.05 ^{+0.1} _{-0.1}	1.93 ^{+0.22} _{-0.22}	4.92 ^{+42.23} _{-1.97}	87.8 ^{+3.8} _{-3.8}	0.051 ^{+0.038} _{-0.023}	557 ⁺⁷⁰⁵ ₋₃₀₃	0.884 ^{+0.114} _{-0.001}	2.92 ^{+27.93} _{-1.24}
TOI-233	21.2 ^{+3.5} _{-2.6}	1.77 ^{+0.46} _{-0.46}	4.29 ^{+13.38} _{-2.0}	90.5 ^{+42.2} _{-42.2}	0.057 ^{+0.044} _{-0.025}	1820 ⁺¹²⁴⁰ ₋₉₅₃	0.512 ^{+0.03} _{-0.001}	1.93 ^{+4.43} _{-1.23}
TOI-2322	7.39 ^{+0.9} _{-1.1}	1.11 ^{+0.39} _{-0.27}	1.29 ^{+2.36} _{-0.797}	90.9 ^{+41.8} _{-42.6}	0.058 ^{+0.046} _{-0.027}	211 ⁺¹⁵³ ₋₁₀₉	0.534 ^{+0.076} _{-0.001}	0.54 ^{+0.76} _{-0.4}
TOI-216	8.48 ^{+0.5} _{-0.7}	5.83 ^{+1.78} _{-1.41}	28.9 ^{+14.76} _{-9.99}	89.1 ^{+43.7} _{-41.6}	0.043 ^{+0.025} _{-0.018}	4440 ⁺²⁷⁷⁰ ₋₂₂₃₀	0.521 ^{+0.14} _{-0.001}	10.53 ^{+1.96} _{-5.75}
TOI-199	42.2 ^{+2.4} _{-2.1}	8.26 ^{+2.35} _{-1.88}	48.91 ^{+23.73} _{-16.39}	88.1 ^{+4.6} _{-3.5}	0.038 ^{+0.023} _{-0.015}	8530 ⁺⁴⁸⁵⁰ ₋₃₈₈₀	0.49 ^{+0.432} _{-0.001}	9.36 ^{+4.82} _{-3.25}
TOI-213	11.7 ^{+24.1} _{-3.0}	1.29 ^{+1.0} _{-0.37}	2.17 ^{+13.53} _{-1.49}	89.5 ^{+43.3} _{-43.2}	0.047 ^{+0.03} _{-0.02}	312 ⁺⁴⁸⁵ ₋₃₈₈₀	0.513 ^{+0.034} _{-0.008}	0.76 ^{+4.0} _{-0.65}
TOI-5126	11.2 ^{+0.8} _{-1.6}	3.85 ^{+1.23} _{-0.94}	14.64 ^{+8.05} _{-5.23}	87.5 ^{+3.8} _{-3.8}	0.047 ^{+0.031} _{-0.02}	810 ⁺⁵¹⁹ ₋₃₉₈	0.543 ^{+0.428} _{-0.001}	3.63 ^{+2.42} _{-1.4}
TOI-119	18.5 ^{+2.7} _{-2.0}	1.86 ^{+0.64} _{-0.49}	4.64 ^{+16.6} _{-1.97}	90.0 ^{+43.0} _{-42.7}	0.057 ^{+0.045} _{-0.025}	432 ⁺³⁰² ₋₂₃₄	0.517 ^{+0.06} _{-0.001}	1.24 ^{+3.48} _{-0.78}
TOI-1444	0.773 ^{+5.0} _{-2.0}	1.63 ^{+1.65} _{-0.54}	4.86 ^{+49.34} _{-3.64}	81.1 ^{+3.7} _{-4.5}	0.05 ^{+0.034} _{-0.021}	270 ⁺⁵⁴⁶ ₋₁₇₉	0.918 ^{+0.001} _{-0.802}	3.52 ^{+42.41} _{-3.07}
TOI-763	19.4 ^{+1.4} _{-1.3}	2.3 ^{+0.74} _{-0.74}	6.49 ^{+3.59} _{-3.59}	89.7 ^{+43.1} _{-43.1}	0.049 ^{+0.031} _{-0.031}	549 ⁺³⁷¹ ₋₃₇₁	0.513 ^{+0.085} _{-0.189}	1.63 ^{+0.68} _{-0.89}
TOI-1404	4.07 ^{+0.4} _{-0.3}	2.53 ^{+0.82} _{-0.82}	7.54 ^{+4.21} _{-4.21}	90.3 ^{+42.0} _{-42.0}	0.045 ^{+0.032} _{-0.019}	507 ⁺³³¹ ₋₂₅₂	0.553 ^{+0.039} _{-0.001}	2.72 ^{+0.89} _{-1.56}
TOI-904	18.5 ^{+1.9} _{-1.3} 46.3 ^{+3.3} _{-3.9}	2.23 ^{+0.71} _{-0.55}	6.18 ^{+3.38} _{-2.23}	90.4 ^{+43.0} _{-42.9}	0.046 ^{+0.03} _{-0.024}	1470 ⁺⁹⁴³ ₋₇₃₃	0.515 ^{+0.055} _{-0.001} 0.51 ^{+0.027} _{-0.001}	2.2 ^{+0.47} _{-1.24} 1.62 ^{+0.35} _{-0.91}
TOI-1670	191.7 ^{+16.1} _{-12.1}	2.28 ^{+0.9} _{-0.59}	6.4 ^{+4.23} _{-2.41}	88.2 ^{+2.8} _{-2.8}	0.034 ^{+0.024} _{-0.015}	251 ⁺¹⁹⁸ ₋₁₃₀	0.275 ^{+0.402} _{-0.001}	0.63 ^{+0.46} _{-0.25}
TOI-1730	3.39 ^{+0.3} _{-0.2}	2.0 ^{+0.67} _{-0.51}	5.9 ^{+3.01} _{-1.93}	89.9 ^{+42.5} _{-42.3}	0.037 ^{+0.031} _{-0.017}	1200 ⁺⁸⁰⁷ ₋₆₁₇	0.536 ^{+0.218} _{-0.001}	3.39 ^{+0.75} _{-1.89}
TOI-1269	14.7 ^{+1.2} _{-1.0}	2.1 ^{+0.69} _{-0.53}	5.62 ^{+3.18} _{-2.07}	89.4 ^{+42.4} _{-42.0}	0.046 ^{+0.032} _{-0.019}	513 ⁺³⁴² ₋₂₆₆	0.513 ^{+0.102} _{-0.001}	1.5 ^{+0.45} _{-0.87}
TOI-1438	16.9 ^{+2.7} _{-1.9}	2.54 ^{+0.86} _{-0.63}	7.59 ^{+4.44} _{-2.75}	90.1 ^{+43.1} _{-42.8}	0.057 ^{+0.044} _{-0.026}	806 ⁺⁵⁵⁵ ₋₄₁₂	0.517 ^{+0.058} _{-0.001}	2.03 ^{+0.66} _{-1.2}
TOI-1757	8.1 ^{+0.7} _{-0.4}	1.51 ^{+0.52} _{-0.37}	3.73 ^{+6.62} _{-2.32}	89.9 ^{+42.8} _{-41.9}	0.046 ^{+0.03} _{-0.019}	383 ⁺²⁷² ₋₁₉₉	0.525 ^{+0.183} _{-0.001}	1.52 ^{+1.94} _{-1.14}
TOI-6655	21.2 ^{+3.4} _{-2.5}	2.31 ^{+0.79} _{-0.58}	6.53 ^{+3.86} _{-2.4}	90.0 ^{+43.0} _{-42.8}	0.057 ^{+0.044} _{-0.025}	542 ⁺³⁷⁵ ₋₂₇₈	0.514 ^{+0.054} _{-0.001}	1.53 ^{+0.51} _{-0.91}
HD63935	5.36 ^{+0.3} _{-0.5}	2.72 ^{+0.85} _{-0.66}	8.46 ^{+4.54} _{-3.01}	89.3 ^{+4.4} _{-3.7}	0.046 ^{+0.032} _{-0.019}	675 ⁺⁴²⁵ ₋₃₁₃	0.843 ^{+0.155} _{-0.001}	3.25 ^{+2.08} _{-1.26}
TOI-1346	3.16 ^{+0.3} _{-0.2}	2.39 ^{+0.77} _{-0.58}	6.89 ^{+3.82} _{-2.45}	90.1 ^{+42.1} _{-42.0}	0.045 ^{+0.029} _{-0.019}	781 ⁺⁵¹³ ₋₃₉₂	0.552 ^{+0.281} _{-0.001}	3.43 ^{+0.89} _{-1.96}
TOI-6022	0.773 ^{+2.0} _{-2.0}	2.39 ^{+0.8} _{-0.6}	6.89 ^{+3.8} _{-2.53}	90.2 ^{+42.9} _{-42.9}	0.058 ^{+0.026} _{-0.026}	3510 ⁺¹⁷⁷⁰ ₋₁₇₇₀	0.581 ^{+0.057} _{-0.057}	9.55 ^{+7.37} _{-7.37}
TOI-4647	4.89 ^{+0.6} _{-0.8}	2.62 ^{+0.89} _{-0.67}	7.97 ^{+4.68} _{-2.97}	90.5 ^{+42.5} _{-42.5}	0.06 ^{+0.046} _{-0.028}	616 ⁺⁴²³ ₋₃₂₁	0.546 ^{+0.105} _{-0.001}	2.82 ^{+1.04} _{-1.66}
TOI-6054	21.2 ^{+3.9} _{-2.6}	2.59 ^{+0.88} _{-0.66}	7.83 ^{+2.91} _{-2.91}	90.3 ^{+42.4} _{-42.6}	0.058 ^{+0.044} _{-0.026}	217 ⁺¹⁴⁹ ₋₁₁₂	0.527 ^{+0.084} _{-0.001}	1.65 ^{+0.58} _{-0.99}
TOI-1706	12.2 ^{+2.2} _{-1.5}	1.72 ^{+0.6} _{-0.44}	4.1 ^{+12.31} _{-1.99}	89.7 ^{+43.5} _{-42.4}	0.059 ^{+0.045} _{-0.027}	264 ⁺¹⁸⁶ ₋₁₃₈	0.522 ^{+0.078} _{-0.001}	1.15 ^{+2.7} _{-0.77}
TOI-1445	15.4 ^{+1.5} _{-1.1}	2.21 ^{+0.72} _{-0.55}	6.09 ^{+3.42} _{-2.22}	90.3 ^{+42.2} _{-43.4}	0.047 ^{+0.031} _{-0.02}	365 ⁺²⁴¹ ₋₁₈₅	0.525 ^{+0.105} _{-0.001}	1.38 ^{+0.43} _{-0.81}
TOI-709	458.1 ^{+35.3} _{-40.1}	1.34 ^{+1.33} _{-0.37}	2.47 ^{+24.18} _{-1.66}	90.8 ^{+42.7} _{-42.4}	0.053 ^{+0.039} _{-0.023}	6980 ⁺¹⁷⁴⁰⁰ ₋₁₁₂₃₀	0.508 ^{+0.005} _{-0.001}	0.33 ^{+4.66} _{-0.27}
TOI-2095	11.7 ^{+1.2} _{-1.7}	1.26 ^{+0.43} _{-0.32}	2.0 ^{+3.5} _{-1.27}	88.4 ^{+4.6} _{-3.6}	0.063 ^{+0.048} _{-0.029}	689 ⁺⁴⁷⁵ ₋₃₅₆	0.497 ^{+0.383} _{-0.001}	0.98 ^{+1.93} _{-0.64}
TOI-1062	14.7 ^{+1.0} _{-0.7}	2.37 ^{+0.75} _{-0.59}	6.8 ^{+3.7} _{-2.47}	86.6 ^{+4.7} _{-3.5}	0.045 ^{+0.028} _{-0.018}	669 ⁺⁴⁴⁷ ₋₃₆₃	0.458 ^{+0.532} _{-0.001}	1.85 ^{+1.08} _{-0.71}
TOI-2076	63.8 ^{+21.6} _{-9.8}	2.95 ^{+1.01} _{-0.76}	9.61 ^{+5.69} _{-3.61}	89.6 ^{+43.0} _{-42.3}	0.042 ^{+0.036} _{-0.02}	1230 ⁺⁸⁴⁵ ₋₆₃₆	0.503 ^{+0.01} _{-0.001}	1.76 ^{+0.49} _{-1.05}
TOI-2112	23.2 ^{+2.2} _{-1.7} 87.9 ^{+5.9} _{-7.0}	4.46 ^{+1.39} _{-1.09}	18.47 ^{+9.89} _{-6.61}	89.6 ^{+42.6} _{-42.6}	0.046 ^{+0.03} _{-0.02}	669 ⁺⁴²⁰ ₋₃₃₁	0.519 ^{+0.107} _{-0.001} 0.505 ^{+0.044} _{-0.001}	3.02 ^{+0.91} _{-1.77} 1.94 ^{+0.59} _{-1.13}
TOI-3353	15.4 ^{+2.4} _{-2.4}	2.2 ^{+0.75} _{-0.64}	6.05 ^{+3.57} _{-2.33}	90.0 ^{+43.0} _{-43.0}	0.057 ^{+0.044} _{-0.028}	391 ⁺²⁶⁹ ₋₂₀₈	0.521 ^{+0.075} _{-0.186}	1.56 ^{+0.92} _{-0.5}
HD28109	145.6 ^{+24.9} _{-40.8}	2.76 ^{+0.94} _{-0.71}	8.65 ^{+3.24} _{-1.5}	88.4 ^{+3.8} _{-3.8}	0.041 ^{+0.02} _{-0.02}	305 ⁺¹⁵⁸ ₋₁₅₈	0.446 ^{+0.001} _{-0.186}	0.9 ^{+0.69} _{-0.4}
TOI-4495	8.48 ^{+0.8} _{-0.4}	2.29 ^{+0.74} _{-0.56}	6.44 ^{+2.31} _{-2.31}	89.9 ^{+42.5} _{-42.4}	0.046 ^{+0.031} _{-0.019}	245 ⁺¹⁶⁰ ₋₁₂₂	0.538 ^{+0.276} _{-0.001}	1.82 ^{+0.54} _{-1.05}
TOI-3485	3.55 ^{+0.3} _{-0.3}	1.6 ^{+0.54} _{-0.4}	4.55 ^{+2.87} _{-2.87}	90.3 ^{+42.0} _{-42.4}	0.047 ^{+0.031} _{-0.02}	363 ⁺²⁵¹ ₋₁₉₀	0.549 ^{+0.219} _{-0.001}	2.38 ^{+3.02} _{-1.79}

Table 1 continued

Table 1 (continued)

Name	Period (d)	Radius (R_{\oplus})	Mass (M_{\oplus})	Inclination (deg)	Eccentricity	Transit Depth (ppm)	Transit Probability	RV Semi-amplitude (m/s)
HD73583	10.2 ^{+0.4} _{-0.5}	2.24 ^{+0.72} _{-0.54}	6.22 ^{+3.44} _{-2.2}	88.7 ^{+4.4} _{-3.6}	0.046 ^{+0.029} _{-0.019}	998 ⁺⁶⁴⁵ ₋₄₈₅	0.583 ^{+0.407} _{-0.001}	2.26 ^{+1.36} _{-0.84}
TOI - 810	46.3 ^{+5.57} _{-5.9}	2.45 ^{+0.79} _{-0.61}	7.17 ^{+3.98} _{-2.61}	89.6 ^{+42.3} _{-41.8}	0.045 ^{+0.03} _{-0.019}	257 ⁺¹⁶⁷ ₋₁₃₀	0.509 ^{+0.047} _{-0.001}	1.26 ^{+0.4} _{-0.73}
TOI - 6293	174.9 ^{+10.9} _{-10.8}	7.65 ^{+2.04} _{-1.78}	43.32 ^{+19.62} _{-14.81}	87.2 ^{+43.7} _{-37.7}	0.045 ^{+0.032} _{-0.018}	5690 ⁺³⁰³⁰ ₋₂₆₅₀	0.484 ^{+0.02} _{-0.001}	5.82 ^{+1.22} _{-3.15}
TOI - 1266	32.1 ^{+4.8} _{-3.5}	1.72 ^{+0.38} _{-0.43}	4.1 ^{+11.83} _{-0.93}	88.4 ^{+3.8} _{-4.4}	0.058 ^{+0.045} _{-0.026}	1410 ⁺⁹⁶⁰ ₋₆₅₂	0.433 ^{+0.21} _{-0.001}	1.45 ^{+4.56} _{-0.74}
TOI - 5143	1.19 ^{+7.0} _{-0.68}	2.7 ^{+1.0} _{-0.68}	8.36 ^{+5.03} _{-3.07}	88.8 ^{+42.5} _{-42.5}	0.048 ^{+0.024} _{-0.021}	840 ⁺⁶⁵² ₋₄₉₃	0.585 ^{+0.078} _{-0.078}	5.38 ^{+4.31} _{-4.31}
TOI - 5696	661.2 ^{+61.3} _{-79.1}	2.85 ^{+1.0} _{-0.73}	9.1 ^{+5.54} _{-3.4}	89.9 ^{+43.0} _{-42.7}	0.074 ^{+0.069} _{-0.036}	991 ⁺⁷⁰² ₋₅₁₇	0.501 ^{+0.005} _{-0.001}	0.72 ^{+0.42} _{-0.24}
TOI - 487	11.7 ^{+1.6} _{-2.0}	2.25 ^{+0.73} _{-0.56}	6.27 ^{+3.5} _{-2.28}	90.4 ^{+42.9} _{-42.8}	0.046 ^{+0.03} _{-0.019}	419 ⁺⁸⁶⁰ ₋₈₆₃	0.53 ^{+0.132} _{-0.024}	1.77 ^{+0.57} _{-1.04}
TOI - 4304	9.29 ^{+0.6} _{-0.9}	2.23 ^{+0.74} _{-0.55}	6.18 ^{+3.54} _{-2.23}	89.8 ^{+43.1} _{-42.2}	0.047 ^{+0.032} _{-0.02}	244 ⁺¹⁶⁴ ₋₁₂₃	0.533 ^{+0.001} _{-0.001}	1.61 ^{+0.55} _{-0.94}
TOI - 5611	6.74 ^{+0.5} _{-0.6}	2.31 ^{+0.75} _{-0.55}	6.53 ^{+3.65} _{-2.28}	89.5 ^{+42.9} _{-42.5}	0.045 ^{+0.03} _{-0.019}	756 ⁺⁵⁰⁵ ₋₃₇₉	0.528 ^{+0.134} _{-0.001}	2.65 ^{+0.74} _{-1.5}
TOI - 6109	15.4 ^{+2.8} _{-1.9}	3.81 ^{+1.29} _{-0.96}	14.4 ^{+8.43} _{-5.3}	90.6 ^{+42.7} _{-42.7}	0.057 ^{+0.044} _{-0.026}	1350 ⁺⁹³¹ ₋₇₀₂	0.526 ^{+0.065} _{-0.001}	3.63 ^{+1.25} _{-2.16}
TOI - 2540	40.3 ^{+5.9} _{-4.4}	2.34 ^{+0.79} _{-0.59}	6.67 ^{+3.89} _{-2.45}	89.9 ^{+43.0} _{-42.3}	0.057 ^{+0.043} _{-0.025}	1050 ⁺⁷⁴³ ₋₅₇₃	0.507 ^{+0.035} _{-0.001}	1.7 ^{+0.57} _{-1.0}
Kepler - 25	3.55 ^{+0.1} _{-0.1}	3.06 ^{+0.98} _{-0.75}	10.19 ^{+5.61} _{-3.65}	89.7 ^{+43.2} _{-41.9}	0.045 ^{+0.03} _{-0.019}	359 ⁺²³⁴ ₋₁₈₁	0.572 ^{+0.428} _{-0.001}	3.85 ^{+0.69} _{-2.08}
TOI - 214	6.15 ^{+0.7} _{-1.0}	1.19 ^{+0.63} _{-0.35}	1.64 ^{+5.46} _{-1.15}	90.7 ^{+42.3} _{-42.5}	0.055 ^{+0.044} _{-0.025}	186 ⁺¹⁹⁸ ₋₁₁₂	0.538 ^{+0.081} _{-0.001}	0.61 ^{+1.67} _{-0.49}
TOI - 5493	5.36 ^{+0.4} _{-0.5}	2.55 ^{+1.98} _{-0.73}	7.64 ^{+11.3} _{-3.23}	89.4 ^{+43.4} _{-42.9}	0.044 ^{+0.028} _{-0.018}	505 ⁺⁷⁸⁶ ₋₃₀₁	0.536 ^{+0.178} _{-0.001}	2.52 ^{+2.63} _{-1.56}
TOI - 1446	10.7 ^{+2.1} _{-1.4}	1.91 ^{+0.66} _{-0.46}	4.84 ^{+18.35} _{-3.84}	90.2 ^{+42.9} _{-42.9}	0.059 ^{+0.046} _{-0.027}	445 ⁺²³² ₋₁₄₁	0.523 ^{+0.071} _{-0.001}	1.53 ^{+0.92} _{-0.62}
TOI - 1812	19.4 ^{+1.8} _{-1.4}	2.78 ^{+0.79} _{-0.79}	8.75 ^{+10.44} _{-3.59}	89.1 ^{+42.7} _{-42.7}	0.045 ^{+0.03} _{-0.019}	1190 ⁺⁶⁸⁸ ₋₆₀₄	0.506 ^{+0.062} _{-0.001}	2.34 ^{+1.89} _{-1.48}
TOI - 2202	60.9 ^{+3.0} _{-3.0}	9.89 ^{+2.58} _{-2.26}	65.01 ^{+28.75} _{-21.9}	87.2 ^{+4.8} _{-4.8}	0.038 ^{+0.023} _{-0.014}	13170 ⁺⁶⁰⁴⁰ ₋₆₀₄₀	0.287 ^{+0.485} _{-0.001}	12.05 ^{+5.77} _{-4.4}
TOI - 201	8.48 ^{+0.8} _{-0.5}	1.15 ^{+0.43} _{-0.29}	1.46 ^{+2.9} _{-0.923}	90.2 ^{+42.5} _{-42.7}	0.052 ^{+0.034} _{-0.023}	63 ⁺⁴⁷ ₋₃₂	0.538 ^{+0.222} _{-0.001}	0.38 ^{+0.58} _{-0.29}
TOI - 2350	18.5 ^{+2.2} _{-1.8}	4.42 ^{+3.38} _{-1.4}	18.21 ^{+26.46} _{-8.23}	90.2 ^{+42.7} _{-42.3}	0.055 ^{+0.041} _{-0.024}	1410 ⁺²¹⁶⁰ ₋₉₀₅	0.523 ^{+0.083} _{-0.001}	4.53 ^{+4.83} _{-2.91}
TOI - 700	5.36 ^{+1.0} _{-1.4}	1.52 ^{+1.43} _{-0.6}	3.89 ^{+33.78} _{-3.14}	89.5 ^{+1.6} _{-1.6}	0.03 ^{+0.029} _{-0.014}	1100 ⁺²⁰⁷⁰ ₋₈₇₅	0.89 ^{+0.101} _{-0.001}	2.53 ^{+25.92} _{-2.12}
LHS1140	12.2 ^{+0.8} _{-1.1}	1.19 ^{+0.39} _{-0.28}	1.64 ^{+2.72} _{-0.99}	88.1 ^{+4.6} _{-3.6}	0.047 ^{+0.029} _{-0.02}	2700 ⁺¹⁷⁷⁰ ₋₁₂₇₀	0.491 ^{+0.325} _{-0.001}	1.43 ^{+2.47} _{-0.87}
TOI - 2000	1.84 ^{+0.1} _{-0.1}	2.71 ^{+1.53} _{-0.72}	8.41 ^{+8.65} _{-3.25}	85.6 ^{+4.6} _{-3.4}	0.051 ^{+0.032} _{-0.022}	483 ⁺⁵⁴⁷ ₋₂₅₉	0.923 ^{+0.077} _{-0.001}	4.16 ^{+4.65} _{-1.77}
TOI - 1246	10.2 ^{+0.8} _{-0.7}	2.95 ^{+0.97} _{-0.73}	9.61 ^{+5.45} _{-3.48}	89.0 ^{+2.0} _{-2.0}	0.027 ^{+0.023} _{-0.013}	989 ⁺⁶⁶⁰ ₋₅₀₃	0.794 ^{+0.205} _{-0.001}	3.11 ^{+1.99} _{-1.22}
TOI - 699	22.2 ^{+7.5} _{-30.6}	2.37 ^{+0.78} _{-0.6}	6.8 ^{+3.86} _{-2.51}	90.6 ^{+42.8} _{-43.8}	0.035 ^{+0.029} _{-0.016}	234 ⁺¹⁵⁵ ₋₁₂₀	0.525 ^{+0.001} _{-0.001}	1.4 ^{+4.83} _{-0.86}
WASP - 84	0.694 ^{+0.0} _{-0.1} , 2.55 ^{+0.5} _{-0.1}	4.67 ^{+1.91} _{-1.2}	19.86 ^{+14.28} _{-7.44}	89.7 ^{+43.3} _{-42.6}	0.045 ^{+0.028} _{-0.019}	2600 ⁺²¹⁴⁰ ₋₁₃₀₀	0.642 ^{+0.358} _{-0.001} , 0.557 ^{+0.443} _{-0.001}	16.0 ^{+5.9} _{-8.89} , 10.37 ^{+3.29} _{-6.03}
HD15337	10.2 ^{+1.9} _{-0.9}	1.79 ^{+0.58} _{-0.46}	4.37 ^{+1.96} _{-1.021}	86.8 ^{+3.7} _{-3.7}	0.048 ^{+0.021} _{-0.021}	364 ⁺¹⁸⁴ ₋₁₃₈	0.497 ^{+0.404} _{-0.001}	1.38 ^{+4.79} _{-0.65}
TOI - 5738	1.19 ^{+7.0} _{-7.0}	1.41 ^{+1.29} _{-0.42}	2.94 ^{+24.75} _{-2.08}	90.8 ^{+42.3} _{-43.1}	0.046 ^{+0.031} _{-0.019}	514 ⁺⁹⁴² ₋₃₀₈	0.576 ^{+0.001} _{-0.001}	2.61 ^{+22.21} _{-2.34}
TOI - 4504	4.07 ^{+0.2} _{-0.2}	2.7 ^{+1.18} _{-0.71}	8.36 ^{+6.46} _{-3.2}	90.9 ^{+43.0} _{-43.0}	0.046 ^{+0.02} _{-0.02}	664 ⁺⁵⁸⁵ ₋₃₅₇	0.561 ^{+0.338} _{-0.001}	3.6 ^{+2.12} _{-2.12}
TOI - 2096	11.7 ^{+0.9} _{-0.5}	1.27 ^{+0.44} _{-0.3}	2.05 ^{+3.68} _{-1.24}	88.5 ^{+4.5} _{-4.5}	0.045 ^{+0.028} _{-0.019}	2560 ⁺¹⁷⁹⁰ ₋₁₂₃₀	0.47 ^{+0.467} _{-0.001}	1.54 ^{+2.93} _{-0.96}
TOI - 270	1.84 ^{+0.3} _{-0.4}	1.5 ^{+1.03} _{-0.52}	3.65 ^{+18.49} _{-2.81}	89.0 ^{+2.2} _{-2.8}	0.041 ^{+0.036} _{-0.02}	1310 ⁺¹⁸⁰⁰ ₋₉₁₁	0.905 ^{+0.091} _{-0.001}	3.57 ^{+20.28} _{-2.8}
TOI - 4093	32.1 ^{+5.4} _{-3.8}	2.92 ^{+0.99} _{-0.74}	9.46 ^{+5.54} _{-3.5}	90.4 ^{+42.5} _{-43.3}	0.057 ^{+0.043} _{-0.026}	1140 ⁺⁷⁸⁶ ₋₅₉₄	0.514 ^{+0.036} _{-0.001}	1.99 ^{+0.65} _{-1.19}
TOI - 714	16.9 ^{+1.5} _{-1.1}	1.37 ^{+0.5} _{-0.32}	2.67 ^{+5.13} _{-1.6}	90.1 ^{+42.6} _{-42.6}	0.046 ^{+0.03} _{-0.02}	714 ⁺⁵²² ₋₃₃₅	0.512 ^{+0.064} _{-0.001}	1.1 ^{+1.38} _{-0.79}
TOI - 1806	26.7 ^{+4.1} _{-2.9}	2.28 ^{+0.75} _{-0.57}	6.4 ^{+3.63} _{-2.34}	89.6 ^{+42.7} _{-42.6}	0.037 ^{+0.032} _{-0.017}	2710 ⁺¹⁷⁹⁰ ₋₁₃₆₀	0.504 ^{+0.03} _{-0.001}	2.55 ^{+0.59} _{-1.45}
TOI - 2086	11.7 ^{+0.8} _{-1.1}	2.37 ^{+0.79} _{-0.58}	6.8 ^{+3.91} _{-2.44}	91.3 ^{+41.6} _{-43.1}	0.046 ^{+0.03} _{-0.019}	570 ⁺³⁸⁵ ₋₂₈₆	0.534 ^{+0.097} _{-0.001}	2.03 ^{+0.66} _{-1.16}
TOI - 1338A	44.2 ^{+2.2} _{-2.4}	6.63 ^{+2.02} _{-1.59}	34.56 ^{+18.02} _{-12.15}	87.6 ^{+4.5} _{-3.6}	0.043 ^{+0.029} _{-0.018}	2090 ⁺¹²⁷⁰ ₋₁₀₀₀	0.488 ^{+0.468} _{-0.001}	5.76 ^{+3.51} _{-2.22}
TOI - 789	3.16 ^{+0.5} _{-0.7}	1.08 ^{+0.36} _{-0.26}	1.17 ^{+1.98} _{-0.89}	89.6 ^{+42.7} _{-42.4}	0.042 ^{+0.037} _{-0.02}	712 ⁺³⁷⁶ ₋₃₀₈	0.527 ^{+0.066} _{-0.001}	1.01 ^{+1.25} _{-0.76}
HD23472	5.36 ^{+0.2} _{-0.2}	1.1 ^{+0.35} _{-0.28}	1.25 ^{+2.23} _{-0.797}	88.6 ^{+1.5} _{-1.5}	0.023 ^{+0.02} _{-0.011}	202 ⁺¹⁰³ ₋₁₀₃	0.926 ^{+0.071} _{-0.001}	0.6 ^{+0.39} _{-0.39}
TOI - 5088	23.2 ^{+4.1} _{-3.0}	1.86 ^{+0.64} _{-0.64}	4.64 ^{+13.79} _{-2.85}	90.5 ^{+42.6} _{-43.1}	0.058 ^{+0.044} _{-0.026}	384 ⁺¹⁰³⁰ ₋₂₆₇	0.519 ^{+0.046} _{-0.001}	1.04 ^{+25.84} _{-0.001}
LTT3780	1.19 ^{+9.0} _{-7.0}	1.41 ^{+0.95} _{-0.41}	2.94 ^{+14.46} _{-2.04}	90.1 ^{+42.4} _{-43.1}	0.048 ^{+0.032} _{-0.02}	1160 ⁺¹⁵⁶⁰ ₋₆₇₆	0.558 ^{+0.001} _{-0.044}	3.39 ^{+17.27} _{-3.02}

Table 1 continued

Table 1 (continued)

Name	Period (d)	Radius (R_{\oplus})	Mass (M_{\oplus})	Inclination (deg)	Eccentricity	Transit Depth (ppm)	Transit Probability	RV Semi-amplitude (m/s)
TOI-2345	1.65 ^{+0.0} _{-0.1}	1.48 ^{+0.52} _{-0.37}	3.48 ^{+6.35} _{-2.19}	89.9 ^{+42.7} _{-43.1}	0.047 ^{+0.032} _{-0.02}	320 ⁺²³⁰ ₋₁₆₇	0.569 ^{+0.431} _{-0.001}	2.33 ^{+3.01} _{-1.74}
LHS1678	1.65 ^{+0.0} _{-0.1}	0.99 ^{+0.27} _{-0.23}	0.869 ^{+1.13} _{-0.52}	88.8 ^{+4.5} _{-3.6}	0.047 ^{+0.029} _{-0.019}	756 ⁺⁴¹⁵ ₋₃₅₄	0.835 ^{+0.164} _{-0.001}	0.97 ^{+1.34} _{-0.59}
TOI-5564	332.3 ^{+20.7} _{-23.6}	8.08 ^{+2.37} _{-1.89}	47.23 ^{+23.67} _{-16.23}	90.1 ^{+42.7} _{-41.2}	0.048 ^{+0.033} _{-0.021}	6930 ⁺⁴¹¹⁰ ₋₃₃₀₀	0.503 ^{+0.012} _{-0.001}	4.31 ^{+1.26} _{-2.45}
TOI-6249	576.2 ^{+52.7} _{-60.8}	2.71 ^{+0.9} _{-0.68}	8.41 ^{+4.82} _{-3.08}	90.2 ^{+42.9} _{-42.6}	0.059 ^{+0.046} _{-0.027}	1090 ⁺⁷⁴³ ₋₆₅₀	0.503 ^{+0.007} _{-0.001}	0.76 ^{+0.24} _{-0.44}
TOI-406	4.07 ^{+0.3} _{-0.31}	1.3 ^{+0.31} _{-0.31}	2.23 ^{+1.36} _{-1.36}	90.0 ^{+42.6} _{-42.6}	0.046 ^{+0.033} _{-0.019}	941 ⁺¹⁶⁵ ₋₁₄₄	0.526 ^{+0.001} _{-0.001}	1.71 ^{+1.25} _{-1.25}
TOI-1453	11.7 ^{+2.0} _{-1.4}	1.43 ^{+0.99} _{-0.48}	3.09 ^{+15.89} _{-2.34}	90.2 ^{+42.6} _{-42.6}	0.059 ^{+0.046} _{-0.027}	341 ⁺⁴⁷⁵ ₋₂₃₄	0.522 ^{+0.001} _{-0.001}	1.0 ^{+0.85} _{-0.85}
TOI-5788	9.29 ^{+0.8} _{-0.6}	1.6 ^{+0.54} _{-0.41}	4.55 ^{+2.87} _{-2.91}	90.5 ^{+43.8} _{-41.7}	0.045 ^{+0.03} _{-0.019}	291 ⁺¹⁹⁸ ₋₁₅₂	0.53 ^{+0.134} _{-0.001}	1.38 ^{+1.68} _{-1.05}
TOI-2104	23.2 ^{+11.3} _{-7.0}	1.46 ^{+0.5} _{-0.38}	3.32 ^{+2.15} _{-2.15}	90.2 ^{+42.8} _{-42.8}	0.022 ^{+0.022} _{-0.01}	346 ⁺²⁴² ₋₁₈₆	0.514 ^{+0.016} _{-0.001}	0.86 ^{+1.28} _{-0.68}
TOI-4305	661.2 ^{+28.6} _{-30.4}	4.63 ^{+1.42} _{-1.11}	19.6 ^{+10.31} _{-6.89}	89.7 ^{+43.1} _{-41.9}	0.041 ^{+0.025} _{-0.017}	238 ⁺¹⁴⁷ ₋₁₁₆	0.501 ^{+0.032} _{-0.001}	1.28 ^{+0.35} _{-0.73}
TOI-1027	1.65 ^{+0.0} _{-0.0}	2.64 ^{+0.9} _{-0.67}	8.07 ^{+4.76} _{-2.99}	89.6 ^{+42.3} _{-42.2}	0.04 ^{+0.036} _{-0.019}	1270 ⁺⁸⁹² ₋₆₈₁	0.564 ^{+0.436} _{-0.001}	5.71 ^{+1.61} _{-3.23}
TOI-178	33.6 ^{+31.1} _{-13.0}	2.13 ^{+0.73} _{-0.55}	5.75 ^{+3.41} _{-2.16}	89.3 ^{+0.8} _{-1.2}	0.018 ^{+0.015} _{-0.009}	903 ⁺⁶¹⁹ ₋₄₆₇	0.5 ^{+0.35} _{-0.001}	1.52 ^{+1.42} _{-0.78}
TOI-2103	3.89 ^{+0.5} _{-0.3} , 12.8 ^{+0.9} _{-1.2}	1.28 ^{+0.456} _{-0.31}	2.11 ^{+3.92} _{-1.3}	90.0 ^{+42.3} _{-42.3}	0.048 ^{+0.033} _{-0.02}	215 ⁺¹⁵⁶ ₋₁₀₈	0.542 ^{+0.219} _{-0.001} , 0.517 ^{+0.087} _{-0.001}	1.0 ^{+1.35} _{-0.74} , 0.67 ^{+0.92} _{-0.5}
TOI-4307	6.44 ^{+0.8} _{-0.6} , 21.2 ^{+1.7} _{-2.2}	1.06 ^{+0.37} _{-0.27}	1.1 ^{+1.99} _{-0.701}	89.4 ^{+42.8} _{-42.1}	0.05 ^{+0.035} _{-0.022}	78 ⁺⁵⁵ ₋₄₀	0.531 ^{+0.166} _{-0.001} , 0.511 ^{+0.064} _{-0.001}	0.35 ^{+0.47} _{-0.26} , 0.23 ^{+0.32} _{-0.18}
TOI-1798	0.694 ^{+5.0} _{-2.0}	1.63 ^{+0.56} _{-0.42}	4.86 ^{+8.6} _{-3.12}	90.0 ^{+43.4} _{-42.4}	0.049 ^{+0.033} _{-0.021}	367 ⁺²⁵⁵ ₋₁₉₃	0.627 ^{+0.001} _{-0.095}	3.84 ^{+5.75} _{-3.38}
K2-275	13.4 ^{+1.3} _{-0.7}	2.08 ^{+0.66} _{-0.63}	5.53 ^{+3.92} _{-3.04}	89.7 ^{+43.6} _{-43.6}	0.045 ^{+0.029} _{-0.019}	764 ⁺³⁸⁵ ₋₃₃₉	0.514 ^{+0.084} _{-0.001}	1.77 ^{+0.62} _{-0.57}
TOI-711	10.7 ^{+0.9} _{-0.7}	2.11 ^{+0.66} _{-0.52}	5.66 ^{+2.04} _{-2.04}	90.3 ^{+42.8} _{-42.8}	0.046 ^{+0.031} _{-0.019}	806 ⁺⁵³⁸ ₋₄₃₉	0.524 ^{+0.098} _{-0.001}	2.13 ^{+0.57} _{-1.22}
K2-266	33.6 ^{+8.9} _{-5.4}	1.57 ^{+0.64} _{-0.64}	4.27 ^{+5.18} _{-3.57}	89.1 ^{+1.9} _{-1.9}	0.03 ^{+0.027} _{-0.015}	423 ⁺⁹³² ₋₃₄₆	0.5 ^{+0.425} _{-0.001}	1.08 ^{+1.42} _{-0.92}
GJ143	11.7 ^{+1.1} _{-0.7}	1.17 ^{+1.14} _{-0.34}	1.55 ^{+14.62} _{-1.07}	88.2 ^{+4.5} _{-4.5}	0.053 ^{+0.035} _{-0.023}	242 ⁺⁴⁷¹ ₋₁₄₂	0.502 ^{+0.48} _{-0.001}	0.54 ^{+5.56} _{-0.39}
HD63433	10.7 ^{+1.3} _{-1.8}	2.22 ^{+0.55} _{-0.55}	6.13 ^{+3.48} _{-2.22}	89.0 ^{+4.5} _{-3.7}	0.049 ^{+0.031} _{-0.021}	500 ⁺³³¹ ₋₂₅₀	0.677 ^{+0.278} _{-0.001}	1.79 ^{+1.25} _{-0.71}
TOI-6454	6.15 ^{+0.4} _{-0.5}	3.78 ^{+1.18} _{-0.92}	14.22 ^{+7.63} _{-5.07}	90.4 ^{+42.0} _{-43.8}	0.044 ^{+0.029} _{-0.019}	1480 ⁺⁹⁴⁰ ₋₇₄₀	0.537 ^{+0.162} _{-0.001}	5.14 ^{+1.32} _{-2.93}
TOI-1752	1.48 ^{+0.0} _{-0.0}	1.87 ^{+0.62} _{-0.48}	4.68 ^{+16.27} _{-1.87}	90.6 ^{+42.7} _{-42.8}	0.046 ^{+0.031} _{-0.019}	1060 ⁺⁷⁰⁵ ₋₅₄₇	0.571 ^{+0.001} _{-0.05}	4.04 ^{+15.71} _{-3.22}
TOI-1746	7.39 ^{+1.2} _{-0.7}	1.36 ^{+0.48} _{-0.34}	2.6 ^{+4.78} _{-1.64}	90.0 ^{+43.0} _{-42.4}	0.059 ^{+0.045} _{-0.027}	923 ⁺⁶⁵⁵ ₋₄₆₆	0.519 ^{+0.074} _{-0.001}	1.57 ^{+1.95} _{-1.18}
TOI-815	437.6 ^{+29.3} _{-36.3}	2.19 ^{+0.71} _{-0.55}	6.0 ^{+3.35} _{-2.2}	91.2 ^{+42.4} _{-42.6}	0.05 ^{+0.037} _{-0.022}	698 ⁺⁴⁵⁸ ₋₃₅₈	0.512 ^{+0.01} _{-0.001}	0.58 ^{+0.18} _{-0.34}
TOI-1288	5.36 ^{+0.4} _{-0.2}	5.05 ^{+2.43} _{-1.3}	22.48 ^{+19.34} _{-8.43}	86.6 ^{+4.5} _{-3.7}	0.049 ^{+0.032} _{-0.021}	2100 ⁺²⁰²⁰ ₋₁₀₈₀	0.653 ^{+0.347} _{-0.001}	8.87 ^{+7.98} _{-3.6}
TOI-2274	4.46 ^{+0.3} _{-0.2}	1.39 ^{+1.04} _{-0.39}	2.8 ^{+16.45} _{-1.9}	90.4 ^{+43.8} _{-41.7}	0.045 ^{+0.029} _{-0.019}	408 ⁺⁶¹¹ ₋₂₃₀	0.54 ^{+0.247} _{-0.001}	1.51 ^{+6.58} _{-1.18}
TOI-6078	14.7 ^{+0.7} _{-0.7}	2.06 ^{+0.58} _{-0.52}	5.45 ^{+3.01} _{-2.01}	89.9 ^{+42.9} _{-41.5}	0.044 ^{+0.018} _{-0.018}	478 ⁺³⁴⁸ ₋₂₄₈	0.519 ^{+0.007} _{-0.001}	1.54 ^{+0.88} _{-0.88}
TOI-1749	15.4 ^{+3.1} _{-3.1}	1.83 ^{+0.62} _{-0.47}	4.52 ^{+15.29} _{-1.92}	87.5 ^{+2.3} _{-2.3}	0.042 ^{+0.036} _{-0.02}	930 ⁺⁶³⁹ ₋₄₈₉	0.407 ^{+0.511} _{-0.001}	1.67 ^{+6.27} _{-0.87}
TOI-2081	3.16 ^{+0.2} _{-0.2}	1.45 ^{+0.35} _{-0.35}	3.24 ^{+5.77} _{-1.99}	90.1 ^{+42.3} _{-42.3}	0.047 ^{+0.031} _{-0.02}	665 ⁺³²³ ₋₂₆₀	0.539 ^{+0.206} _{-0.001}	2.21 ^{+2.56} _{-1.61}
TOI-4010	29.2 ^{+4.3} _{-3.0}	3.75 ^{+2.89} _{-1.29}	14.04 ^{+20.59} _{-6.83}	88.3 ^{+1.5} _{-1.5}	0.028 ^{+0.025} _{-0.013}	1720 ⁺²⁶⁴⁰ ₋₁₁₈₀	0.494 ^{+0.482} _{-0.001}	3.17 ^{+5.12} _{-1.65}
TOI-712	27.9 ^{+2.1} _{-2.8} , 145.6 ^{+22.1} _{-14.2}	2.29 ^{+0.77} _{-0.58}	6.44 ^{+3.74} _{-2.38}	88.8 ^{+2.7} _{-2.3}	0.039 ^{+0.032} _{-0.018}	982 ⁺⁶⁶³ ₋₅₀₁	0.5 ^{+0.44} _{-0.001} , 0.446 ^{+0.148} _{-0.001}	1.68 ^{+1.14} _{-0.67} , 0.97 ^{+0.66} _{-0.4}
HD109833	4.07 ^{+0.4} _{-0.4}	2.63 ^{+0.88} _{-0.65}	8.02 ^{+4.63} _{-2.9}	87.2 ^{+4.4} _{-4.4}	0.057 ^{+0.041} _{-0.025}	581 ⁺³⁹² ₋₂₉₁	0.701 ^{+0.295} _{-0.001}	3.05 ^{+1.88} _{-1.21}
TOI-790	25.5 ^{+1.8} _{-2.3} , 63.8 ^{+6.8} _{-4.1}	2.47 ^{+2.9} _{-3.0}	7.26 ^{+17.51} _{-3.01}	89.9 ^{+42.1} _{-42.9}	0.047 ^{+0.031} _{-0.02}	240 ⁺⁵⁶⁵ ₋₁₃₉	0.517 ^{+0.083} _{-0.001} , 0.509 ^{+0.058} _{-0.001}	1.19 ^{+2.28} _{-0.74} , 0.88 ^{+1.65} _{-0.55}
TOI-2494	3.89 ^{+0.176} _{-0.0}	2.14 ^{+0.81} _{-0.54}	5.79 ^{+3.13} _{-2.13}	90.2 ^{+42.6} _{-42.1}	0.048 ^{+0.029} _{-0.02}	475 ⁺³⁶⁴ ₋₂₄₆	0.547 ^{+0.453} _{-0.001}	2.47 ^{+0.87} _{-1.43}
TOI-4468	12.2 ^{+1.1} _{-0.7}	3.44 ^{+1.27} _{-0.85}	12.25 ^{+7.88} _{-4.43}	90.7 ^{+42.6} _{-43.0}	0.047 ^{+0.03} _{-0.02}	1590 ⁺¹¹⁸⁰ ₋₇₈₈	0.526 ^{+0.109} _{-0.001}	3.88 ^{+1.25} _{-2.23}
TOI-1347	3.16 ^{+0.3} _{-0.2} , 7.39 ^{+0.7} _{-0.4}	1.59 ^{+0.52} _{-0.41}	4.46 ^{+7.37} _{-2.86}	90.7 ^{+42.4} _{-42.5}	0.049 ^{+0.032} _{-0.021}	297 ⁺¹⁹⁶ ₋₁₅₆	0.554 ^{+0.29} _{-0.001} , 0.532 ^{+0.185} _{-0.001}	2.07 ^{+2.21} _{-1.56} , 1.56 ^{+1.65} _{-1.17}
HD260655	1.65 ^{+0.1} _{-0.1}	1.25 ^{+0.43} _{-0.36}	1.94 ^{+3.45} _{-1.57}	88.4 ^{+4.7} _{-4.7}	0.048 ^{+0.032} _{-0.021}	678 ⁺³⁶⁷ ₋₂₆₇	0.868 ^{+0.13} _{-0.001}	1.82 ^{+3.51} _{-1.41}
TOI-1238	1.19 ^{+0.0} _{-0.0}	1.42 ^{+0.99} _{-0.42}	3.02 ^{+15.7} _{-2.12}	89.7 ^{+42.6} _{-42.6}	0.048 ^{+0.032} _{-0.021}	441 ⁺⁶¹⁶ ₋₂₆₂	0.576 ^{+0.001} _{-0.001}	2.55 ^{+2.01} _{-2.01}
TOI-880	26.7 ^{+6.1} _{-4.1}	3.33 ^{+2.31} _{-1.1}	11.64 ^{+15.12} _{-5.46}	90.2 ^{+42.0} _{-42.8}	0.04 ^{+0.036} _{-0.019}	1390 ⁺¹⁹³⁰ ₋₉₃₁	0.514 ^{+0.036} _{-0.001}	2.87 ^{+2.7} _{-1.9}
TOI-1659	9.29 ^{+1.8} _{-1.2}	1.45 ^{+1.03} _{-0.5}	3.24 ^{+17.42} _{-2.49}	90.2 ^{+42.8} _{-43.1}	0.059 ^{+0.019} _{-0.027}	175 ⁺²⁴⁹ ₋₁₂₂	0.529 ^{+0.085} _{-0.001}	0.93 ^{+4.03} _{-0.79}

Table 1 continued

Table 1 (continued)

Name	Period (d)	Radius (R_{\oplus})	Mass (M_{\oplus})	Inclination (deg)	Eccentricity	Transit Depth (ppm)	Transit Probability	RV Semi-amplitude (m/s)
TOI - 1064	22.2 $^{+2.4}_{-1.9}$	2.51 $^{+0.85}_{-0.63}$	7.45 $^{+4.36}_{-2.73}$	90.0 $^{+3.6}_{-4.6}$	0.057 $^{+0.043}_{-0.025}$	994 $^{+674}_{-500}$	0.55 $^{+0.386}_{-0.001}$	2.06 $^{+1.38}_{-0.83}$
TOI - 512	11.2 $^{+1.3}_{-1.2}$, 30.6 $^{+2.6}_{-2.1}$	1.5 $^{+0.51}_{-0.37}$	3.65 $^{+6.36}_{-2.27}$	90.6 $^{+42.1}_{-42.3}$	0.047 $^{+0.03}_{-0.02}$	243 $^{+167}_{-123}$	0.53 $^{+0.083}_{-0.001}$	1.1 $^{+1.47}_{-0.83}$, 0.79 $^{+1.02}_{-0.59}$
TOI - 5398	2.28 $^{+15.0}_{-12.0}$	3.52 $^{+2.08}_{-0.97}$	12.71 $^{+13.74}_{-5.07}$	89.9 $^{+3.7}_{-4.3}$	0.043 $^{+0.026}_{-0.018}$	945 $^{+1120}_{-521}$	0.949 $^{+0.001}_{-0.296}$	5.63 $^{+13.85}_{-3.92}$
TOI - 1692	9.29 $^{+1.1}_{-1.3}$	5.38 $^{+1.83}_{-1.39}$	24.84 $^{+4.61}_{-1.71}$	89.9 $^{+42.8}_{-42.1}$	0.056 $^{+0.041}_{-0.025}$	1140 $^{+786}_{-589}$	0.538 $^{+0.117}_{-0.001}$	6.17 $^{+2.45}_{-1.68}$
TOI - 266	18.5 $^{+2.9}_{-2.1}$	1.92 $^{+0.97}_{-0.69}$	4.88 $^{+1.12}_{-0.92}$	89.8 $^{+42.1}_{-42.1}$	0.058 $^{+0.026}_{-0.026}$	367 $^{+298}_{-196}$	0.515 $^{+0.039}_{-0.001}$	1.15 $^{+0.62}_{-0.37}$
TOI - 703	13.4 $^{+0.7}_{-0.7}$, 36.8 $^{+2.9}_{-2.5}$	2.17 $^{+0.71}_{-0.53}$	5.92 $^{+3.34}_{-2.12}$	89.6 $^{+41.9}_{-41.9}$	0.045 $^{+0.029}_{-0.019}$	478 $^{+316}_{-237}$	0.519 $^{+0.142}_{-0.001}$, 0.508 $^{+0.061}_{-0.001}$	1.66 $^{+0.5}_{-0.95}$, 1.19 $^{+0.37}_{-0.68}$
TOI - 553	19.4 $^{+3.1}_{-3.2}$	2.28 $^{+0.76}_{-0.56}$	6.4 $^{+3.68}_{-2.63}$	90.0 $^{+42.6}_{-43.1}$	0.046 $^{+0.03}_{-0.019}$	565 $^{+382}_{-285}$	0.515 $^{+0.043}_{-0.001}$	1.62 $^{+0.54}_{-0.95}$
K2 - 285	23.2 $^{+10.4}_{-6.2}$	2.39 $^{+0.83}_{-0.61}$	6.89 $^{+4.15}_{-2.57}$	89.0 $^{+1.9}_{-1.5}$	0.03 $^{+0.03}_{-0.014}$	769 $^{+536}_{-395}$	0.605 $^{+0.324}_{-0.001}$	1.75 $^{+1.41}_{-0.79}$
TOI - 1803	3.55 $^{+0.2}_{-0.3}$	3.07 $^{+0.96}_{-0.76}$	10.24 $^{+5.5}_{-3.71}$	89.3 $^{+42.4}_{-41.1}$	0.044 $^{+0.029}_{-0.019}$	1660 $^{+1080}_{-873}$	0.537 $^{+0.203}_{-0.001}$	5.01 $^{+1.44}_{-2.84}$
TOI - 451	5.87 $^{+0.4}_{-0.4}$	2.26 $^{+0.77}_{-0.57}$	6.31 $^{+3.72}_{-2.32}$	88.4 $^{+2.8}_{-2.2}$	0.039 $^{+0.031}_{-0.018}$	554 $^{+380}_{-282}$	0.841 $^{+0.159}_{-0.001}$	2.32 $^{+1.5}_{-0.9}$
TOI - 1533	2.05 $^{+14.0}_{-11.0}$	2.96 $^{+2.25}_{-0.8}$	9.66 $^{+13.95}_{-3.79}$	88.9 $^{+43.1}_{-42.4}$	0.046 $^{+0.029}_{-0.02}$	951 $^{+1450}_{-525}$	0.569 $^{+0.001}_{-0.058}$	5.45 $^{+11.37}_{-4.3}$
TOI - 932	4.89 $^{+0.3}_{-0.5}$	1.78 $^{+0.59}_{-0.45}$	4.33 $^{+13.34}_{-1.92}$	90.5 $^{+42.3}_{-43.8}$	0.044 $^{+0.029}_{-0.018}$	494 $^{+337}_{-262}$	0.54 $^{+0.142}_{-0.001}$	2.07 $^{+4.82}_{-1.3}$
TOI - 500	110.6 $^{+13.3}_{-9.1}$	1.69 $^{+2.74}_{-0.62}$	3.99 $^{+148.89}_{-2.85}$	82.8 $^{+1.5}_{-2.0}$	0.028 $^{+0.024}_{-0.013}$	519 $^{+1680}_{-382}$	0.009 $^{+0.013}_{-0.001}$	0.64 $^{+25.1}_{-0.47}$
TOI - 1208	6.44 $^{+0.8}_{-1.0}$	2.04 $^{+0.68}_{-0.52}$	5.37 $^{+3.09}_{-2.0}$	90.4 $^{+42.7}_{-42.8}$	0.038 $^{+0.032}_{-0.018}$	516 $^{+348}_{-268}$	0.532 $^{+0.082}_{-0.001}$	1.87 $^{+0.66}_{-1.11}$
TOI - 4643	16.9 $^{+1.4}_{-1.1}$	1.27 $^{+0.45}_{-0.31}$	2.05 $^{+3.39}_{-1.4}$	90.8 $^{+42.3}_{-42.8}$	0.047 $^{+0.032}_{-0.02}$	505 $^{+339}_{-283}$	0.519 $^{+0.072}_{-0.001}$	0.8 $^{+0.89}_{-1.09}$
TOI - 261	5.36 $^{+0.9}_{-0.9}$	2.93 $^{+0.95}_{-0.73}$	9.51 $^{+5.31}_{-3.46}$	89.9 $^{+42.8}_{-42.8}$	0.045 $^{+0.019}_{-0.02}$	440 $^{+223}_{-223}$	0.55 $^{+0.129}_{-0.001}$	3.33 $^{+1.99}_{-1.99}$
TOI - 4511	36.8 $^{+4.0}_{-4.0}$	2.66 $^{+0.93}_{-0.66}$	8.16 $^{+4.95}_{-2.96}$	90.3 $^{+42.3}_{-42.3}$	0.057 $^{+0.043}_{-0.026}$	593 $^{+419}_{-300}$	0.514 $^{+0.044}_{-0.001}$	1.55 $^{+0.55}_{-0.91}$
HD219134	692.2 $^{+61.2}_{-78.9}$	3.32 $^{+10.39}_{-1.89}$	11.59 $^{+97.32}_{-8.52}$	86.8 $^{+1.2}_{-1.8}$	0.018 $^{+0.016}_{-0.009}$	1560 $^{+9780}_{-1780}$	0.019 $^{+0.015}_{-0.001}$	0.96 $^{+8.69}_{-0.72}$
TOI - 1272	22.2 $^{+0.9}_{-0.9}$	4.08 $^{+1.23}_{-0.95}$	16.05 $^{+8.29}_{-5.49}$	90.1 $^{+43.1}_{-44.0}$	0.039 $^{+0.022}_{-0.016}$	2240 $^{+1360}_{-1060}$	0.514 $^{+0.105}_{-0.001}$	4.07 $^{+0.62}_{-2.22}$
TOI - 125	1.84 $^{+0.2}_{-0.3}$	2.74 $^{+0.92}_{-0.7}$	8.55 $^{+4.96}_{-3.19}$	89.9 $^{+2.2}_{-2.8}$	0.04 $^{+0.035}_{-0.019}$	873 $^{+587}_{-447}$	0.984 $^{+0.016}_{-0.001}$	4.94 $^{+3.59}_{-2.03}$
TOI - 4405	1.65 $^{+1.0}_{-1.0}$	1.44 $^{+1.03}_{-0.41}$	3.17 $^{+17.21}_{-2.17}$	89.8 $^{+42.2}_{-42.4}$	0.048 $^{+0.031}_{-0.021}$	369 $^{+532}_{-220}$	0.568 $^{+0.04}_{-0.001}$	2.22 $^{+13.37}_{-1.81}$
TOI - 4311	1.48 $^{+0.2}_{-0.1}$	1.56 $^{+1.19}_{-0.48}$	4.11 $^{+25.33}_{-3.0}$	90.6 $^{+42.8}_{-42.5}$	0.047 $^{+0.032}_{-0.02}$	283 $^{+432}_{-177}$	0.59 $^{+0.41}_{-0.001}$	2.57 $^{+12.56}_{-2.1}$
HD108236	46.3 $^{+27.7}_{-12.8}$	2.04 $^{+0.71}_{-0.52}$	5.37 $^{+3.24}_{-2.0}$	88.4 $^{+1.5}_{-1.1}$	0.023 $^{+0.021}_{-0.011}$	452 $^{+315}_{-230}$	0.417 $^{+0.369}_{-0.001}$	1.05 $^{+0.9}_{-0.51}$
Kepler - 411	1.65 $^{+0.1}_{-0.2}$	2.19 $^{+1.44}_{-0.62}$	6.0 $^{+7.34}_{-2.46}$	90.0 $^{+42.6}_{-42.3}$	0.044 $^{+0.028}_{-0.018}$	754 $^{+998}_{-442}$	0.574 $^{+0.253}_{-0.001}$	3.57 $^{+2.75}_{-2.09}$
TOI - 2267	5.87 $^{+1.5}_{-1.0}$	1.08 $^{+0.36}_{-0.27}$	1.17 $^{+1.99}_{-0.739}$	90.0 $^{+42.8}_{-42.3}$	0.042 $^{+0.038}_{-0.02}$	1660 $^{+1110}_{-720}$	0.515 $^{+0.041}_{-0.001}$	1.16 $^{+1.48}_{-0.89}$
TOI - 713	3.16 $^{+0.2}_{-0.2}$	1.23 $^{+0.37}_{-0.37}$	1.84 $^{+1.15}_{-0.82}$	89.9 $^{+43.0}_{-43.0}$	0.047 $^{+0.032}_{-0.02}$	300 $^{+187}_{-187}$	0.543 $^{+0.405}_{-0.001}$	1.05 $^{+0.84}_{-0.84}$
TOI - 4567	1.33 $^{+0.0}_{-0.0}$	1.51 $^{+1.05}_{-0.44}$	3.73 $^{+19.32}_{-2.59}$	90.6 $^{+42.4}_{-42.7}$	0.047 $^{+0.031}_{-0.02}$	518 $^{+720}_{-303}$	0.578 $^{+0.422}_{-0.001}$	3.07 $^{+11.32}_{-2.4}$
TOI - 1836	3.16 $^{+7.9}_{-0.2}$	2.77 $^{+3.0}_{-0.8}$	8.7 $^{+19.04}_{-3.62}$	89.6 $^{+43.2}_{-42.5}$	0.045 $^{+0.031}_{-0.019}$	246 $^{+533}_{-143}$	0.583 $^{+0.417}_{-0.045}$	3.25 $^{+5.36}_{-2.41}$
TOI - 2079	2.28 $^{+3.1}_{-0.2}$	1.25 $^{+0.45}_{-0.3}$	1.94 $^{+9.67}_{-1.19}$	90.2 $^{+42.1}_{-42.6}$	0.048 $^{+0.031}_{-0.021}$	570 $^{+411}_{-275}$	0.546 $^{+0.185}_{-0.01}$	1.54 $^{+1.95}_{-1.22}$
TOI - 786	23.2 $^{+2.3}_{-2.8}$	2.07 $^{+0.69}_{-0.52}$	5.49 $^{+3.16}_{-2.02}$	90.1 $^{+42.4}_{-42.6}$	0.046 $^{+0.03}_{-0.019}$	210 $^{+141}_{-107}$	0.521 $^{+0.068}_{-0.001}$	1.19 $^{+0.38}_{-0.69}$

Table 2. DYNAMITE v3 predictions for the 2023 dataset with the PRM model

Name	Period (d)	Radius (R_{\oplus})	Mass (M_{\oplus})	Inclination (deg)	Eccentricity	Transit Depth (ppm)	Transit Probability	RV Semi-amplitude (m/s)
TOI - 512	40.3 ^{15.2}	1.62 ^{0.56}	4.75 ^{8.49}	90.1 ^{43.0}	0.071 ^{0.064}	283 ¹⁹⁸	0.511 ^{0.022}	0.94 ^{1.35}
HD63935	40.3 ^{16.2}	2.93 ^{1.03}	9.51 ^{5.8}	90.0 ^{0.38}	0.072 ^{0.063}	783 ⁵⁵⁴	0.535 ^{0.25}	1.87 ^{1.51}
TOI - 6022	7.3 ^{39.5}	3.85 ^{1.94}	14.64 ^{8.94}	90.0 ^{43.7}	0.075 ^{0.037}	9110 ⁸²⁰⁰	0.517 ^{0.001}	1.86 ^{1.85}
TOI - 789	23.2 ^{10.2}	1.11 ^{0.29}	1.29 ^{0.836}	89.8 ^{42.6}	0.045 ^{0.044}	75 ²³⁹⁵	0.505 ^{0.011}	9.58 ^{7.98}
TOI - 451	4.07 ^{0.9}	2.33 ^{0.59}	6.53 ^{3.92}	88.4 ^{2.8}	0.045 ^{0.043}	579 ⁴⁰³	0.907 ^{0.001}	0.57 ^{0.74}
TOI - 487	50.7 ^{25.2}	2.43 ^{0.84}	7.08 ^{4.24}	90.1 ^{43.1}	0.07 ^{0.063}	488 ¹⁰³⁰	0.51 ^{0.04}	2.71 ^{2.06}
HR858	25.5 ^{5.2}	2.05 ^{0.7}	5.41 ^{2.04}	86.5 ^{2.2}	0.044 ^{0.043}	488 ¹⁰¹⁰	0.51 ^{0.009}	1.23 ^{0.46}
TOI - 125	40.3 ^{14.8}	2.79 ^{0.96}	8.83 ^{2.4}	89.9 ^{2.2}	0.044 ^{0.043}	906 ⁶²⁴	0.555 ^{0.001}	1.07 ^{0.86}
TOI - 880	27.9 ^{6.9}	3.66 ^{1.34}	13.52 ^{6.94}	89.9 ^{42.7}	0.045 ^{0.022}	1670 ²¹³⁰	0.511 ^{0.001}	1.82 ^{1.39}
TOI - 2086	10.2 ^{1.6}	2.55 ^{0.88}	7.64 ^{2.88}	90.2 ^{42.9}	0.07 ^{0.061}	660 ⁴⁶¹	0.525 ^{0.055}	3.28 ^{2.97}
TOI - 4010	2.5 ^{0.1}	3.71 ^{2.81}	13.81 ^{9.85}	88.3 ^{1.9}	0.028 ^{0.026}	1680 ²⁵⁴⁰	0.98 ^{0.02}	2.39 ^{1.9}
TOI - 2202	73.2 ^{29.1}	12.15 ^{4.09}	89.99 ^{52.39}	86.9 ^{3.7}	0.069 ^{0.061}	19880 ¹³⁴⁰⁰	0.259 ^{0.074}	7.04 ^{3.55}
HD109833	33.6 ^{7.1}	2.71 ^{0.93}	8.41 ^{3.12}	86.5 ^{4.5}	0.071 ^{0.065}	617 ⁴²⁷	0.356 ^{0.178}	15.71 ^{13.81}
TOI - 1272	25.5 ^{5.8}	4.64 ^{1.6}	19.66 ^{7.74}	90.1 ^{43.2}	0.072 ^{0.039}	2900 ²⁰⁰	0.511 ^{0.004}	1.58 ^{1.21}
TOI - 5126	36.8 ^{3.5}	4.11 ^{1.43}	16.74 ^{9.88}	88.1 ^{4.5}	0.071 ^{0.034}	960 ⁶⁵⁷	0.468 ^{0.001}	4.77 ^{2.81}
TOI - 1446	12.8 ^{5.5}	1.96 ^{0.51}	5.04 ^{3.03}	89.7 ^{43.2}	0.073 ^{0.035}	468 ³²⁸	0.518 ^{0.001}	2.79 ^{2.14}
TOI - 1782	9.2 ^{1.1}	2.42 ^{0.62}	7.03 ^{2.63}	89.9 ^{42.7}	0.044 ^{0.042}	468 ²⁴⁸	0.518 ^{0.001}	1.51 ^{0.94}
TOI - 815	5.8 ^{0.7}	2.34 ^{0.8}	6.67 ^{3.94}	90.1 ^{42.8}	0.068 ^{0.06}	1100 ⁷⁷⁷	0.531 ^{0.001}	2.77 ^{1.63}
TOI - 213	46.3 ^{21.4}	1.64 ^{1.13}	4.96 ^{2.33}	90.1 ^{42.5}	0.07 ^{0.063}	797 ⁵⁵¹	0.521 ^{0.085}	2.71 ^{0.92}
TOI - 904	183.1 ^{43.7}	2.44 ^{0.63}	7.12 ^{2.63}	89.8 ^{42.5}	0.069 ^{0.033}	1770 ¹²⁰	0.508 ^{0.014}	1.14 ^{0.77}
TOI - 6729	15.4 ^{4.1}	1.99 ^{0.5}	5.16 ^{1.89}	90.0 ^{42.7}	0.073 ^{0.035}	96 ⁴⁹	0.534 ^{0.001}	1.18 ^{0.79}
HD93963A	7.39 ^{1.8}	2.03 ^{0.74}	5.33 ^{3.16}	85.3 ^{3.4}	0.074 ^{0.069}	320 ²⁷⁸	0.41 ^{0.001}	1.16 ^{0.54}
L98 - 59	25.5 ^{5.9}	1.29 ^{0.46}	2.17 ^{4.04}	87.0 ^{2.0}	0.031 ^{0.029}	1550 ¹¹⁵⁰	0.126 ^{0.326}	1.63 ^{3.19}
TOI - 1438	18.5 ^{1.1}	2.63 ^{0.92}	8.02 ^{4.86}	89.7 ^{42.6}	0.072 ^{0.067}	865 ⁶¹⁴	0.513 ^{0.024}	1.03 ^{2.4}
TOI - 2095	9.2 ^{1.7}	1.28 ^{0.45}	2.11 ^{3.85}	88.4 ^{3.6}	0.073 ^{0.064}	711 ⁵⁰⁴	0.519 ^{0.343}	2.09 ^{0.89}
HD23472	53.1 ^{14.9}	1.11 ^{0.29}	1.29 ^{0.836}	88.2 ^{1.1}	0.023 ^{0.011}	205 ¹⁰⁸	0.267 ^{0.001}	1.11 ^{2.36}
TOI - 4418	53.1 ^{11.9}	2.47 ^{0.86}	7.26 ^{2.7}	90.2 ^{42.5}	0.07 ^{0.062}	763 ⁵³⁹	0.509 ^{0.015}	0.29 ^{0.2}
TOI - 6078	53.1 ^{12.2}	2.24 ^{0.77}	6.22 ^{2.35}	90.1 ^{43.0}	0.071 ^{0.034}	566 ³⁹⁴	0.509 ^{0.016}	1.31 ^{0.82}
TOI - 1757	9.2 ^{2.7}	1.65 ^{0.42}	3.84 ^{4.48}	89.8 ^{43.0}	0.074 ^{0.068}	458 ³³¹	0.521 ^{0.001}	1.15 ^{0.72}
TOI - 261	6.44 ^{0.7}	3.17 ^{1.11}	10.77 ^{6.54}	90.1 ^{42.7}	0.071 ^{0.034}	515 ²⁶⁷	0.546 ^{0.188}	1.53 ^{0.48}
TOI - 836	18.5 ^{1.9}	1.93 ^{0.67}	4.92 ^{1.94}	89.2 ^{4.3}	0.073 ^{0.066}	697 ⁴⁵⁵	0.544 ^{0.272}	3.55 ^{1.19}
LP791 - 18	10.3 ^{2.9}	1.59 ^{0.65}	4.46 ^{3.73}	89.2 ^{2.2}	0.044 ^{0.044}	1030 ⁸⁰⁰	0.532 ^{0.001}	1.54 ^{0.08}
TOI - 1288	6.44 ^{2.2}	6.54 ^{2.29}	33.82 ^{56.28}	86.6 ^{3.7}	0.067 ^{0.06}	6560 ⁵⁴¹⁰	0.532 ^{0.001}	4.88 ^{4.9}
TOI - 786	80.2 ^{30.9}	2.21 ^{0.77}	6.09 ^{2.68}	90.2 ^{42.9}	0.07 ^{0.061}	3520 ²⁴⁷⁰	0.592 ^{0.376}	12.57 ^{6.92}
TOI - 1208	5.8 ^{0.6}	2.1 ^{0.72}	5.62 ^{2.11}	90.3 ^{42.5}	0.045 ^{0.022}	239 ¹⁶⁸	0.511 ^{0.001}	0.87 ^{0.54}
TOI - 2300	36.8 ^{12.5}	4.21 ^{1.52}	16.86 ^{19.19}	90.3 ^{43.0}	0.07 ^{0.064}	547 ²⁸⁷	0.534 ^{0.001}	2.02 ^{0.67}
TOI - 5493	53.1 ^{28.6}	3.42 ^{1.64}	12.14 ^{17.84}	90.2 ^{43.7}	0.07 ^{0.062}	2350 ²⁹¹⁰	0.512 ^{0.019}	3.27 ^{2.28}
TOI - 214	36.8 ^{8.6}	1.31 ^{0.64}	2.28 ^{1.68}	89.7 ^{42.7}	0.072 ^{0.035}	909 ²³⁰	0.511 ^{0.017}	1.87 ^{2.24}
						225 ¹⁴⁷	0.507 ^{0.001}	0.46 ^{0.39}

Table 2 continued

Table 2 (continued)

Name	Period (d)	Radius (R_{\oplus})	Mass (M_{\oplus})	Inclination (deg)	Eccentricity	Transit Depth (ppm)	Transit Probability	RV Semi-amplitude (m/s)
TOI - 1266	36.8 ^{+14.1} _{-8.4}	1.78 ^{+0.61} _{-0.46}	4.33 ^{+13.86} _{-4.3}	88.4 ^{+3.8} _{-4.3}	0.072 ^{+0.064} _{-0.035}	1510 ⁺¹⁰⁴⁰ ₋₇₉₃	0.433 ^{+0.068} _{-0.001}	1.46 ^{+5.41} _{-7.7}
TOI - 2274	5.36 ^{+2.2} _{-1.3}	1.85 ^{+1.2} _{-0.72}	4.6 ^{+7.58} _{-2.6}	89.9 ^{+42.6} _{-42.6}	0.074 ^{+0.071} _{-0.036}	723 ⁺³⁹ ₋₅₆₄	0.529 ^{+0.05} _{-0.001}	2.34 ^{+15.29} _{-1.89}
TOI - 1659	11.7 ^{+1.3} _{-0.9}	1.6 ^{+0.61} _{-0.4}	4.55 ^{+20.9} _{-6.9}	90.1 ^{+42.6} _{-42.6}	0.074 ^{+0.038} _{-0.033}	213 ⁺¹⁶³ ₋₆₃₇	0.524 ^{+0.009} _{-0.001}	1.21 ^{+1.02} _{-0.61}
TOI - 5611	58.2 ^{+34.3} _{-24.8}	2.5 ^{+0.87} _{-0.65}	7.49 ^{+2.82} _{-4.8}	90.6 ^{+42.9} _{-42.9}	0.07 ^{+0.063} _{-0.033}	900 ⁺⁶³⁷ ₋₄₈₅	0.512 ^{+0.014} _{-0.001}	1.49 ^{+0.61} _{-0.95}
TOI - 1749	18.7 ⁺⁵ _{-4.4}	1.85 ^{+0.63} _{-0.48}	4.1 ^{+6.06} _{-3.3}	87.9 ^{+2.3} _{-2.3}	0.045 ^{+0.044} _{-0.022}	951 ⁺⁵⁰⁴ ₋₅₀₄	0.388 ^{+0.001} _{-0.001}	1.6 ^{+0.8} _{-0.8}
TOI - 4495	11.7 ^{+4.6} _{-2.8}	2.44 ^{+0.85} _{-0.63}	7.12 ^{+3.43} _{-2.68}	89.9 ^{+43.0} _{-43.0}	0.073 ^{+0.069} _{-0.036}	279 ⁺¹⁹⁶ ₋₁₄₆	0.53 ^{+0.056} _{-0.001}	1.81 ^{+0.78} _{-1.13}
LHS1140	53.1 ^{+28.4} _{-11.9}	1.31 ^{+0.46} _{-0.33}	2.28 ^{+1.47} _{-1.45}	88.2 ^{+4.4} _{-4.4}	0.07 ^{+0.063} _{-0.033}	3270 ⁺²³⁰⁰ ₋₁₆₅₀	0.441 ^{+0.056} _{-0.001}	1.22 ^{+2.51} _{-0.83}
TOI - 1225	29.2 ^{+11.5} _{-7.3}	2.79 ^{+0.97} _{-0.71}	8.8 ^{+3.37} _{-3.7}	90.0 ^{+43.3} _{-43.3}	0.071 ^{+0.065} _{-0.034}	829 ⁺⁵⁸⁴ ₋₄₃₃	0.512 ^{+0.021} _{-0.001}	1.87 ^{+0.78} _{-1.16}
TOI - 2392	11.7 ^{+3.1} _{-2.1}	3.1 ^{+2.09} _{-1.8}	10.5 ^{+3.95} _{-3.95}	89.8 ^{+42.8} _{-42.8}	0.073 ^{+0.035} _{-0.035}	264 ⁺¹³⁸ ₋₁₃₈	0.537 ^{+0.001} _{-0.001}	2.61 ^{+1.63} _{-1.63}
TOI - 2441	29.2 ^{+11.2} _{-6.8}	2.31 ^{+0.8} _{-0.59}	6.5 ^{+3.92} _{-4.3}	89.9 ^{+43.1} _{-43.1}	0.071 ^{+0.065} _{-0.034}	2050 ⁺¹⁴³⁰ ₋₁₀₅₀	0.507 ^{+0.015} _{-0.001}	2.26 ^{+0.73} _{-1.35}
TOI - 4311	29.2 ^{+11.9} _{-7.6}	1.93 ^{+1.3} _{-0.75}	4.92 ^{+6.49} _{-3.32}	89.8 ^{+43.3} _{-43.3}	0.071 ^{+0.065} _{-0.034}	433 ⁺⁵⁸⁵ ₋₃₄₀	0.51 ^{+0.018} _{-0.001}	1.12 ^{+0.25} _{-0.9}
K2 - 266	36.8 ^{+14.0} _{-8.2}	1.74 ^{+1.68} _{-0.79}	4.17 ^{+5.43} _{-3.42}	88.7 ^{+1.9} _{-1.5}	0.031 ^{+0.029} _{-0.015}	519 ⁺¹⁰⁰⁰ ₋₄₇₃	0.497 ^{+0.344} _{-0.001}	1.03 ^{+0.22} _{-0.87}
TOI - 2494	29.3 ^{+8.3} _{-5.2}	3.69 ^{+7.19} _{-1.78}	13.69 ^{+61.9} _{-8.85}	89.8 ^{+42.7} _{-42.8}	0.071 ^{+0.068} _{-0.034}	1410 ⁺⁵⁵¹⁰ ₋₁₃₇₀	0.513 ^{+0.003} _{-0.001}	3.37 ^{+13.04} _{-2.64}
K2 - 285	26.7 ^{+10.7} _{-7.6}	2.41 ^{+0.83} _{-0.62}	6.98 ^{+4.16} _{-2.92}	89.4 ^{+1.5} _{-1.3}	0.031 ^{+0.031} _{-0.015}	782 ⁺⁵⁴⁰ ₋₄₆₉	0.575 ^{+0.337} _{-0.001}	1.69 ^{+1.34} _{-1.76}
TOI - 969	3.5 ^{+1.0} _{-0.6}	2.75 ^{+0.7} _{-0.4}	8.6 ^{+3.19} _{-3.19}	85.2 ^{+3.8} _{-3.8}	0.07 ^{+0.034} _{-0.034}	1420 ⁺⁷²² ₋₆₆₉	0.499 ^{+0.425} _{-0.001}	4.44 ^{+1.97} _{-1.97}
TOI - 713	76.6 ^{+30.3} _{-30.3}	1.63 ^{+0.69} _{-0.69}	4.86 ^{+32.74} _{-4.13}	90.1 ^{+43.3} _{-43.3}	0.07 ^{+0.061} _{-0.033}	527 ⁺⁸⁵⁸ ₋₄₅₅	0.506 ^{+0.006} _{-0.001}	0.96 ^{+0.03} _{-0.87}
TOI - 5738	58.2 ^{+16.2} _{-16.2}	1.86 ^{+0.76} _{-0.76}	4.65 ^{+2.47} _{-3.39}	90.4 ^{+43.0} _{-43.0}	0.07 ^{+0.062} _{-0.033}	895 ⁺¹⁴²⁰ ₋₇₃₄	0.51 ^{+0.009} _{-0.001}	1.13 ^{+0.49} _{-0.94}
TOI - 1130	29.2 ^{+11.6} _{-7.0}	5.61 ^{+2.33} _{-2.51}	26.54 ^{+16.03} _{-16.14}	88.8 ^{+4.4} _{-4.4}	0.074 ^{+0.069} _{-0.036}	5560 ⁺²⁴⁴⁰⁰ ₋₄₉₇₀	0.5 ^{+0.248} _{-0.001}	6.94 ^{+1.42} _{-4.54}
Kepler - 25	26.7 ^{+10.7} _{-6.8}	3.28 ^{+1.15} _{-0.85}	11.37 ^{+6.91} _{-4.29}	90.1 ^{+43.2} _{-43.2}	0.072 ^{+0.065} _{-0.035}	413 ⁺²⁹⁴ ₋₂₂₀	0.519 ^{+0.034} _{-0.001}	2.2 ^{+0.7} _{-1.32}
TOI - 1812	23.2 ^{+1.0} _{-1.1}	3.57 ^{+1.4} _{-1.4}	12.99 ^{+0.29} _{-0.29}	90.3 ^{+43.7} _{-43.7}	0.068 ^{+0.058} _{-0.001}	1960 ⁺²⁰⁵⁰ ₋₁₁₃₀	0.516 ^{+0.059} _{-0.001}	3.28 ^{+2.85} _{-2.23}
TOI - 790	19.4 ^{+4.5} _{-4.6}	84.0 ^{+12.3} _{-11.7}	11.53 ^{+6.57} _{-6.1}	90.3 ^{+42.6} _{-42.6}	0.065 ^{+0.053} _{-0.033}	432 ⁺³⁵⁹ ₋₁₅₁₅	0.525 ^{+0.041} _{-0.001}	2.08 ^{+5.01} _{-1.28}
TOI - 5696	15.4 ^{+2.7} _{-2.7}	2.8 ^{+0.98} _{-0.73}	9.05 ^{+3.39} _{-3.35}	90.1 ^{+42.9} _{-42.9}	0.07 ^{+0.064} _{-0.034}	98 ⁺⁶⁸⁶ ₋₅₁₅	0.518 ^{+0.001} _{-0.001}	2.51 ^{+0.92} _{-1.49}
HD28109	159.6 ^{+6.2} _{-40.9}	2.79 ^{+0.95} _{-0.73}	8.8 ^{+5.18} _{-3.35}	88.5 ^{+2.3} _{-2.3}	0.044 ^{+0.042} _{-0.021}	311 ⁺¹²³ ₋₁₆₄	0.449 ^{+0.058} _{-0.001}	0.89 ^{+0.74} _{-0.42}
TOI - 6293	4.89 ^{+0.6} _{-0.8}	9.12 ^{+3.02} _{-2.27}	57.19 ^{+32.68} _{-20.81}	89.9 ^{+42.8} _{-42.8}	0.068 ^{+0.059} _{-0.032}	8080 ⁺⁵³⁵⁰ ₋₄₀₃₀	0.546 ^{+0.113} _{-0.001}	25.4 ^{+7.89} _{-14.6}
TOI - 1803	29.2 ^{+11.0} _{-6.9}	3.38 ^{+1.17} _{-0.88}	11.92 ^{+7.14} _{-4.52}	90.2 ^{+43.1} _{-43.1}	0.071 ^{+0.065} _{-0.034}	2020 ⁺¹⁴⁴⁰ ₋₁₁₁₀	0.512 ^{+0.002} _{-0.001}	2.91 ^{+1.7} _{-1.8}
HD22946	20.3 ^{+1.4} _{-1.4}	2.03 ^{+0.53} _{-0.53}	5.33 ^{+1.99} _{-1.99}	90.3 ^{+43.7} _{-43.7}	0.045 ^{+0.022} _{-0.001}	276 ⁺¹²² ₋₁₂₂	0.52 ^{+0.005} _{-0.001}	1.17 ^{+0.35} _{-0.35}
HIP9618	121.2 ^{+29.5} _{-29.5}	3.56 ^{+0.91} _{-0.91}	12.94 ^{+7.81} _{-4.82}	90.2 ^{+43.0} _{-43.0}	0.069 ^{+0.058} _{-0.033}	1130 ⁺⁷⁸⁹ ₋₅₇₉	0.507 ^{+0.009} _{-0.001}	1.65 ^{+0.64} _{-0.99}
TOI - 2076	69.9 ^{+32.0} _{-21.9}	2.99 ^{+1.02} _{-0.78}	9.82 ^{+3.73} _{-3.73}	90.0 ^{+43.1} _{-43.1}	0.044 ^{+0.042} _{-0.021}	1270 ⁺⁸⁶⁵ ₋₆₆₂	0.505 ^{+0.007} _{-0.001}	1.74 ^{+0.64} _{-1.07}
TOI - 810	12.2 ^{+2.6} _{-2.8}	191.7 ^{+76.3} _{-47.8}	8.11 ^{+4.88} _{-3.04}	90.3 ^{+42.9} _{-42.9}	0.069 ^{+0.059} _{-0.033}	301 ⁺²¹¹ ₋₁₅₇	0.535 ^{+0.061} _{-0.001}	2.23 ^{+0.89} _{-1.34}
TOI - 4504	230.3 ^{+22.6} _{-55.5}	3.99 ^{+8.37} _{-1.66}	15.49 ^{+7.97} _{-8.7}	90.6 ^{+42.9} _{-42.9}	0.066 ^{+0.056} _{-0.031}	1450 ⁺⁶⁰⁸⁰ ₋₁₂₂₀	0.509 ^{+0.007} _{-0.001}	1.74 ^{+7.41} _{-1.29}
Kepler - 411	16.9 ^{+7.1} ₋₃	2.81 ^{+0.73} _{-0.53}	8.85 ^{+10.08} _{-4.36}	90.3 ^{+43.0} _{-43.0}	0.072 ^{+0.066} _{-0.035}	1230 ⁺¹⁵³⁰ ₋₉₂₆	0.518 ^{+0.028} _{-0.001}	2.43 ^{+1.94} _{-1.68}
TOI - 700	69.9 ^{+32.2} _{-22.2}	1.6 ^{+0.66} _{-0.46}	4.55 ^{+3.83} _{-3.83}	89.5 ^{+1.5} _{-1.5}	0.031 ^{+0.015} _{-0.015}	1220 ⁺¹⁰¹⁰ ₋₇₁₀	0.498 ^{+0.008} _{-0.001}	1.28 ^{+1.11} _{-1.11}
TOI - 663	15.4 ^{+6.1} _{-6.1}	2.4 ^{+0.62} _{-0.62}	6.94 ^{+2.61} _{-4.16}	89.7 ^{+42.7} _{-42.7}	0.045 ^{+0.043} _{-0.022}	1840 ⁺¹²⁸⁰ ₋₉₅₉	0.51 ^{+0.001} _{-0.001}	2.8 ^{+0.88} _{-1.87}
TOI - 4342	23.2 ^{+5.7} _{-4.6}	2.38 ^{+0.6} _{-0.6}	6.62 ^{+2.48} _{-2.48}	88.4 ^{+3.7} _{-3.7}	0.072 ^{+0.067} _{-0.035}	1270 ⁺⁶⁵⁴ ₋₄₀₈	0.479 ^{+0.001} _{-0.001}	2.02 ^{+1.53} _{-0.9}
TOI - 1670	252.4 ^{+104.0} _{-65.9}	3.25 ^{+8.39} _{-1.3}	11.2 ^{+72.89} _{-26.2}	88.2 ^{+2.2} _{-2.2}	0.044 ^{+0.039} _{-0.022}	510 ⁺²⁶³⁰ ₋₄₀₈	0.258 ^{+0.13} _{-0.001}	1.07 ^{+0.36} _{-0.6}
HD73583	38.5 ^{+15.0} _{-8.1}	2.42 ^{+0.84} _{-0.62}	7.03 ^{+4.23} _{-2.63}	89.4 ^{+3.3} _{-3.3}	0.071 ^{+0.064} _{-0.034}	1170 ⁺⁸¹² ₋₆₀₁	0.5 ^{+0.144} _{-0.001}	1.65 ^{+1.24} _{-0.73}
TOI - 2103	40.3 ^{+16.6} _{-10.9}	1.38 ^{+0.48} _{-0.36}	2.73 ^{+4.92} _{-3.6}	90.0 ^{+43.1} _{-43.1}	0.072 ^{+0.065} _{-0.035}	250 ⁺¹⁷⁷ ₋₁₇₇	0.509 ^{+0.018} _{-0.001}	0.59 ^{+0.85} _{-0.47}
TOI - 4156	26.7 ^{+10.9} _{-6.8}	2.61 ^{+0.67} _{-0.67}	7.92 ^{+2.96} _{-2.96}	90.1 ^{+42.6} _{-42.6}	0.071 ^{+0.034} _{-0.034}	529 ⁺²⁷⁷ ₋₂₇₇	0.514 ^{+0.001} _{-0.001}	1.59 ^{+0.69} _{-0.69}
TOI - 201	132.8 ^{+53.7} _{-32.4}	1.77 ^{+0.76} _{-0.76}	4.29 ^{+583.03} _{-3.36}	90.2 ^{+42.9} _{-42.9}	0.067 ^{+0.058} _{-0.032}	149 ⁺¹⁷⁹⁰ ₋₁₂₉	0.508 ^{+0.001} _{-0.001}	0.45 ^{+11.66} _{-0.39}
TOI - 1798	15.4 ^{+6.3} _{-4.1}	1.72 ^{+0.6} _{-0.44}	4.1 ^{+1.31} _{-1.31}	89.9 ^{+43.0} _{-43.0}	0.073 ^{+0.067} _{-0.036}	409 ⁺²⁸⁸ ₋₂₁₃	0.516 ^{+0.001} _{-0.001}	1.16 ^{+2.94} _{-0.79}

Table 2 continued

Table 2 (continued)

Name	Period (d)	Radius (R_{\oplus})	Mass (M_{\oplus})	Inclination (deg)	Eccentricity	Transit Depth (ppm)	Transit Probability	RV Semi-amplitude (m/s)
TOI - 4468	16.9 ^{+8.4} _{-4.4}	5.53 ^{+12.41} _{-2.41}	25.95 ^{+82.21} _{-15.44}	90.0 ^{+42.8} _{-43.1}	0.073 ^{+0.067} _{-0.036}	4120 ⁺¹²¹⁰⁰ ₋₃₅₉₀	0.515 ^{+0.028} _{-0.001}	7.39 ^{+19.1} _{-5.53}
TOI - 711	73.2 ^{+28.9} _{-28.9}	2.28 ^{+0.79} _{-0.39}	6.4 ^{+3.84} _{-2.41}	90.3 ^{+42.9} _{-42.9}	0.07 ^{+0.061} _{-0.034}	941 ⁺⁶⁸⁷ ₋₅₃₃	0.509 ^{+0.006} _{-0.001}	1.27 ^{+0.65} _{-0.79}
TOI - 199	36.8 ^{+10.7} _{-10.7}	9.03 ^{+5.05} _{-2.15}	56.3 ^{+38.46} _{-15.15}	89.2 ^{+41.5} _{-41.5}	0.047 ^{+0.019} _{-0.019}	10190 ⁺⁷⁹⁰⁰ ₋₇₉₀₀	0.505 ^{+0.001} _{-0.001}	11.29 ^{+1.79} _{-1.79}
TOI - 1873	12.8 ^{+1.0} _{-1.0}	3.39 ^{+1.15} _{-0.86}	11.97 ^{+4.43} _{-4.43}	90.1 ^{+42.5} _{-42.5}	0.041 ^{+0.036} _{-0.036}	1030 ⁺⁷⁰⁴ ₋₅₃₂	0.522 ^{+0.111} _{-0.001}	3.24 ^{+1.04} _{-1.89}
TOI - 3353	18.9 ^{+4.8} _{-4.8}	2.28 ^{+0.59} _{-0.59}	6.43 ^{+2.41} _{-2.41}	90.0 ^{+43.3} _{-43.3}	0.073 ^{+0.067} _{-0.035}	420 ⁺²⁹⁰ ₋₂₂₁	0.518 ^{+0.031} _{-0.001}	1.55 ^{+0.63} _{-0.97}
TOI - 1470	55.6 ^{+12.4} _{-12.4}	2.30 ^{+0.86} _{-0.62}	6.49 ^{+3.91} _{-2.6}	88.7 ^{+4.4} _{-4.4}	0.07 ^{+0.064} _{-0.034}	2010 ⁺¹⁴⁰⁰ ₋₁₀₃₀	0.496 ^{+0.001} _{-0.001}	1.86 ^{+0.85} _{-0.61}
TOI - 4304	63.8 ^{+34.8} _{-34.8}	2.39 ^{+0.82} _{-0.62}	6.89 ^{+4.09} _{-2.6}	89.8 ^{+43.2} _{-43.2}	0.071 ^{+0.062} _{-0.034}	280 ⁺¹⁹⁴ ₋₁₄₈	0.508 ^{+0.014} _{-0.001}	0.95 ^{+0.45} _{-0.61}
TOI - 553	84.0 ^{+34.0} _{-34.0}	2.47 ^{+0.86} _{-0.63}	7.26 ^{+4.38} _{-2.6}	90.2 ^{+43.1} _{-43.1}	0.069 ^{+0.06} _{-0.033}	663 ⁺⁴⁶⁸ ₋₃₄₆	0.508 ^{+0.008} _{-0.001}	1.13 ^{+0.55} _{-0.7}
TOI - 421	36.8 ^{+7.7} _{-7.7}	3.61 ^{+1.38} _{-1.38}	13.23 ^{+7.37} _{-5.03}	86.7 ^{+3.7} _{-3.7}	0.07 ^{+0.033} _{-0.033}	1450 ⁺¹¹¹⁰ ₋₁₁₁₀	0.343 ^{+0.001} _{-0.001}	2.84 ^{+1.66} _{-1.66}
TOI - 270	21.9 ^{+4.4} _{-4.4}	1.62 ^{+1.03} _{-0.61}	4.75 ^{+3.21} _{-2.21}	88.4 ^{+2.2} _{-2.2}	0.045 ^{+0.043} _{-0.022}	1530 ⁺¹⁹⁴⁰ ₋₁₁₅₀	0.491 ^{+0.162} _{-0.001}	2.06 ^{+10.58} _{-1.71}
TOI - 1445	20.8 ^{+6.6} _{-6.6}	2.37 ^{+0.82} _{-0.61}	6.8 ^{+4.08} _{-2.55}	90.1 ^{+42.9} _{-42.9}	0.072 ^{+0.067} _{-0.035}	420 ⁺²⁹³ ₋₂₂₀	0.517 ^{+0.028} _{-0.001}	1.41 ^{+0.65} _{-0.89}
TOI - 5564	15.3 ^{+2.4} _{-2.4}	9.38 ^{+3.16} _{-2.4}	59.79 ^{+32.31} _{-22.31}	89.6 ^{+42.8} _{-42.8}	0.068 ^{+0.058} _{-0.032}	9340 ⁺⁶³⁵⁰ ₋₄₈₅₀	0.516 ^{+0.038} _{-0.001}	15.19 ^{+5.2} ₋₁₅
TOI - 1752	73.2 ^{+33.1} _{-25.2}	2.03 ^{+0.7} _{-0.53}	5.33 ^{+3.18} _{-2.02}	90.4 ^{+42.7} _{-42.7}	0.07 ^{+0.061} _{-0.033}	1250 ⁺⁸⁶³ ₋₆₅₅	0.507 ^{+0.005} _{-0.001}	1.26 ^{+0.49} _{-0.76}
TOI - 178	36.8 ^{+13.8} _{-13.8}	2.13 ^{+0.74} _{-0.54}	5.75 ^{+3.46} _{-2.15}	88.9 ^{+1.2} _{-1.2}	0.018 ^{+0.015} _{-0.009}	903 ⁺⁶²⁸ ₋₄₆₈	0.498 ^{+0.443} _{-0.001}	1.47 ^{+1.18} _{-0.6}
TOI - 1346	11.7 ^{+2.9} _{-2.9}	2.61 ^{+0.67} _{-0.67}	7.92 ^{+2.96} _{-2.96}	89.8 ^{+42.4} _{-42.4}	0.073 ^{+0.035} _{-0.035}	931 ⁺⁴⁹² ₋₄₉₂	0.517 ^{+0.001} _{-0.001}	2.56 ^{+1.58} _{-1.58}
TOI - 1338A	576.9 ^{+67.1} _{-67.1}	7.49 ^{+2.54} _{-1.89}	41.9 ^{+4.49} _{-4.49}	88.5 ^{+4.4} _{-4.4}	0.059 ^{+0.044} _{-0.026}	2670 ⁺¹⁸¹⁰ ₋₁₃₅₀	0.375 ^{+0.105} _{-0.001}	2.97 ^{+1.23} _{-1.23}
TOI - 2345	87.9 ^{+33.8} _{-26.6}	1.58 ^{+0.55} _{-0.44}	4.36 ^{+2.77} _{-1.89}	90.1 ^{+43.0} _{-43.0}	0.07 ^{+0.063} _{-0.034}	365 ⁺²⁶⁰ ₋₁₉₃	0.505 ^{+0.008} _{-0.001}	0.78 ^{+1.19} _{-0.6}
WASP - 132	18.9 ^{+8.0} _{-8.0}	3.12 ^{+1.52} _{-1.52}	10.5 ^{+6.94} _{-4.4}	88.4 ^{+3.4} _{-3.4}	0.072 ^{+0.068} _{-0.035}	1450 ⁺⁷⁶³⁰ ₋₁₄₂₀	0.501 ^{+0.255} _{-0.001}	3.02 ^{+2.72} _{-2.09}
TOI - 2540	46.3 ^{+16.9} _{-16.9}	2.42 ^{+0.85} _{-0.62}	7.03 ^{+4.28} _{-2.63}	90.1 ^{+43.7} _{-43.7}	0.071 ^{+0.062} _{-0.034}	1130 ⁺⁸²⁴ ₋₆₂₁	0.508 ^{+0.017} _{-0.001}	1.71 ^{+0.69} _{-1.06}
HD63433	36.8 ^{+15.5} _{-15.5}	2.36 ^{+0.81} _{-0.61}	6.76 ^{+4.01} _{-2.4}	89.8 ^{+3.7} _{-3.7}	0.071 ^{+0.065} _{-0.034}	565 ⁺³⁹⁰ ₋₂₉₄	0.512 ^{+0.221} _{-0.001}	1.31 ^{+1.91} _{-1.91}
TOI - 1260	26.7 ^{+1.6} _{-1.6}	2.83 ^{+0.98} _{-0.73}	9.0 ^{+3.38} _{-2.4}	88.7 ^{+1.9} _{-1.9}	0.03 ^{+0.029} _{-0.015}	1500 ⁺¹⁰⁴⁰ ₋₇₇₅	0.496 ^{+0.001} _{-0.001}	2.49 ^{+1.83} _{-1.83}
TOI - 1062	18.7 ^{+1.1} _{-1.1}	2.53 ^{+0.87} _{-0.65}	7.54 ^{+4.49} _{-2.82}	86.7 ^{+3.6} _{-3.6}	0.073 ^{+0.067} _{-0.035}	762 ⁺⁵⁴⁹ ₋₄₂₄	0.439 ^{+0.271} _{-0.001}	1.90 ^{+1.43} _{-0.84}
TOI - 1052	92.0 ^{+38.3} _{-23.7}	4.01 ^{+1.61} _{-1.61}	15.55 ^{+25.64} _{-6.6}	88.4 ^{+3.7} _{-3.7}	0.068 ^{+0.061} _{-0.032}	847 ⁺¹⁴⁴⁰ ₋₆₈₃	0.496 ^{+0.046} _{-0.001}	1.95 ^{+3.83} _{-1.19}
TOI - 2269	5.36 ^{+0.6} _{-0.6}	1.58 ^{+0.55} _{-0.44}	4.36 ^{+2.77} _{-1.89}	90.2 ^{+42.7} _{-42.7}	0.071 ^{+0.065} _{-0.034}	694 ⁺⁴⁸⁶ ₋₃₅₅	0.528 ^{+0.096} _{-0.001}	2.42 ^{+2.88} _{-1.79}
TOI - 4305	692.2 ^{+11.0} _{-28.7}	4.88 ^{+1.53} _{-1.18}	21.29 ^{+1.47} _{-1.47}	89.9 ^{+43.2} _{-43.2}	0.047 ^{+0.03} _{-0.019}	264 ⁺¹⁶⁷ ₋₁₃₀	0.504 ^{+0.033} _{-0.001}	1.37 ^{+0.39} _{-0.78}
TOI - 2322	40.3 ^{+8.9} _{-8.9}	1.15 ^{+0.29} _{-0.29}	1.46 ^{+2.93} _{-1.46}	90.0 ^{+42.1} _{-42.1}	0.072 ^{+0.035} _{-0.035}	227 ⁺¹⁵¹ ₋₁₅₁	0.509 ^{+0.008} _{-0.001}	0.35 ^{+0.27} _{-0.27}
TOI - 4093	36.8 ^{+2.4} _{-2.4}	3.02 ^{+1.05} _{-0.78}	9.98 ^{+3.75} _{-2.93}	89.9 ^{+42.7} _{-42.7}	0.071 ^{+0.064} _{-0.034}	1220 ⁺⁸⁶² ₋₆₄₆	0.509 ^{+0.019} _{-0.001}	2.01 ^{+1.25} _{-1.25}
TOI - 4405	11.7 ^{+3.1} _{-3.1}	1.80 ^{+0.67} _{-0.67}	4.31 ^{+1.04} _{-0.86}	90.0 ^{+42.8} _{-42.8}	0.073 ^{+0.068} _{-0.035}	577 ⁺⁷¹² ₋₄₄₁	0.519 ^{+0.033} _{-0.001}	1.61 ^{+1.96} _{-1.3}
TOI - 1404	29.2 ^{+11.2} _{-11.2}	2.71 ^{+0.94} _{-0.69}	8.41 ^{+5.05} _{-3.12}	90.2 ^{+42.8} _{-42.8}	0.071 ^{+0.065} _{-0.034}	582 ⁺⁴⁰⁶ ₋₃₀₀	0.515 ^{+0.022} _{-0.001}	1.57 ^{+0.67} _{-0.97}
TOI - 776	32.1 ^{+2.6} _{-2.6}	1.94 ^{+0.66} _{-0.51}	4.96 ^{+1.96} _{-1.87}	87.9 ^{+4.4} _{-4.4}	0.071 ^{+0.065} _{-0.034}	1080 ⁺⁷⁴² ₋₅₇₆	0.475 ^{+0.057} _{-0.001}	1.51 ^{+6.84} _{-0.69}
TOI - 5143	13.4 ^{+5.5} _{-5.5}	4.93 ^{+3.13} _{-2.47}	21.64 ^{+79.23} _{-14.42}	90.0 ^{+42.8} _{-42.8}	0.073 ^{+0.07} _{-0.036}	2800 ⁺⁹²⁴⁰ ₋₂₈₂₀	0.521 ^{+0.034} _{-0.001}	6.22 ^{+19.6} _{-4.98}
TOI - 554	15.4 ^{+7.7} _{-7.7}	1.92 ^{+0.66} _{-0.66}	4.88 ^{+3.59} _{-2.6}	89.9 ^{+42.9} _{-42.9}	0.072 ^{+0.034} _{-0.034}	152 ⁺¹³⁹ ₋₁₃₉	0.526 ^{+0.001} _{-0.001}	1.08 ^{+0.91} _{-0.91}
TOI - 1746	7.39 ^{+2.0} _{-2.0}	1.42 ^{+0.36} _{-0.36}	3.02 ^{+5.53} _{-1.92}	90.3 ^{+42.8} _{-42.8}	0.074 ^{+0.07} _{-0.036}	1010 ⁺¹⁵¹² ₋₅₁₅	0.521 ^{+0.027} _{-0.001}	1.82 ^{+5.55} _{-1.41}
GJ143	15.4 ^{+1.6} _{-1.6}	1.64 ^{+1.38} _{-1.38}	4.96 ^{+4.23} _{-2.3}	88.0 ^{+3.8} _{-3.8}	0.07 ^{+0.061} _{-0.033}	475 ⁺⁴⁰⁷ ₋₃₀₀	0.496 ^{+0.001} _{-0.001}	1.58 ^{+12.68} _{-1.36}
TOI - 4307	66.8 ^{+34.9} _{-34.9}	1.14 ^{+0.43} _{-0.3}	1.41 ^{+2.85} _{-1.92}	89.8 ^{+43.2} _{-43.2}	0.072 ^{+0.066} _{-0.035}	91 ⁺⁶⁹ ₋₄₈	0.505 ^{+0.012} _{-0.001}	0.20 ^{+0.36} _{-0.16}
TOI - 431	23.9 ^{+6.1} _{-6.1}	2.01 ^{+0.81} _{-0.81}	5.2 ^{+2.99} _{-2.99}	85.1 ^{+2.2} _{-2.2}	0.045 ^{+0.043} _{-0.022}	631 ⁺¹¹⁴⁰ ₋₅₅₀	0.108 ^{+0.255} _{-0.001}	1.37 ^{+3.09} _{-0.9}
TOI - 4443	20.3 ^{+6.6} _{-6.6}	1.91 ^{+0.67} _{-0.67}	4.84 ^{+18.84} _{-3.33}	89.7 ^{+43.0} _{-43.0}	0.072 ^{+0.067} _{-0.033}	296 ⁺²¹⁰ ₋₁₆₅	0.513 ^{+0.028} _{-0.001}	1.13 ^{+7.6} _{-0.68}
TOI - 1730	25.5 ^{+6.2} _{-6.2}	2.09 ^{+0.54} _{-0.54}	5.58 ^{+2.3} _{-2.3}	90.1 ^{+42.9} _{-42.9}	0.045 ^{+0.022} _{-0.001}	1310 ⁺⁶⁸³ ₋₆₈₃	0.51 ^{+0.001} _{-0.001}	1.86 ^{+1.11} _{-1.11}
TOI - 4567	50.7 ^{+25.4} _{-25.4}	1.86 ^{+0.68} _{-0.68}	4.64 ^{+37.54} _{-3.05}	90.0 ^{+42.8} _{-42.8}	0.07 ^{+0.063} _{-0.033}	785 ⁺¹⁰¹⁰ ₋₅₇₆	0.507 ^{+0.001} _{-0.001}	1.14 ^{+7.89} _{-0.89}
TOI - 2016	12.8 ^{+1.3} _{-1.3}	3.04 ^{+0.78} _{-0.78}	10.08 ^{+6.03} _{-3.77}	90.0 ^{+42.7} _{-42.7}	0.044 ^{+0.041} _{-0.021}	1100 ⁺⁷⁷² ₋₅₈₀	0.52 ^{+0.081} _{-0.001}	3.01 ^{+0.98} _{-1.77}

Table 2 continued

Table 2 (continued)

Name	Period (d)	Radius (R_{\oplus})	Mass (M_{\oplus})	Inclination (deg)	Eccentricity	Transit Depth (ppm)	Transit Probability	RV Semi-amplitude (m/s)
TOI - 797	7.39 ^{+3.3} ₋₀	1.20 ⁺⁴¹ ₋₃₁	1.69 ^{+2.97} _{-1.09}	90.2 ^{+42.5} _{-42.6}	0.046 ^{+0.045} _{-0.023}	539 ⁺³⁷⁰ ₋₂₈₁	0.521 ^{+0.03} _{-0.001}	0.92 ^{+1.22} _{-0.71}
TOI - 1706	15.4 ^{+3.3} ₋₀	1.77 ^{+0.62} _{-0.45}	4.29 ^{+15.9} _{-0.45}	90.0 ^{+42.8} _{-42.8}	0.073 ^{+0.068} _{-0.035}	280 ⁺¹⁹⁸ ₋₁₄₅	0.518 ^{+0.034} _{-0.001}	1.11 ^{+3.04} _{-0.74}
TOI - 6655	26.7 ^{+6.9} _{-0.7}	2.38 ^{+0.84} _{-0.69}	6.85 ^{+2.15} _{-0.935}	90.0 ^{+42.9} _{-42.9}	0.072 ^{+0.035} _{-0.001}	575 ⁺³⁰¹ ₋₁₆₅	0.513 ^{+0.001} _{-0.001}	1.49 ^{+0.94} _{-0.94}
TOI - 1238	7.39 ^{+1.7} _{-0.7}	1.78 ^{+0.67} _{-0.67}	4.33 ^{+29.05} _{-0.04}	89.8 ^{+42.8} _{-42.8}	0.074 ^{+0.036} _{-0.001}	693 ⁺⁸³⁴ ₋₅₂₃	0.522 ^{+0.043} _{-0.001}	1.99 ^{+0.5} _{-1.6}
TOI - 2104	27.9 ^{+1.3} _{-0.3}	1.46 ^{+0.51} _{-0.37}	3.22 ^{+6.01} _{-1.1}	89.6 ^{+43.4} _{-43.4}	0.023 ^{+0.021} _{-0.011}	346 ⁺²⁴⁶ ₋₁₈₂	0.507 ^{+0.017} _{-0.001}	0.81 ^{+1.19} _{-0.63}
TOI - 2096	15.4 ^{+5.6} _{-3.3}	1.42 ^{+0.49} _{-0.37}	3.02 ^{+3.37} _{-1.95}	88.4 ^{+3.8} _{-4.4}	0.073 ^{+0.068} _{-0.035}	3200 ⁺²²³⁰ ₋₁₆₉₀	0.445 ^{+0.001} _{-0.001}	2.07 ^{+1.31} _{-1.42}
TOI - 4511	46.3 ^{+16.9} _{-9.6}	2.76 ^{+0.96} _{-0.71}	8.65 ^{+2.21} _{-3.24}	90.1 ^{+43.0} _{-43.0}	0.07 ^{+0.064} _{-0.033}	638 ⁺⁴⁴⁹ ₋₃₃₅	0.51 ^{+0.021} _{-0.001}	1.53 ^{+0.58} _{-0.94}
TOI - 4643	20.3 ^{+2.5} _{-3.8}	1.41 ^{+0.48} _{-0.37}	2.94 ^{+1.15} _{-0.87}	90.4 ^{+42.7} _{-42.7}	0.072 ^{+0.066} _{-0.035}	623 ⁺⁴²⁶ ₋₃₂₉	0.515 ^{+0.015} _{-0.001}	1.07 ^{+1.42} _{-0.84}
TOI - 872	9.2 ^{+5.6} _{-1.6}	2.54 ^{+0.66} _{-0.58}	7.59 ^{+2.87} _{-1.91}	90.0 ^{+42.7} _{-42.7}	0.074 ^{+0.036} _{-0.001}	939 ⁺⁵⁰³ ₋₃₀₅	0.524 ^{+0.001} _{-0.001}	2.71 ^{+1.75} _{-1.0}
TOI - 1269	18.5 ^{+4.9} _{-1.8}	2.25 ^{+0.58} _{-0.58}	6.27 ^{+2.35} _{-2.35}	89.9 ^{+42.6} _{-42.6}	0.072 ^{+0.067} _{-0.035}	589 ⁺⁴¹⁴ ₋₃₁₁	0.515 ^{+0.001} _{-0.001}	1.55 ^{+0.67} _{-0.97}
TOI - 1444	32.1 ^{+1.8} _{-0.8}	2.07 ^{+0.79} _{-0.89}	5.49 ^{+2.1} _{-2.3}	80.3 ^{+4.5} _{-3.7}	0.072 ^{+0.066} _{-0.035}	435 ⁺⁷⁵² ₋₃₇₄	0.05 ^{+0.045} _{-0.001}	1.15 ^{+2.26} _{-0.73}
TOI - 561	139.0 ^{+1.6} _{-37.2}	2.38 ^{+0.82} _{-0.61}	6.85 ^{+4.08} _{-2.56}	90.0 ^{+1.1} _{-1.5}	0.023 ^{+0.021} _{-0.011}	675 ⁺⁴⁶⁵ ₋₃₄₆	0.511 ^{+0.001} _{-0.001}	0.97 ^{+0.81} _{-0.45}
TOI - 6109	18.5 ^{+7.9} _{-4.8}	3.96 ^{+1.37} _{-1.02}	15.31 ^{+9.17} _{-5.75}	90.3 ^{+42.6} _{-43.0}	0.072 ^{+0.067} _{-0.035}	1460 ⁺¹⁰³⁰ ₋₇₇₅	0.52 ^{+0.028} _{-0.001}	3.63 ^{+1.52} _{-2.26}
HD260655	11.7 ^{+5.4} _{-1.0}	1.36 ^{+0.48} _{-0.35}	2.6 ^{+4.78} _{-1.4}	88.5 ^{+4.5} _{-4.5}	0.073 ^{+0.069} _{-0.035}	803 ⁺⁵⁶⁷ ₋₄₀₈	0.502 ^{+0.263} _{-0.001}	1.27 ^{+2.73} _{-1.77}
TOI - 216	84.0 ^{+26.3} _{-3.0}	6.78 ^{+1.74} _{-1.74}	35.8 ^{+13.39} _{-3.39}	90.2 ^{+42.9} _{-42.9}	0.068 ^{+0.032} _{-0.001}	6010 ⁺⁴²²⁰ ₋₃₁₈₀	0.508 ^{+0.001} _{-0.001}	6.24 ^{+3.74} _{-3.74}
TOI - 2081	20.3 ^{+5.6} ₋₆	1.58 ^{+0.56} _{-0.41}	4.36 ^{+2.81} _{-0.6}	90.3 ^{+43.1} _{-42.6}	0.072 ^{+0.066} _{-0.035}	789 ⁺⁵⁶² ₋₄₁₂	0.515 ^{+0.015} _{-0.001}	1.61 ^{+2.25} _{-0.97}
TOI - 763	24.10 ⁺² _{-3.2}	2.43 ^{+0.84} _{-0.62}	7.08 ^{+4.24} _{-2.63}	89.7 ^{+43.3} _{-42.7}	0.072 ^{+0.067} _{-0.034}	613 ⁺³¹³ ₋₃₁₃	0.511 ^{+0.001} _{-0.001}	1.66 ^{+0.53} _{-0.99}
TOI - 1246	10.9 ^{+0.9} _{-0.9}	3.08 ^{+1.06} _{-0.79}	10.29 ^{+6.13} _{-3.85}	88.6 ^{+1.9} _{-1.5}	0.03 ^{+0.03} _{-0.014}	1080 ⁺⁵⁷³ ₋₅₆₇	0.797 ^{+0.202} _{-0.001}	3.33 ^{+2.27} _{-1.35}
TOI - 714	20.3 ^{+5.4} _{-4.4}	1.52 ^{+0.53} _{-0.39}	3.82 ^{+6.89} _{-2.44}	90.0 ^{+42.8} _{-42.8}	0.072 ^{+0.067} _{-0.035}	879 ⁺⁶¹⁴ ₋₄₅₃	0.51 ^{+0.016} _{-0.001}	1.48 ^{+1.99} _{-1.14}
TOI - 699	7.39 ^{+1.2} _{-0.7}	2.48 ^{+0.86} _{-0.73}	7.31 ^{+2.79} _{-1.91}	89.9 ^{+43.0} _{-42.9}	0.043 ^{+0.043} _{-0.001}	256 ⁺¹⁷⁹ ₋₁₀₉	0.541 ^{+0.11} _{-0.001}	2.18 ^{+0.83} _{-0.77}
HD219134	11.7 ^{+0.6} _{-0.6}	2.97 ^{+1.6} _{-1.6}	9.72 ^{+6.86} _{-4.64}	86.8 ^{+0.8} _{-0.8}	0.018 ^{+0.015} _{-0.009}	1250 ⁺⁸⁰⁴⁰ ₋₁₃₅₀	0.236 ^{+0.001} _{-0.001}	3.15 ^{+2.69} _{-2.69}
TOI - 1027	20.3 ^{+9.4} _{-3.6}	2.71 ^{+0.93} _{-0.7}	8.41 ^{+4.99} _{-13.16}	90.2 ^{+42.8} _{-42.9}	0.045 ^{+0.043} _{-0.022}	1330 ⁺⁹⁴⁶ ₋₇₂₉	0.515 ^{+0.001} _{-0.001}	2.58 ^{+1.62} _{-1.62}
TOI - 3485	24.36 ⁺⁴ _{-4.4}	1.77 ^{+0.59} _{-0.45}	4.12 ^{+2.07} _{-2.05}	89.9 ^{+42.9} _{-42.4}	0.072 ^{+0.067} _{-0.035}	419 ⁺²⁹⁵ ₋₂₂₉	0.513 ^{+0.022} _{-0.001}	1.13 ^{+2.83} _{-0.79}
TOI - 6054	26.7 ^{+0.5} _{-0.5}	2.66 ^{+0.92} _{-0.68}	8.16 ^{+4.89} _{-3.04}	89.7 ^{+43.3} _{-42.8}	0.072 ^{+0.066} _{-0.035}	229 ⁺¹⁶⁰ ₋₁₁₉	0.519 ^{+0.037} _{-0.001}	1.59 ^{+0.66} _{-0.99}
TOI - 286	80.2 ^{+30.8} _{-29.3}	1.57 ^{+0.55} _{-0.41}	4.27 ^{+7.76} _{-2.76}	90.3 ^{+42.9} _{-43.0}	0.071 ^{+0.062} _{-0.034}	332 ⁺²³⁶ ₋₁₇₈	0.508 ^{+0.006} _{-0.001}	0.71 ^{+1.14} _{-0.55}
TOI - 4600	9.2 ^{+5.6} _{-1.6}	7.69 ^{+1.98} _{-1.98}	43.68 ^{+6.39} _{-3.9}	89.3 ^{+4.5} _{-4.5}	0.076 ^{+0.037} _{-0.001}	7580 ⁺³²⁴⁰ ₋₃₂₄₀	0.645 ^{+0.001} _{-0.001}	14.4 ^{+6.77} _{-6.77}
TOI - 703	46.3 ^{+17.9} _{-10.0}	2.36 ^{+0.82} _{-0.61}	6.76 ^{+2.54} _{-1.6}	90.0 ^{+43.0} _{-42.6}	0.07 ^{+0.063} _{-0.033}	565 ⁺³⁹⁶ ₋₂₉₆	0.51 ^{+0.018} _{-0.001}	1.26 ^{+0.52} _{-0.78}
TOI - 1064	26.7 ^{+6.4} _{-6.4}	2.6 ^{+0.67} _{-0.67}	7.87 ^{+2.96} _{-2.96}	89.9 ^{+4.4} _{-4.4}	0.072 ^{+0.064} _{-0.035}	1070 ⁺⁷³⁹ ₋₅₅₀	0.526 ^{+0.001} _{-0.001}	2.05 ^{+0.93} _{-0.93}
TOI - 1347	9.2 ^{+4.1} _{-2.5}	1.68 ^{+0.59} _{-0.43}	3.95 ^{+11.27} _{-2.01}	90.1 ^{+42.8} _{-42.8}	0.074 ^{+0.069} _{-0.036}	331 ⁺²³⁵ ₋₁₇₃	0.525 ^{+0.038} _{-0.001}	1.28 ^{+2.83} _{-0.88}
TOI - 6249	7.39 ^{+1.0} _{-1.2}	2.78 ^{+0.95} _{-0.71}	8.75 ^{+5.17} _{-3.26}	90.1 ^{+43.1} _{-42.5}	0.067 ^{+0.058} _{-0.032}	1150 ⁺⁸⁰⁴ ₋₆₁₀	0.527 ^{+0.073} _{-0.001}	3.4 ^{+2.1} _{-2.1}
LHS1678	8.1 ^{+3.3} _{-1.9}	1.10 ^{+0.39} _{-0.28}	1.25 ^{+2.31} _{-0.797}	89.5 ^{+3.8} _{-3.8}	0.074 ^{+0.07} _{-0.036}	934 ⁺⁶⁵⁵ ₋₄₇₉	0.536 ^{+0.287} _{-0.001}	0.82 ^{+1.77} _{-0.56}
TOI - 2079	18.5 ^{+4.9} _{-1.9}	1.36 ^{+0.35} _{-0.35}	2.61 ^{+4.6} _{-1.6}	89.9 ^{+43.1} _{-42.9}	0.072 ^{+0.035} _{-0.001}	675 ⁺³⁴⁸ ₋₃₄₈	0.51 ^{+0.001} _{-0.001}	1.03 ^{+0.8} _{-0.8}
TOI - 1533	20.7 ⁺⁶ _{-3.7}	4.35 ^{+3.83} _{-1.86}	17.70 ^{+30.4} _{-10.4}	90.0 ^{+43.0} _{-43.0}	0.072 ^{+0.067} _{-0.035}	2050 ⁺³⁶²⁰ ₋₁₇₇₀	0.516 ^{+0.001} _{-0.001}	4.68 ^{+3.9} _{-3.9}
TOI - 1806	32.1 ^{+1.5} _{-1.5}	2.38 ^{+0.81} _{-0.62}	6.85 ^{+4.03} _{-2.6}	90.2 ^{+42.6} _{-42.6}	0.044 ^{+0.043} _{-0.021}	2950 ⁺²⁰²⁰ ₋₁₅₅₀	0.508 ^{+0.012} _{-0.001}	2.57 ^{+0.82} _{-1.55}
TOI - 2000	20.38 ^{+2.5} _{-4.85}	4.28 ^{+5.06} _{-1.97}	17.31 ^{+10.78} _{-3.6}	85.7 ^{+4.5} _{-3.6}	0.073 ^{+0.066} _{-0.036}	1210 ⁺²⁸⁵⁰ ₋₁₁₁₀	0.353 ^{+0.334} _{-0.001}	3.85 ^{+1.96} _{-2.59}
TOI - 5398	26.7 ^{+10.5} _{-6.3}	5.37 ^{+6.36} _{-2.37}	24.77 ^{+60.35} _{-14.9}	89.8 ^{+3.8} _{-4.3}	0.071 ^{+0.066} _{-0.034}	2200 ⁺⁵²¹⁰ ₋₁₉₄₀	0.581 ^{+0.258} _{-0.001}	4.84 ^{+3.37} _{-3.11}
TOI - 2267	7.39 ^{+2.8} _{-1.6}	1.11 ^{+0.38} _{-0.39}	1.29 ^{+2.27} _{-0.76}	90.0 ^{+42.9} _{-42.9}	0.045 ^{+0.045} _{-0.022}	1760 ⁺¹²¹⁰ ₋₈₂₆	0.514 ^{+0.026} _{-0.001}	1.19 ^{+1.59} _{-0.53}
TOI - 6276	12.2 ^{+3.2} _{-2.2}	1.11 ^{+0.28} _{-0.28}	1.29 ^{+6.81} _{-1.9}	90.2 ^{+42.7} _{-42.7}	0.074 ^{+0.036} _{-0.001}	260 ⁺¹³⁹ ₋₁₃₉	0.519 ^{+0.001} _{-0.001}	0.44 ^{+0.34} _{-0.34}
TOI - 266	20.3 ^{+0.9} _{-0.9}	1.98 ^{+0.69} _{-0.52}	5.12 ^{+3.09} _{-1.96}	90.3 ^{+42.8} _{-42.8}	0.072 ^{+0.067} _{-0.035}	390 ⁺²⁷⁴ ₋₂₀₈	0.517 ^{+0.023} _{-0.001}	1.17 ^{+0.52} _{-0.74}
TOI - 1692	69.9 ^{+29.3} _{-29.3}	5.59 ^{+1.95} _{-1.43}	26.39 ^{+9.84} _{-9.84}	89.8 ^{+42.6} _{-42.6}	0.069 ^{+0.06} _{-0.033}	1240 ⁺⁸⁷⁰ ₋₆₄₃	0.508 ^{+0.001} _{-0.001}	3.35 ^{+2.01} _{-2.11}

Table 2 continued

Table 2 (continued)

Name	Period (d)	Radius (R_{\oplus})	Mass (M_{\oplus})	Inclination (deg)	Eccentricity	Transit Depth (ppm)	Transit Probability	RV Semi-amplitude (m/s)
TOI - 1136	73.229.5	2.58 ^{0.9} _{0.66}	7.78 ^{4.7} _{2.9}	88.9 ^{1.2} _{0.8}	0.018 ^{0.016} _{0.009}	595 ⁴¹⁸ ₃₀₈	0.499 ^{0.178} _{0.001}	1.17 ^{1.12} _{0.53}
TOI - 5088	26.710.8	2.37 ^{2.56} _{1.06}	6.8 ^{4.84} _{1.14}	90.1 ^{43.1} _{42.8}	0.072 ^{0.066} _{0.034}	624 ¹³⁵⁰ ₅₆₁	0.513 ^{0.021} _{0.001}	1.46 ^{2.64} _{1.11}
TOI - 1468	33.67 ^{8.5} ₅	1.43 ^{0.37} _{0.37}	3.09 ^{1.90} _{0.93}	90.0 ^{1.5} _{0.93}	0.071 ^{0.034} _{0.034}	1490 ⁷⁷⁴ ₀	0.503 ^{0.005} _{0.001}	1.26 ^{0.86} _{0.05}
TOI - 6454	50.72 ^{1.5} _{1.5}	4.11 ^{1.43} _{1.06}	16.48 ^{9.83} _{6.14}	90.0 ^{42.2} _{0.034}	0.07 ^{0.062} _{0.034}	1790 ¹²⁵⁰ ₉₃₄	0.508 ^{0.017} _{0.001}	2.95 ^{1.16} _{1.86}
HD15337	9.29 ^{0.9} _{0.9}	1.87 ^{0.66} _{0.48}	4.68 ^{1.75} _{1.87}	86.8 ^{3.7} _{4.5}	0.071 ^{0.063} _{0.034}	397 ²⁸¹ ₂₀₅	0.497 ^{0.479} _{0.001}	1.53 ^{0.66} _{0.65}
TOI - 2112	332.312 ^{7.5} ₆	4.86 ^{1.65} _{1.26}	21.16 ^{12.42} _{9.9}	90.5 ^{42.7} _{0.031}	0.067 ^{0.057} _{0.031}	795 ⁵⁴³ ₄₁₆	0.508 ^{0.007} _{0.001}	1.43 ^{0.62} _{0.9}
K2 - 275	16.97 ⁶ ₆	2.27 ^{0.79} _{0.58}	6.35 ^{3.83} _{2.37}	90.0 ^{42.8} _{4.4}	0.072 ^{0.068} _{0.035}	910 ⁶³⁴ ₄₆₆	0.514 ^{0.001} _{0.001}	1.89 ^{0.62} _{1.12}
LTT3780	25.510 ⁷ _{6.3}	1.73 ^{1.07} _{0.64}	4.14 ^{2.26} _{0.64}	90.2 ^{42.6} _{0.035}	0.072 ^{0.065} _{0.035}	1740 ²¹⁶⁰ ₂₉₀	0.509 ^{0.014} _{0.001}	1.72 ^{0.44} _{1.4}
TOI - 2350	20.35 ¹ ₁	5.23 ^{2.02} _{0.67}	23.76 ^{12.77} _{7.7}	90.3 ^{43.1} _{0.035}	0.072 ^{0.035} _{0.035}	1970 ¹⁵⁴⁰ ₀	0.521 ^{0.001} _{0.001}	5.74 ^{4.14} _{1.4}
HD191939	15.4 ^{0.9} _{0.9}	4.04 ^{1.81} _{1.36}	15.82 ^{5.2} _{5.4}	88.6 ^{0.8} _{0.8}	0.017 ^{0.016} _{0.008}	1550 ⁶⁷⁷⁰ ₁₀₅₀	0.869 ^{0.131} _{0.001}	4.67 ^{2.35} _{0.99}
HD108236	53.113 ^{1.1} _{1.1}	2.05 ^{0.71} _{0.52}	5.41 ^{3.24} _{1.2}	88.4 ^{1.5} _{1.1}	0.023 ^{0.021} _{0.011}	456 ²³² ₀	0.415 ^{0.344} _{0.001}	1.01 ^{0.83} _{0.48}
TOI - 5788	32.118 ^{0.8} _{0.8}	1.72 ^{0.59} _{0.45}	4.12 ^{2.07} _{2.05}	90.3 ^{42.8} _{0.035}	0.072 ^{0.065} _{0.035}	336 ²³³ ₁₇₉	0.513 ^{0.019} _{0.001}	0.82 ^{2.04} _{0.57}
TOI - 406	26.711 ³ ₃	1.45 ^{0.5} _{0.37}	3.24 ^{5.77} _{2.07}	90.1 ^{42.5} _{0.034}	0.071 ^{0.065} _{0.034}	1170 ⁸¹⁰ ₆₀₁	0.509 ^{0.013} _{0.001}	1.33 ^{1.79} _{1.03}
TOI - 712	22.22 ⁷ ₇	2.35 ^{0.81} _{0.67}	6.71 ^{4.0} _{1.9}	88.8 ^{2.7} _{0.034}	0.044 ^{0.041} _{0.032}	1030 ¹¹⁵ ₅₃₂	0.507 ^{0.456} _{0.001}	1.88 ^{1.31} _{0.77}
TOI - 932	40.38 ⁷ ₇	1.93 ^{0.5} _{0.5}	4.92 ^{1.83} _{1.94}	90.0 ^{43.8} _{0.034}	0.071 ^{0.063} _{0.034}	581 ⁴¹⁴ ₃₁₆	0.509 ^{0.001} _{0.001}	1.17 ^{0.71} _{0.01}
TOI - 4647	23.25 ⁸ ₈	2.69 ^{0.94} _{0.7}	8.31 ^{5.03} _{13.15}	89.8 ^{42.8} _{0.035}	0.072 ^{0.066} _{0.035}	649 ⁴⁵⁸ ₃₄₄	0.514 ^{0.025} _{0.001}	1.75 ^{0.72} _{1.09}
TOI - 2404	9.29 ^{1.6} _{2.0}	5.01 ^{1.74} _{1.74}	22.13 ^{2.8} _{10.87}	89.8 ^{42.8} _{0.038}	0.042 ^{0.038} _{0.02}	1510 ²³⁵⁰ ₁₀₆₀	0.53 ^{0.069} _{0.001}	6.1 ^{2.22} _{4.11}
TOI - 2525	167.02 ⁸ _{36.3}	9.21 ^{3.18} _{2.36}	58.09 ^{34.72} _{21.7}	88.6 ^{4.3} _{0.034}	0.071 ^{0.06} _{0.034}	11420 ⁷⁹⁴⁰ ₅₉₂₀	0.484 ^{0.015} _{0.001}	7.53 ^{5.88} _{3.4}
TOI - 1453	12.85 ⁴ ₄	1.58 ^{0.99} _{0.59}	4.36 ^{1.9} _{3.49}	89.9 ^{43.3} _{42.5}	0.073 ^{0.068} _{0.035}	416 ⁵²⁵ ₃₁₆	0.517 ^{0.029} _{0.001}	1.38 ^{5.15} _{1.21}
TOI - 500	12.21 ⁴ ₄	2.07 ^{2.09} _{1.5}	5.49 ^{15.06} _{10.6}	82.4 ^{1.9} _{0.034}	0.031 ^{0.029} _{0.034}	779 ²¹⁰⁰ ₀	0.016 ^{0.744} _{0.001}	1.85 ^{5.10} _{1.0}
TOI - 709	12.82 ⁵ ₅	1.86 ^{0.75} _{0.75}	4.64 ^{107.55} _{3.35}	90.3 ^{43.0} _{0.032}	0.068 ^{0.061} _{0.032}	13460 ³⁷⁶⁰⁰ ₂₃₀₄₀	0.507 ^{0.028} _{0.001}	2.02 ^{1.73} _{0.81}
TOI - 1836	48.421 ⁷ ₈	4.11 ^{1.84} _{1.84}	16.17 ^{9.92} _{8.6}	90.1 ^{42.9} _{0.034}	0.07 ^{0.062} _{0.034}	538 ¹³⁴⁰ ₄₈₅	0.514 ^{0.028} _{0.001}	2.44 ^{5.32} _{1.87}
TOI - 119	21.28 ⁷⁴ ₇	1.92 ^{0.67} _{0.5}	4.88 ^{19.12} _{1.86}	89.8 ^{42.7} _{0.035}	0.072 ^{0.066} _{0.035}	461 ³²⁶ ₂₄₆	0.512 ^{0.023} _{0.001}	1.25 ^{4.18} _{0.78}
TOI - 233	25.510 ⁶ ₆	1.84 ^{0.63} _{0.47}	4.56 ^{15.81} _{1.89}	90.3 ^{43.0} _{0.034}	0.071 ^{0.066} _{0.034}	1970 ¹³⁵⁰ ₁₀₁₀	0.51 ^{0.014} _{0.001}	1.93 ^{5.33} _{1.22}
WASP - 84	23.28 ⁸ _{5.9}	7.22 ^{6.59} _{3.01}	39.5 ^{22.68} ₀	89.9 ^{42.3} _{0.035}	0.072 ^{0.067} _{0.035}	6210 ¹¹⁴⁰⁰ ₅₂₁₀	0.514 ^{0.026} _{0.001}	9.91 ^{13.18} _{7.2}